PALACKÝ UNIVERSITY IN OLOMOUC
FACULTY OF SCIENCE

DISSERTATION THESIS

Analysis of the mathematical models for unsaturated porous media flow

Department of Mathematical Analysis and Application of Mathematics
Supervisor: **RNDr. Rostislav Vodák, Ph.D.**
Submitted by: **Mgr. Jakub Kmec**
Programme: P1102 Mathematics
Branch: Mathematical Analysis
Form: Full-time
Year of submission: 2021

BIBLIOGRAPHICAL IDENTIFICATION

Author: Mgr. Jakub Kmec

Title: Analysis of the Mathematical Models for Unsaturated Porous Media Flow

Type of thesis: Dissertation thesis

Department: Department of Mathematical Analysis and Application of Mathematics

Supervisor: RNDr. Rostislav Vodák, Ph.D.

The year of presentation: 2021

Abstract: Modelling unsaturated porous media flow is a complex problem with many important applications. There is sufficient experimental and theoretical evidence of porous media flow regimes that are impossible to explain by the standard continuum mechanics models. In this thesis, a semi-continuum model is presented that combines the virtues of the continuum and discrete models based on invasion percolation. The medium is divided into blocks of finite (not infinitesimal) size that retain the characteristics of a porous medium. Each block sample of porous medium is characterized by its porosity, permeability, and the retention curve. The semi-continuum model describes pressure and saturation as fields that are continuous in time but piecewise constant in space. The model repeats three successive rules: saturation update in each block, pressure update in each block and flux update between neighbouring blocks. The limit of the semi-continuum model is very substantial and is not compatible with continuum mechanics approach. It is demonstrated that the model captures well (1) all the features of one dimensional unsaturated porous media flow (i.e. three dimensional flow in a thin tube), (2) all the features of two dimensional unsaturated porous media flow (i.e. three dimensional flow in a Hele-Shaw cells).

Keywords: Porous media flow, Saturation overshoot, Wetting front instability, Semi-continuum model, Darcy-Buckingham law, Invasion percolation, Richards' equation, Finger flow

Number of pages: 120

Number of appendices: 1

Language: English

Declaration

I declare that this thesis was composed by myself, that the work contained herein is my own except where explicitly stated otherwise in the text, and that this work has not been submitted for any other degree or processional qualification except as specified. Parts of this work have been published in [65, 66]; specifically parts of chapters 2 and 3 have been published in [65], parts of the chapter 4 have been published in [66], and parts of the chapter 5 have been published in [65, 66].

In Olomouc ....
Signature

Contents

Acknowledgement

Chapter 1

Introduction

A porous medium is a material, which contains pores. Pores are filled with one or more different fluids, for instance air, water or oil. Skeletal structure of porous medium is called matrix and is usually very complex with fractal structure. In terminology of hydrology, the porous medium is saturated if all the pores contain water and is unsaturated if some pores are filled with water and some with air. The saturation is defined as the fraction of the total volume of the fluid and pore volume. There exist many natural porous substances such as soil, rocks, wood, cork or bones.

Flow of liquids through porous media is a long standing, well researched, yet still not fully understood problem. There are two broad areas that draw heavily on understanding porous media flow – oil recovery [69], and vadose zone hydrology [29], [137]. In oil recovery applications, two immiscible and incompressible fluids – water and oil – move in a complex space of pores in a reservoir rock. In vadose zone hydrology, the two fluids are water (incompressible and wetting) and air (compressible and non-wetting). Many other applications of porous media flow have been investigated, such as carbon sequestration [118], transport of radionuclides in the soil [14], filtration [117], hydrogen storage [2], geothermal engineering [8], and applications in biological systems and biotechnology [123]. This thesis concentrates on the flow of water through soil which is not fully saturated. Lack of understanding of vadose zone hydrology is one of the main bottlenecks in our understanding of the hydrological cycle [68].

Problems concerning fluid flow are notoriously difficult due to non-linearity caused by inertial forces (the so-called convective term in the Navier-Stokes equations). In the porous media setting, the flow velocity is usually so small that inertial forces can be neglected. Still, the problem is difficult because the pressure in the wetting fluid at each point is determined by an interplay between hydro-

static forces due to gravity, and capillary forces due to the presence of menisci of air-water interfaces which are in turn determined by the geometry of the porous matrix. Since the geometry of the matrix is so complex that it cannot be fully resolved in any reasonable model, some simplification or approximation is needed.

Over the years, there has been a growing body of experimental evidence of observed unsaturated porous media flow regimes that were not easy to describe or explain by the known mathematical models [29], [137]. These persistent and important flow regimes will be described in Section 1.1. In Section 1.2, we will derive the most celebrated equation associated with homogeneous porous media flow in the context of hydrology, the so-called Richards' equation.

1.1. Flow regimes in unsaturated homogeneous porous media

The purpose of this section is to briefly describe each of the regimes in porous media flow. All of the regimes share the following setting: the porous medium is homogeneous, i.e. it does not contain any macropores, cracks, or preferential channels. The porous medium is unsaturated, i.e. some of the pores are filled with wetting fluid and some with gas. Gravity and capillary forces both play important roles and neither can be neglected.

Finger flow

The so-called finger flow, or gravity-driven fingering, rates among the most intriguing of the flow regimes in unsaturated homogeneous porous media (UHPM). This phenomenon has been studied extensively since the early 1970s [59], more detailed reference is provided in Section 2.1. The regime can be reached e.g. as follows: let us start with a sample of initially dry homogeneous porous medium, usually fine grain sand. Wetting fluid is supplied to a single point at the upper boundary of the sample at a small constant rate. Under a wide range of experimental conditions (see Section 2.1), a single macroscopic finger forms and proceeds downwards at almost constant velocity (see Figure 1.1). The finger tip can be almost fully saturated.

The proceeding finger leaves an under-saturated trace. Subsequent infiltration follows the path wetted by the first finger. The key feature of this regime is the non-monotonicity of the saturation, i.e. a ratio of the total volume of the fluid to the pore volume. At certain points (through which the finger tip passes)
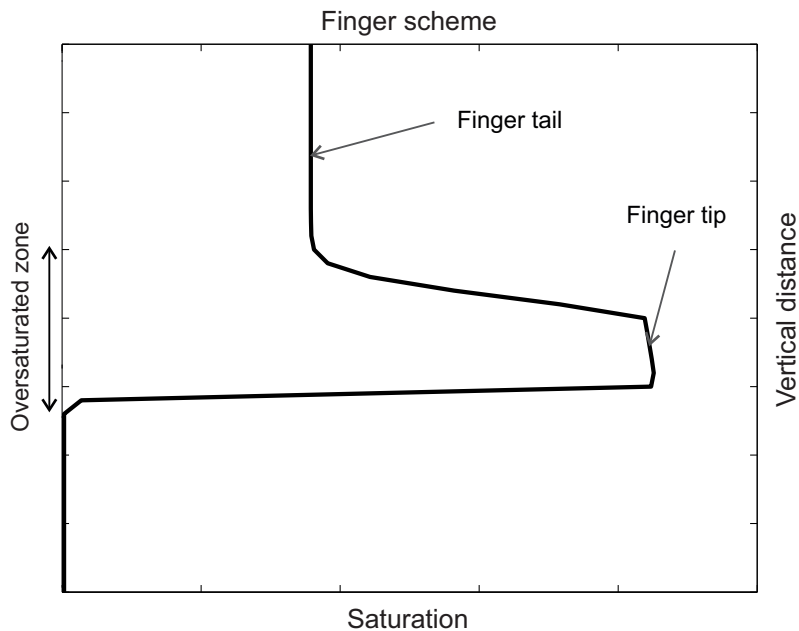
Figure 1.1: A schematic representation of a single one-dimensional finger.

saturation is a non-monotone function of time, first it increases abruptly as the over-saturated fingertip arrives, and then it gradually decreases as the undersaturated fingertail passes. This effect is called saturation overshoot as it is characteristic for finger flow.

Wetting front instability

Earlier studies of wetting front instability were presented by Raats [101]. Let us start with a sample of initially dry homogeneous porous medium. Water is supplied to the entire upper boundary at a small constant rate (usually by spraying). In experiments, a complicated structure of rivulets (preferential pathways, fingers) is formed in the porous matrix [106]. Large parts of the matrix remain dry even if the experiment continues for a long time (months), see Figure 1.2. Subsequent infiltration follows the preferential pathways formed by the first event. The paths can be erased either by over-drying or by complete wetting of the matrix pore space. Fingers were observed to merge (often) and bifurcate (rarely). Each finger can exhibit saturation overshoot at its tip. For a deeper understanding of wetting front instability, we recommend a detailed experimental work provided in a series of papers from Glass et al. [46, 50, 48, 49, 45, 41].

Figure 1.2: Demonstration of wetting front instability. The experiment was realized at Mlaky II near Sekule in 2010 [76]. Water was supplied across the top boundary at a small constant rate. Substantial part of the matrix remained dry after long time of steady infiltration.

Buoyancy destabilized non-wetting invasion

A sample of initially wet porous medium is placed into a box. Air is supplied to one point near the bottom of the box at a small constant rate. In experiments, a beautiful structure of jellyfish-like clusters of air is formed, one on top of another. The clusters are interconnected with pore-scale fingers. The clusters pulsate: once a cluster is large enough (to become buoyancy destabilized) it sends a pulse of air through the pore-scale finger to the cluster above and so on. For more details, see experiments from Glass et al. [42], [52].

Draining by air overpressure: the problem of residual moisture

The main draining branch is usually measured in the following way [100]: start with a sample of initially wet homogeneous porous medium. The water is displaced from matrix by gradually increasing overpressure of the ambient air, which is supplied at the entire upper boundary. The main draining branch is then measured as the dependence of air pressure and outflowed water. The ex-

perimental procedure is usually done by using pressure plate apparatus [105]. Some isolated clusters of water always remain inside the porous matrix, even if huge overpressure is used. This residual moisture can be removed only by increasing temperature inside the porous matrix e.g. by burning.

Free evaporation

A sample of initially wet homogeneous porous medium is left to dry by evaporation from its upper boundary [98]. A rich networks of dry fingers and wet islands is formed inside the porous matrix. There is no simple interface between the dry and wet regions.

Oscillation water discharge

A sample of initially dry homogeneous porous medium is placed into a box. Water is supplied to the entire upper boundary at a small constant rate. It is a black-box experiment, only the discharge (outflow as a function of time) is measured. Experimental records are scarce [99], [134]. Two distinct discharge regimes are observed:

- Monotonic sigmoid-like discharge stabilizing at a constant rate, which is equaled to the influx rate. This is predicted by the continuum theory. It is observed for instance in very fine sands or clays, where the diffusion-like behavior appears.

- Oscillation water discharge: the discharge never stabilizes at a constant rate, it keeps fluctuating. The oscillations are chaotic rather than periodic. Sometimes a peak initial discharge appears before oscillatory discharge. It is shown in [134], that the varying discharge from the soil is a manifestation of the finger flow.

Old and new water

Start with a sample of initially partially wet homogeneous porous medium. Old water is distributed throughout the porous medium, usually sitting in the small pores. New water is supplied to the entire upper boundary at a constant rate. It is a black-box experiment, only the proportion of old and new water in the discharge is measured. Old and new water can be distinguished by chemical or physical tracers. Experimental records are again scarce, however some field studies are available [121], [131], [132]. Initially, a mixture of old and new water

emerges, then mostly new water flows out, followed again by a mixture of old and new water. Another experiments showed significant old water portion during rainfall and snowmelt events in the Canadian Prairies [107].

1.2. Governing equations

Let us first introduce physical variables, which are usually used for the description of porous media flow:

- Saturation S [–]: a relative moisture content, i.e. a ratio of the total volume of the fluid to the pore volume.

- Pressure P [kg/ms^2].

- Flux q [m/s].

- Porosity θ [–]: a ratio of the total volume of voids to the total volume of the porous material.

- Intrinsic permeability κ [m^2]: a property of the soil to transfer fluid through a porous medium.

- Dynamic viscosity μ [kg/ms]: a fluid's resistance to flow.

- Relative permeability k [–]: a function of saturation calculated as a ratio of the effective permeability of the particular saturation to the intrinsic permeability. Values are bounded between 0 and 1.

- Gravitational acceleration g [m/s^2].

- Density ρ [kg/m^3].

We begin with the standard fractional flow formulation of two-phase flow system [13], [84], [12], [120], [69], [119], when the first fluid (e.g water) displace the second fluid (e.g gas or oil). Two-phase flow system is characterized by the wetting phase (denoted by index w) and non-wetting phase (denoted by index n). If no external force is given, the mass balance law for each phase is represented by the equation

$$\partial_t \theta \rho_i S_i + \operatorname{div}(\rho_i q_i) = 0, \tag{1.1}$$

where i denotes index for each phase. Saturation S_i, densities ρ_i and fluxes q_i are functions of space $\mathbf{x} \in \Omega \subset \mathbb{R}^3$ and time $t \in \mathbb{R}$. The following constitutive relation holds for the two-phase flow

$$S_w + S_n = 1. \tag{1.2}$$

In the fractional flow formulation it is usually assumed incompressibility of both fluids [33, 58, 109, 142], therefore we can write

$$\rho_w(\mathbf{x}, t) = \rho_w = \text{const},$$
$$\rho_n(\mathbf{x}, t) = \rho_n = \text{const}. \tag{1.3}$$

By assuming, that the porous medium is homogeneous, we can get another great simplification

$$\theta(\mathbf{x}, t) = \theta = \text{const}. \tag{1.4}$$

Using assumptions (1.3) and (1.4) in the mass balance Equation (1.1) yields

$$\theta \partial_t S_n + \text{div}(q_n) = 0 \tag{1.5}$$

for the non-wetting phase and

$$\theta \partial_t S_w + \text{div}(q_w) = 0 \tag{1.6}$$

for the wetting phase. Fluxes q_i for each phase are given by the Darcy-Buckingham law [5]

$$q_i = -\frac{k_i(S_i)}{\mu_i} \kappa \Big(\nabla P_i + (0, 0, \rho_i g) \Big) = -\lambda_i(S_i) \kappa \Big(\nabla P_i + (0, 0, \rho_i g) \Big), \tag{1.7}$$

where $\lambda_i(S_i) = \frac{k_i(S_i)}{\mu_i}$ is the mobility of the phase i. The flux of the wetting phase can be derived in terms of phase mobilities, phase densities and phases pressure difference. Let's denote

$$Q = q_w + q_n, \tag{1.8}$$

and

$$\lambda_T = \lambda_w + \lambda_n, \tag{1.9}$$

where Q and λ_T is the total volume flux and total mobility, respectively. Adding Equations (1.5) and (1.6), and using Equation (1.2) shows

$$\text{div}(q_w + q_n) = \text{div}(Q) = 0. \tag{1.10}$$

The equation above implies, that the total volume flux is independent of space for a one-dimensional case. Moreover, Hilfer et al. [58] claim that the independency of space also applies for higher dimension, although the proof is unclear. Hence, we can write

$$q_w(\mathbf{x}, t) + q_n(\mathbf{x}, t) = Q(t). \tag{1.11}$$

Using Equations (1.8) and (1.9), we can write

$$\left(1 - \frac{\lambda_n}{\lambda_T}\right) q_w = \frac{\lambda_w}{\lambda_T}(Q - q_n). \tag{1.12}$$

The flux of the wetting phase can be then expressed as

$$q_w = \frac{\lambda_w}{\lambda_T}Q - \frac{\lambda_w}{\lambda_T}q_n + \frac{\lambda_n}{\lambda_T}q_w. \tag{1.13}$$

Substitute relation (1.7) for both phases into Equation (1.13) to eliminate q_n gives the result

$$
\begin{aligned}
q_w &= \frac{\lambda_w}{\lambda_T}Q + \frac{\lambda_n \lambda_w}{\lambda_T}\kappa\Big(\nabla P_n + (0, 0, \rho_n g)\Big) - \frac{\lambda_n \lambda_w}{\lambda_T}\kappa\Big(\nabla P_w + (0, 0, \rho_w g)\Big) \\
&= \frac{\lambda_w}{\lambda_T}Q\Big[1 + \frac{\lambda_n}{Q}\kappa\Big(\nabla P_c + (0, 0, \rho_n - \rho_w)g\Big)\Big],
\end{aligned} \tag{1.14}
$$

where the capillary pressure P_c is usually given as a function of the wetting phase saturation:

$$P_c = P_c(S_w) = P_n - P_w. \tag{1.15}$$

Here, the capillary pressure $P_c(S_w)$ represents the so-called retention curve (hysteresis operator). Let us note, that the capillary pressure is always given as a suction. The retention curve consists of the main wetting and draining branches and is assumed to be non-increasing [128] (see Figure 1.3 for a simplified model of the retention curve). It is well known, that retention curve exhibit substantial hysteresis, thus the pressure-saturation relation depends also on history of a system. Some approaches of modelling hysteresis of the retention curve can be found in [85, 70, 96].

The fractional flow equation is then obtaint by inserting Equation (1.14) into Equation (1.6):

$$\theta \partial_t S_w + \mathrm{div}\left(\frac{\lambda_w(S_w)}{\lambda_T(S_w)}Q\Big[1 + \frac{\lambda_n(S_w)}{Q}\kappa\Big(\nabla P_c(S_w) + (0, 0, \rho_n - \rho_w)g\Big)\Big]\right) = 0. \tag{1.16}$$
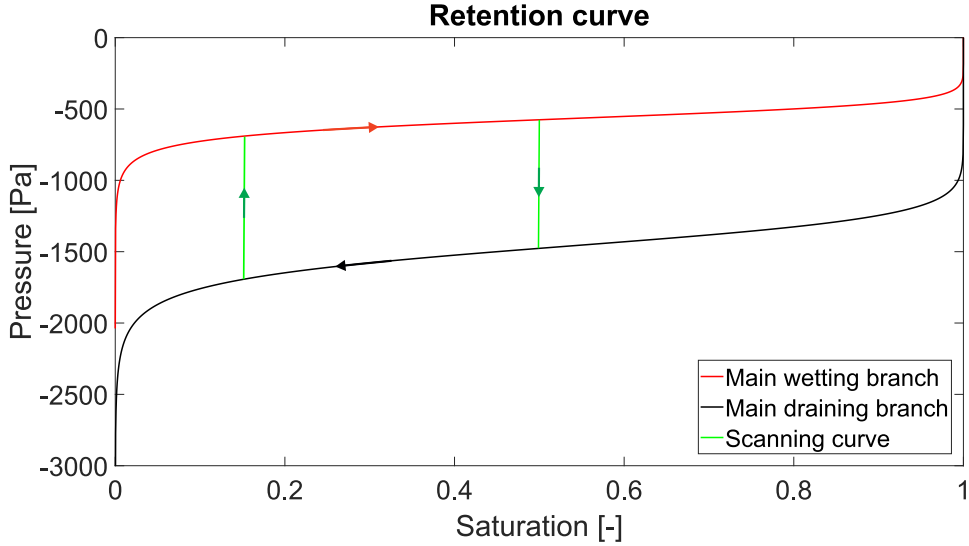
Figure 1.3: A simplified retention curve. The pressure is given as a underpressure and thus the retention curve is non-decreasing.

In controlled experiments in which water is injected into the porous medium, the total volume flux $Q(t)$ is known. Moreover, if a constant boundary flux q is used, then we can write $Q(t) = q$.

For a very small intrinsic permeability or when gravity and capillary effects can be neglected, the Equation (1.16) reduces to the Buckley-Leverett equation [13]

$$\theta \partial_t S_w + \text{div}\Big(\frac{\lambda_w(S_w)}{\lambda_T(S_w)}Q\Big) = 0. \tag{1.17}$$

For applications in hydrology (w corresponds to water and n to air), one can assume $\rho_n = 0$ and $P_n = 0$ and then Equation (1.7) implies $q_n = 0$. Therefore, the non-wetting phase vanishes from the problem and inserting Darcy-Buckingham equation (1.7) for the wetting phase into the Equation (1.6) gives the Richards' equation [104] (RE); for the simplicity, we will denote the wetting phase without index w:

$$\theta \partial_t S(t, \mathbf{x}) + \text{div}\left[\frac{\kappa k(S(t, \mathbf{x}))}{\mu}\Big(\nabla P_c(S(t, \mathbf{x})) - (0, 0, \rho g)\Big)\right] = 0. \tag{1.18}$$

In other words, the RE is the limit of the fractional flow equation (1.16), when the mobility of the air-phase tends to infinity. Thus, if we assume that the dynamic viscosity of the air cannot be neglected, we will receive more general case of the

RE. The RE is usually stated in the following form:

$$\theta \partial_t S(t, \mathbf{x}) + \mathrm{div}\left[K(S(t,\mathbf{x}))\nabla h(S(t,\mathbf{x})) - \Big(0, 0, K(S(t,\mathbf{x}))\Big)\right] = 0, \qquad (1.19)$$

where $K = \frac{\kappa k(S)}{\mu}\rho g$ [m/s] denotes the hydraulic conductivity and the function h [m] denotes the capillary height. The hydraulic conductivity is assumed to be non-negative and non-decreasing function of the saturation. The capillary pressure $P_c(S)$ is related to the capillary height $h(S)$ by the simple rescaling relation

$$P_c(S(t,\mathbf{x})) = \rho g h(S(t,\mathbf{x})).$$

The Richards' equation is fundamental in hydrology, while the Buckley-Leverett equation is usually used for applications in petroleum engineering.

Chapter 2

Different approaches of modelling unsaturated porous media flow

Let us now introduce different approaches of modelling UHPM. We will focus mostly on the most intriguing and the famous regime, the so-called saturation overshoot (see Section 1.1). Porous media flow is usually modeled in the framework of continuum mechanics [5], [29], [137]. This approach has been popular because the mathematical tools of continuum mechanics (differential calculus and partial differential equations) were well established and very successful in science and technology.

In Section 2.1, the experimental evidence of saturation overshoot will be presented followed by Sections 2.2–2.4, where different approaches of modelling are described. Finally we will suggest methodology for evaluation different models in Section 2.5. Sections 2.1-2.4 are taken from Kmec et al. [65], and are extended in this thesis.

2.1. Experimental evidence of saturation overshoot

Saturation overshoot in gravity-driven fingers was experimentally observed by Glass et al. [47], Liu et al., [77]. and Selker et al. [111]. To our knowledge, the most comprehensive experimental work was done by DiCarlo (see [23] and [26] and the reference and discussion therein) and Bauters et al. [3]. The main experimental results of DiCarlo and Bauters et al. can be summarized as follows:

- Finger flow accompanied by saturation overshoot is observed in wide range of homogeneous porous media types – soils, sands, and artificial glass beads,

uniformly or randomly packed. It is observed for wide range of flow rates, and for wide range of initial saturation levels.

- The overshoot effect is observed in three-dimensional, two dimensional (Hele-Shaw cells) and one-dimensional (narrow tubes) settings.

- The finger behavior depends on the initial saturation of the matrix. With increasing initial saturation, the fingers first become more narrow and faster, then they widen and slow down and the saturation overshoot decreases. For initial saturation close to the residual moisture limit, the fingering regime disappears and diffusion-like front forms with no overshoot.

- The saturation overshoot magnitude (i.e. the difference between the saturation in the tip and the saturation in the tail) increases with increasing flow rate up to a certain value, beyond which it decreases until it disappears completely. However, there is also a lower limit – saturation overshoot is not observed for very small flow rates.

- Glass et al. [49] observed, that the finger width is increasing with increasing flux. Moreover, Yao et al. [138] showed the increase in finger width at very low applied fluxes. DiCarlo [29] compared these results (see Figure 2 in [29]). The increase in the finger width for high applied fluxes is predicted by Chuoke et al. [20] and Parlange et al. [97]. However, they do not predict the finger width increase for very low fluxes.

- Saturation overshoot depends on the shape of the porous matrix grains. The effect is less pronounced for spherical sand grains than for sands with more angular (irregular) shapes. Materials with very similar macroscopic continuum properties exhibit different saturation overshoot patterns.

- The finger-tip is not always fully saturated, its saturation depends on the flow rate and on initial saturation of the medium.

- Capillary pressure overshoot is consistent with the saturation overshoot, and the pressure-saturation relation does not seem to depend on the finger velocity, although other sources (see e.g. [39]) report some evidence for velocity dependent behavior.

- The overshoot behavior depends on the ratio of capillary and gravitational forces captured in [94] by the so-called Bond number.

2.2. Continuum modelling

Naturally, there have been many attempts to capture gravity-driven fingers and especially the saturation overshoot by continuum mechanics based models. Continuum mechanics uses the concept of reference volume element to transition from naturally discontinuous pore-level quantities to continuous and differentiable macroscopic fields (e.g. pressure, saturation). Various forms of conservation laws such as balance of mass, momentum and energy for these fields are then derived in the form of partial differential equations. The "canonical" equation used for UHPM flow is the celebrated Richard's equation [104] (see Section 1.2 for the derivation).

For a long time, it had not been known whether the RE admits solutions that exhibit saturation overshoot, although it was widely doubted because of the parabolic nature of the equation. In 1996, Nieber [92] claimed to have produced a finger-like solution of the RE numerically which exhibited saturation overshoot. However, Eliassi and Glass [35] demonstrated why the finger-like solution was a numerical artifact. The arguments used by Eliassi and Glass were numerical in their nature: the authors went through the numerical methods used in [92] and explained why the computed finger-like solution was incorrect. This issue was finally settled in [40] where the authors show by means of a mathematical proof that the RE, in principle, cannot admit saturation overshoot for three-dimensional homogeneous unsaturated porous media flow, subject to monotone boundary conditions. The authors prove that any solution to the RE, under the above boundary conditions, is non-decreasing in time at all points. The result is not dependent on any particular form of the hydraulic conductivity or the retention curve, and it holds for any type of hysteretic behavior of the retention curve. Together with the references [127], and [34] it can be concluded that the RE is completely stable, to infinitesimal and finite-size perturbations, with or without hysteresis, and both in asymptotic and transient sense (see the discussion in [21]). Thus, the finger flow and saturation overshoot have been proven to be outside the scope of the RE based modelling.

Thus, it is obvious that in order to model saturation overshoot with continuum models, some extra terms in the governing equation are needed. Hassanizadeh et al. [55], [57], [56], [54] proposed to include a dynamical term into the pressure-saturation equation to yield a formula

$$P_{dyn}(S) = P_{stat}(S) - \tau(S)\frac{\partial S}{\partial t}, \tag{2.1}$$

where S stands again for the saturation, $P_{cs}(S)$ is the equilibrium pressure-

19

saturation curve, and $\tau(S)$ is a saturation dependent coefficient. This leads to a new term in the governing equation which is second order in space, and first order in time. DiCarlo [24] showed that solutions to such an extension of RE are not necessarily monotone in time, thus they can exhibit saturation overshoot. However, the function $\tau(S)$ represents the third unknown material function (together with the equilibrium pressure-saturation curve, and the hydraulic conductivity-saturation curve). Moreover, DiCarlo [24] notes that the parameter $\tau(S)$ is not clearly related to any measurable property of the porous medium. Even if τ is assumed to be saturation independent, its value has to be adjusted over two orders of magnitude to match experimental results in two media which are very similar from the macroscopic point of view. Experimental results have not brought conclusive evidence that the dynamical term in Equation (2.1) is necessary to characterize the pressure-saturation relation [27]. It is well known, that the dynamical term can produce solutions that exceed unity (due to pseudo-parabolic behavior of equations), as observed in [126]. However, if the relative permeabilities are vanishing for given values of saturation (0 or 1 in this case), then the saturation remains between these two bounds [18], [81].

Leroux and Pomeroy [75] developed a new model using the dynamic extension. A new approach for estimating residual water content in the hysteretic retention curves is used. This model reproduces well pressure overshoot experimentally measured in snowpack water flow [62]. However, the three model parameters were manually varied to match the experimental data. One of the model parameters defines the main imbibition curve, thus the retention curve varies for different input fluxes in the same medium. The main imbibition curve should remain the same for one porous medium. Other models using the dynamic extensions can be found e.g. in [91], [90], [19], [64], [102], and [82].

Eliassi and Glass published a series of papers [35], [36], [37] where they introduced the hold-back–pile-up effect to explain the saturation overshoot. They proposed three different extensions of the RE: a hypodiffusive model (which includes a term with the second order derivative of the saturation with respect to space), a hyperbolic model (with the second order derivative of the saturation with respect to time), and a mixed model (second order in space and first order in time). All the three extensions admit non-monotonic solutions and thus allow for saturation overshoot modelling. The hypodiffusive model is equivalent to the use of a non-monotonic pressure-saturation relation [32], [37]. All these extensions were analyzed by DiCarlo [32]. It is reported that the hypodiffusive and hyperbolic models are not well posed and require a regularization term. Solutions

(of the regularized equation) in the form of a traveling wave are found and their ability to match the experimentally observed features is discussed. The mixed model can be related to the dynamic capillary pressure concept of Hassanizadeh and Gray [55], [57], [56], [54] (see the discussion in the previous paragraph). Cueto-Felgueroso and Juanes [21] further question the above model extensions because they can produce overshoot which is not bounded between 0 and 1.

The approach presented in [21] represents another attempt to extend the RE for saturation overshoot modelling. The authors notice an analogy between the finger behavior and the flow of a thin fluid film along an inclined plane. An extension of the RE is presented which includes a fourth order space derivative of the saturation field. The governing equation (abbreviated here as CFJ) reads

$$\theta \partial_t S(t,x) = \mathrm{div} \left[K(S(t,x)) \nabla h(S(t,x)) + (0,0,K(S(t,x)) + \alpha \nabla \Delta S(t,x)) \right].$$
(2.2)

The model is then derived from free energy [9] in the framework of phase fields models [17], [16] (without any explicit reference to the thin film equation). The model introduces one new parameter α, however the authors link it to (well measurable) material parameter already presented in the RE. The authors then show by means of numerical simulation in one and two dimensions that the model is capable of reproducing many features of finger flow, including saturation overshoot and its dependence on initial saturation and flow rate.

The spatial patterns produced by the equation match very well the patterns observed for film flow on an inclined plane (see the Figure 2 in [21]). However, fingers in porous media tend to exhibit much more complicated structures. Gomez et al. [53] added spatial heterogeneity in the permeability field. By this approach, fingers are not "straight" anymore, they can meander, merge (two fingers meet) and breakup (a single finger splits). This is a remarkable success, however, there are several issues that bring even this model into question:

- It is experimentally observed, that the saturation overshoot has usually a plateau form [23]. However, the saturation overshoot of two and three dimensional fingers simulated by CFJ model has always a drop-like shape [53]. The authors claim [21], that simulations with a finer grid will lead to a sharper wetting front and larger saturation overshoot at the finger tip.

- The pressure-saturation relation has to be amended to prevent saturation from exceeding the unity. This is achieved by introducing a "compressibility term" to the capillary energy-saturation dependence. This term activates

(and becomes dominant) near saturation ($S = 1$) and prevents the saturation to increase any further, which is physically incorrect.

- DiCarlo [28] describes a simple experiment, in which an initially wet porous medium is allowed to drain under the force of gravity. After an equilibrium is reached, saturation is measured as a function of height. The zero-flux situation in the RE yields the equation $P_w(S) = z$, where z stands for the vertical coordinate. Measuring $S(z)$ allows one to obtain the pressure-saturation curve directly from this simple experiment. In the CFJ model, the zero-flux situation yields the relation

$$P_c(S) = z - \frac{\partial^2 S}{\partial z^2},$$

which seems to produce non-monotonic pressure-saturation curves. This is certainly an issue to be considered. The authors of the model reply to this criticism in [22] by arguing that their model is capable of capturing the draining experiment without the need for non-monotonic pressure-saturation curves. We believe this is an answer to a slightly different question. We think that the stationary model should be compatible with experiments.

- To solve the model, one needs boundary conditions that contain higher order derivatives of the saturation field. It is not clear how second or third derivatives can be obtained experimentally and what physical quantity they represent. In the thin-film context, the boundary conditions can be clearly related to (well measurable) geometry of the film, however, in the porous media flow context this is no longer possible.

- DiCarlo reports in [23] that saturation overshoot depends on the shape of the porous matrix grains. Materials with very similar macroscopic continuum properties exhibit different over-saturation patterns. This observation naturally challenges *any* continuum model of saturation overshoot (see the title of DiCarlo's article [23]).

Another very interesting approach is that of Brindt et al. [10] who treat the flow in 1D as a free-boundary problem. The model is based on the fact that a contact angle of the invading fluid should not be neglected [135]. The domain is divided into two subdomains with a sharp boundary between them. The upper subdomain (behind the wetting front) consists of water and air, whose proportion

is calculated by the RE. The lower subdomain (in front of the wetting front) consists of initially dry porous medium and the saturation remains constant in this region. The wetting front will propagate only if the capillary pressure head at the wetting front is lower than water-entry pressure Ψ_{we}, otherwise the flux through the boundary is equal zero. In case of finger flow, this is yet another way to ensure water accumulation in the fingertip. The presented model is in good agreement with experiments from DiCarlo [23] (see Figure 2 in [10]). However, the saturation overshoot is still pronounced for the lowest flux although it was not observed experimentally. On the other hand, the model can capture well the transition between saturation overshoot and diffusive like behavior for increasing boundary fluxes (see Figure 8 in [10]). Unfortunately, more simulations in 1D are not available (e.g. dependence on initial saturation).

Next, the moving-boundary approach has been implemented in 2D [11] (the authors claim, that the model is not a naive straightforward extension of the 1D). The authors produce physically correct gravity-driven finger, which is consistent with the experimentally measured finger in [3]. They also produced stable 2D flow, however different parameters to simulate stable and unstable flow were used including different retention curve, boundary flux and other important parameters of the model. Moreover, the dependence on initial saturation is not available in [11], thus any detailed comparison with experiments of Bauters et al. [3] is not possible. The price the authors pay for this approach is the necessity to indirectly prescribe the flow across the free boundary as an input to the model. We would rather see this to be an output. The division of the matrix into two domains is rather arbitrary -– in reality it is a single domain through which water and air move. There is no clear physical process (e.g. phase change as in the case of continuous casting modelling) which would define the position of the boundary. We are not sure how Brindt's modelling strategy allows for reproducing the dependence of flow characteristics on initial saturation of the matrix. Moreover, is it possible to define the free boundary, if the matrix is not in equilibrium at the start of new infiltration?

DiCarlo et al. [33] compared the standard fractional flow approach (see Equation 1.16) [13], [84], [120], [69], [119] to the Richards' equation (see Equation 1.18) [104]. The aim of the research was not focused on a prediction of the saturation overshoot. On the contrary, the authors claim that the saturation overshoot is not allowed from the continuum multiphase equations because they are parabolic. It is postulated that the saturation overshoot does occur over an infinitesimal distance and then they compare saturation behavior for the frac-

tional flow approach and the RE. It is shown, that the effect of non-wetting phase is negligible for infiltrations with fluxes less than half of the saturated conductivity. Hilfer et al. [58] proposed model which is based on fractional flow equation with hysteresis in the relative permeability. Schneider et al. [109] then extended recent predictions for stability of the saturation overshoot within the traditional generalized Darcy model. In [115], some comparison with experimental results of DiCarlo [23] were performed. The authors claim in [58], that the traditional theory has been abandoned prematurely because of its failure of producing the saturation overshoot. However, initial buildup of the saturation overshoot is modeled as a time-dependent Dirichlet condition. We conjecture that this is not appropriate for modelling fingering flow. The model is not able to produce the saturation overshoot with constant time-independent boundary condition. Finally, Zhang and Zegeling [142, 140, 141] implemented dynamic capillary pressure into a fractional flow equation and suggested hysteresis in the $\tau(S) - S$ relationship. They successfully compared results with experiments of one dimensional profiles. However as was already mentioned, the function $\tau(S)$ represents the third unknown material function, which is not clearly related to any measurable property of porous medium.

To sum up, current continuum models are struggling to capture the rich variety of complex UHPM flow regimes. For the saturation overshoot modelling, several extensions of the RE were proposed [29] (most of these extensions are described above). While they usually succeed in allowing saturation overshoot solutions, all of them have drawbacks and none seems to be able to capture the complexity of UHMP flow regimes entirely. Let us now turn to a completely different possibility of UHPM flow modelling, which we call discrete modelling.

2.3. Discrete modelling

The interest in discrete dynamical systems goes back to the work of Ulam [122] and von Neumann [130]. The field of discrete models, often called cellular automata, was usually considered as a part of statistical physics, and had almost no overlap with porous media flow modelling. In the 1970s, a new branch of discrete dynamical systems science emerged, which became known as percolation theory. The most important early contributions can be traced back to Kirkpatrick [63] and Stauffer [113].

It was soon recognized that percolation theory can be used to model immiscible fluid flow in porous media. The theory was used to predict the fractal

structure of the percolating clusters of fluids, capture the critical behavior of pressure and hydraulic conductivity dependence on saturation near the percolation threshold, and point out the universality of the various scaling relations [136]. Lenormand et al. conducted an extensive research in this direction, both experimental and theoretical, which clarified the mechanisms by which individual pores are filled and drained by wetting and non-wetting fluids [74, 73, 72, 71], see also [7] for important contributions to the understanding of collective pore filling mechanisms. Based on these seminal papers, there has been an explosion of theoretical and experimental results which used percolation theory to capture the flow of immiscible fluids in two or there dimensional porous media at the pore level, under various combinations of viscous and capillary forces and the force of gravity. The porous medium is usually modeled as two or three dimensional regular or random network of pores and/or throats, of various types of cross-sectional shapes and various types of connectivity. Usually two (sometimes three) immiscible fluids are allowed to move inside this network. Pores and throats are usually filled with one fluid, or the other, intermediate levels of saturation inside a single pore are seldom considered. These models are typically called Invasion Percolation (IP) models or, if they also include an external force field, Modified Invasion Percolation (MIP). Meheust et al. [80] reports an extensive experimental study of water-air interface patterns in synthetic two-dimensional porous media under the combined effect of viscous and capillary forces and the force of gravity. Various IP and MIP models devised for modelling the patterns can be found in [1], [6], [38], [78], [79], [124], [125].

The binary nature majority of these models (a pore is either empty or full) suggests that it is not possible to model the saturation of the porous matrix as a continuous variable. Accordingly, there have been almost no attempts to capture saturation overshoot directly by these models. However, the non-monotonicity of flow can be captured by allowing the pores to fill with the fluid and then desaturate (empty) again. Birovljev et al. [6] studied the migration of a gas cluster in water filled two dimensional random porous media and used MIP model to capture repeated withdrawal and invasion of water at the pore level. The proposed MIP model was shown to match the experimental results well. The purpose of their model did not include saturation overshoot modelling, they were trying to capture fragmentation and migration of air clusters, not water clusters. However, the MIP model had to allow for both invasion and withdrawal, which is something other MIP models rarely dealt with.

Further attempt was made by DiCarlo [25] who used a state-of-the-art dis-

crete model of Valvante and Blunt [124], [125] to model the advancing water front at the pore level. Saturation was recovered from the discrete model by averaging over space. The model included viscous and capillary forces but the force of gravity was not included, as it was argued that it can be neglected at the pore-scale. This comes to us as a surprise because it suggests that saturation overshoot should be observable for horizontal imbibition, which we find no experimental evidence of. The author himself compares the predictions of the model to experiments performed on *vertical* sand columns. We argue that gravity cannot be disregarded because it influences the distribution of pressure throughout an entire cluster (connected region of water filled pores) which is macroscopic, so pore-scale arguments are not valid. Nevertheless, the model exhibits some qualitative agreement with vertical infiltration experiments, including the dependence of the overshoot on the influx magnitude.

To sum up, various IP and MIP (discrete) models have been used to capture UHPM flow. Few of them aimed at saturation overshoot modelling. Although some features of the UHMP flow may be captured very well by the IP and MIP models, discrete models have several disadvantages:

- The models usually treat saturation as a binary quantity. To obtain continuous values of saturation, some kind of time and/or space averaging must be performed.

- In any of these models, one needs to define the shapes of the pores and/or throats and their connectivity. This is often done in an arbitrary way (using circular or rectangular pores, and using regular or random network of pores). It then becomes difficult to link the properties of the artificial pore network to a real porous matrix (see the discussion in [89]). Consequently, one can never be sure whether the predictions of the models are due to correct underlying physics of the model, or whether they are artifacts of the arbitrary geometry of the model.

- Most of the models do not capture time in a physically meaningful way. The local percolation rules are executed one at a time, in an order which usually reflects the energetic accessibility of the states. Consequently, the order of the pore-filling (or draining) events is physically correct, however, the exact times of the filling and draining events may be artificial.

2.4. Semi-continuum modelling

It is natural to try to combine the advantages of both the continuum-based and discrete approaches. Let us call these models *semi-continuum models* borrowing the term from [30]. To our knowledge, there have been only two attempts in this direction.

DiCarlo et al. [30] performed extensive experimental study of overshoot phenomena in quasi-one-dimensional vertical sand columns. They define the so-called overshoot flux – a critical flux below which no overshoot is observed. When the overshoot flux is plotted against the grain size on a log-log scale, it exhibits a power-law behavior and suggests a critical grain size for which no overshoot should be observed. It is also found that overshoot flux scales with the mean grain size D as D^{-3}. Moreover, a linear relationship is found between the overshoot flux and the ratio of surface tension to viscosity. DiCarlo proposes a clever heuristic way to explain these two observations. Continuum theory is used to capture the motion of the water front. Then a thin film equation is proposed to capture the movement of the films ahead of the water front. The film equation is considered at the level of a single grain/pore. Combining these two approaches, DiCarlo is able to produce a formula that matches the overshoot flux dependence on surface tension, viscosity and grain size. Thus, this semi-continuum model is not used to capture the UHPM flow, it is only used to explain certain experimentally observed scaling relations.

Another semi-continuum model was reported by Glass et al. in [52] following a series of papers [50], [51], [44], [43]. Let us note that the authors themselves call the approach "mechanistic modelling", or Macro Modified Invasion Percolation (MMIP), they never use the term "semi-continuum model". In their MMIP model, the porous medium is represented as a regular grid of rectangular sites (called blocks) in two or three dimensions, with certain specified type of connectivity. Each block is a small part of the original porous medium (hence our "semi-continuum" label) completely described by two numbers:

- P_w is the pressure needed for the invading phase to fully percolate the block (that means to form a connected network of filled pores throughout the block so that the block becomes conductive for that phase).

- P_d is the pressure needed for the defending (retreating) phase to reinvade the block.

The pressure can be related to a radius of curvature by means of the formula

$$P_i = -\frac{2\sigma \cos\phi}{R_i}, \tag{2.3}$$

where i stands either for w or d, σ is the surface tension between the phases and ϕ is the contact angle. Thus, each block can be assigned a critical wetting radius R_w and a critical draining radius R_d.

The MMIP conceptualization has the great advantage (over IP and MIP models) of not having to worry about the particular geometry of the pores and throats. It is important to note that the radii R_i in Equation (2.3) do not represent any dimension of any actual (real) pore in the block – they represent the capillary pressures given in units of capillary radii. Each block is either full (percolated by the invading fluid) or empty (not percolated). The model is binary in nature as almost all IP and MIP models, it does not capture saturation as a continuous variable. The percolation rules for invasion and withdrawal are based on local pressure considerations and global gradient of the force of gravity (although the authors are not particularly clear in this matter). The process of facilitation (preferential filling of pores which are surrounded by already full pores) is included if the invading phase is wetting.

The model is used to capture the following three situations:

- The formation of a single macroscopic gravity-driven finger for water infiltration from a point source into initially dry UHPM.

- Buoyancy-driven migration of CO_2 injected at constant rate at the bottom of heterogeneous sand column, initially fully water saturated.

- The formation of a single gravity-driven water finger for infiltration from a point source located at the top of a dry, vertical rough-walled fracture formed by two textured glass plates.

The agreement of this MMIP model with experiments in all the three cases is astonishing. For the gravity driven UHPM fingering, saturation overshoot is not only reproduced qualitatively but also the finger width and the size of the overshoot zone are captured well. Two discrepancies are reported by Glass et al:

- Behind the saturated finger tip, the wetting phase becomes fully fragmented with a narrow backbone that quasi-periodically connects the source to the advancing finger-tip. This is not observed in experiments and the authors attribute this discrepancy to the failure of the model to account for film flow.

28

- Multiple pathways (finger divergence) are never produced by the model, although they are observed in experiments. This is due to the deterministic nature of the algorithm – the filling and vacating pressures for the blocks are almost always distinguishable.

In our opinion, the MMIP model by Glass et al. is the most successful approach presented so far to capture the overshoot phenomenon. The model is reasonably simple, it does not introduce any free parameters (not related to measurable properties of the porous medium) and it is able to capture three very different flow regimes by means of a unified approach. To the best of our knowledge, no attempts were made to capture the effects of initial saturation or influx magnitude by the MMIP model. Due to the discrete nature of saturation in the MMIP model, it may not be possible at all.

2.5. Benchmarking

There exist many different models for modelling multiphase flow of porous media. Therefore there has been interest how to compare and evaluate such models. DiCarlo in [29] proposed rules of evaluation which model is "the most appropriate" for modelling UHPM. The model should satisfy the following benchmarks [29]:

1. *Have a minimum of adjustable parameters, and parameters should have a defined and natural scaling as a function of grain size, fluid pairs, and initial conditions.*

2. *Reduce to the Richards' equation in nonovershoot and static profiles.*

3. *Produce a good match of the observed one dimensional profiles, e.g. the magnitude of the saturation and pressure overshoot, the dependence on boundary influx, the dependence on initial saturation, the finger velocity and the finger build up.*

4. *Can produce predictions of the two and three dimensional preferential flow in terms of finger widths, finger velocities and finger spacing.*

The main advantage of evaluating the models in terms of one dimensional flow is reducing three-dimensional nonlinear partial differential equation into a one-dimensional nonlinear partial differential equation. It is then possible to

compare quickly 1D experiments with simulations as a function of different parameters such as initial saturation dependence or boundary flux dependence. In the next step, more complex evaluation of model can be provided by comparing 2D experiments of unstable flow in terms of finger characteristics. Many models succeed in one or more items mentioned above. However, none seems to be able to capture all at once. Especially none can fully satisfy the predictions of the two dimensional preferential flow. For this reason, a different approach of modelling UHPM will be presented in this thesis.

Chapter 3

1D semi-continuum model

In this chapter, we present a semi-continuum model for fluid flow in unsaturated porous medium in one spatial dimension. This model reproduces qualitatively and quantitatively all of the features of saturation overshoot behavior reported by DiCarlo [27] (see the summary in Section 2.1).

In Section 3.1, the physics of the model will be presented and the resulting model will be fully described. Then, the ability of the model to reproduce experimental observations will be demonstrated in Section 3.2 followed by Section 3.3, where the limit of the semi-continuum model will be explained. Finally, this chapter will be closed with the discussion in Section 3.4. Sections 3.1, 3.2 (except Section 3.2.5) and 3.4 are taken from Kmec et al. [65], and are slightly extended here. Parts from Section 3.4 are also published in [66]. Some parts from Section 3.3 are also published in [65, 66].

3.1. Model derivation

The model is based only on well-established physics, measurable parameters and material characteristics. The porous material is characterized by porosity, intrinsic permeability, the main wetting and draining branches of the retention curve, and the saturation dependence on the relative permeability. The fluid is characterized by its density and dynamic viscosity. The only physics involved is the mass balance of fluid together with the Darcy-Buckingham law for fluid flow in unsaturated porous media.

Let us suppose a long narrow vertical tube filled with homogeneous porous medium, e.g. 20/30 sand as in the experiments of DiCarlo [27]. The tube has a cross-section of A [m^2], the height of the tube is L [m]. Lets subdivide the tube into small blocks of height dx and cross sectional area A. These blocks

represent "pieces" of the original porous medium and they are not to be considered infinitesimal. For a given time, the key physical quantities (see below) are considered constant within a single block. This is a direct reference to the semi-continuum approach of Glass and Yarrington [52]. The tube now consists of slices $[ndx, (n+1)dx]$ with $n = 0, 1, \ldots N$. The key quantities that we want to track are

- Saturation S_i [-] in each block. Saturation is assumed to be uniform throughout each block but continuously varying in time.

- Capillary pressure P_i [Pa] in each block i.e. the average pressure difference across the menisci (wetting fluid–gas interfaces) in the block. For simplicity, air pressure is set to zero everywhere. Pressure is assumed to be uniform throughout each block but continuously varying in time.

- Fluxes $q_{i,j}$ [m/s] between the blocks i and j. Real fluxes in [m³/s] can be recovered as $Aq_{i,j}$. Naturally, only fluxes between neighbouring blocks are non-zero in this setting. Fluxes are assumed to be continuous in time.

Gravity is directed downward along the long axis of the tube, which is called the $x-$axis here. A constant (in time) influx q_B [m/s] at the top boundary $(x = 0)$ is assumed. Zero discharge (i.e. zero flux) at the bottom boundary $(x = L)$ is assumed.

3.1.1. Saturation update

Naturally, a mass balance has to hold. Here, we use the form

$$\theta \partial_t S(t, x) + \partial_x q(t, x) = 0,$$

where θ [-] stands for the porosity of the material. This can be understood in the semi-continuum setting as a simple explicit discrete scheme

$$\frac{\theta}{dt} \left[S_i(t) - S_i(t - dt) \right] = \frac{1}{dx} \left[q_{i-1,i}(t - dt) - q_{i,i+1}(t - dt) \right], \qquad (3.1)$$

where dx and dt are discretization parameters. The specific form of the fluxes $q_{i,j}$ are given by (3.6). Thus, knowing the fluxes at time $t - dt$, one can update the saturation in each block in this straightforward way at time t.

3.1.2. Pressure update

Next, the pressure in each block has to be updated, because the fluxes are governed by pressure gradients. Hysteresis of the retention curve has to be addressed in this step because it is known [103] that, in the case of fingering, the (over-saturated) finger tip is in the imbibition mode while the under-saturated finger tail is in the draining mode. Consequently, no reasonable model of the saturation overshoot can ignore hysteresis. Let us use the following very simple approach. Suppose that the material has a well-defined main wetting branch of the retention curve denoted by

$$P_i(t) = F_W(S_i(t)). \tag{3.2}$$

This means that if a block starts at zero saturation and becomes more and more wet, the capillary pressure in the block will be dependent on its saturation through Equation (3.2). Analogously, there is the main draining branch of the retention curve

$$P_i(t) = F_D(S_i(t)). \tag{3.3}$$

For any block that starts at unit saturation and becomes less and less wet, the capillary pressure will be given by (3.3). A typical retention curve of a 20/30 sand is shown in Figure 3.1. The wetting and draining branch are both modeled by the logistic functions with small corrections at the $S = 0$ and $S = 1$ ends.
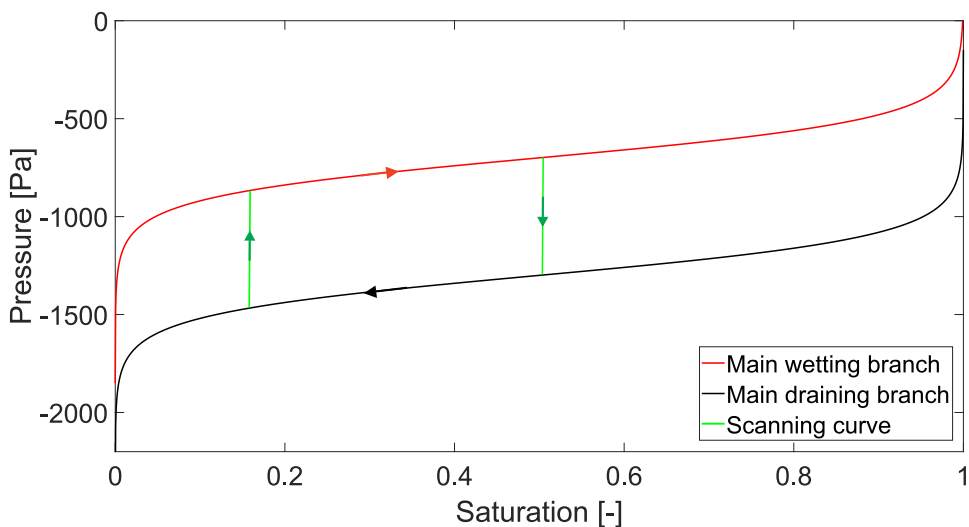

Figure 3.1: The retention curve used for one dimensional simulations. The curve roughly matches 20/30 sand used in the article of DiCarlo [27].

If a block first undergoes imbibition but then switches to draining, it moves in the saturation-pressure diagram (Figure 3.1) between the two main branches. In experiments, significant changes in pressure are observed with almost no change in saturation [27]. There are many approaches to hysteresis modelling [85, 70, 96]. Here, we adopt the simplest modelling approach and describe this process by a relation

$$\frac{dP}{dS} = K_{PS} \tag{3.4}$$

with some large constant K_{PS}. It means that between the main branches, saturation changes with pressure very rapidly, following a line with a very large slope K_{PS} (such scanning curve is plotted in Figure 3.1). One may think of the saturation jumping from the wetting to the draining branch discontinuously (i.e. vertically) but this would cause unnecessary numerical issues in the model; hence this approximation. We believe there is a simple explanation for this rapid behavior: capillary pressure originates as an average of the pressure drops across the fluid–gas menisci. As a block switches between imbibition and draining, the shape of the menisci changes (they become more pronounced with smaller radii), which causes almost no measurable change in volume, but a dramatic increase in the pressure drop across the menisci. Relation (3.4) holds anywhere between the main wetting and the main draining branches. Once a block in the draining mode reaches the main draining branch, it sticks to it and continues along it. Analogously, once a block in the imbibition mode reaches the main wetting branch, it sticks to it. In this way, we update the pressures in all the blocks using the current (already updated) levels of the saturation.

3.1.3. Flux update

At last, we have to update the fluxes. This is where we slightly depart from the usual Richards' equation formulation (1.19). It is understood that the advancing of the finger tip is where the classical theory fails. The overshoot can be understood as fluid piling up behind the fingertip because the dry medium ahead of the fingertip has insufficient hydraulic conductance; thus the flux across the fingertip cannot keep up with the flux in the tail of the finger. Therefore, fluid piles up behind the fingertip which increases the hydraulic gradient across the finger tip until the large gradient "matches" the low conductivity and the flux across the fingertip equals the flux in the tail. Then, a stable finger with an oversaturated tip proceeds with a constant velocity downwards.

The original Darcy-Buckingham law for unsaturated porous media flow [5]

states:

$$q = \frac{\kappa}{\mu} k(S) \left(\rho g - \nabla P \right),$$

where κ [m^2] is the intrinsic permeability of the medium, μ [Pas] is the dynamic viscosity of the fluid, ρg is the gradient of the gravitational potential, and P [Pa] is the capillary pressure. Here $k(S)$ [-] stands for the relative permeability which is very sensitive to S and is usually modeled by a power law relation

$$k(S) = S^m \tag{3.5}$$

with m usually around 3 or 4 (some sources report m as high as 10 [21] but since saturation may vary over three orders of magnitude, this would result in relative permeability varying over 30 orders of magnitude, which may not be reasonable).

In view of the two preceding paragraphs, it is crucial how we model the conductance at the finger tip, where ∇P is large, and S changes abruptly from small values in front of the fingertip to large values inside the fingertip. We propose the following discrete implementation of the Darcy-Buckingham law:

$$q_{i,j}(t) = \begin{cases} \frac{\kappa}{\mu} \sqrt{k(S_i(t)) k(S_j(t))} \left(\rho g - \frac{P_j(t) - P_i(t)}{dx} \right) & \text{for } j = i + 1 \\ 0 & \text{otherwise} \end{cases} \tag{3.6}$$

Thus, for the relative permeability at the finger tip edge, we simply take the *geometric* mean of the permeability of the respective blocks. The geometric mean $\sqrt{ab}$ has the desirable property of being small if one of the numbers a and b is small. It is also possible to use the *harmonic* mean with similar results. The more common (arithmetic) mean does not behave in this way. Further justification for using this type of averaging comes from [61], where the authors show that the geometric mean is appropriate by means of numerical experiments in random pore networks. Detailed explanation is left to Discussion section. Notice that if the saturation vanishes in a block, the flux to/from the neighbouring blocks becomes zero. Therefore, the initial saturation in all blocks has to be set to a nonzero value.

Notice that in the limit $dt \to 0$, $dx \to 0$, the numerical scheme (with geometric or arithmetic mean) converges back to the RE which is known [40] to be incapable of producing any overshoot. Thus, the issue of the limit of this semi-continuum model is an important one and it is left to Section 3.3.

3.1.4. Model description

The resulting model in one dimension works as follows:

1. The size of the blocks dx is chosen and an appropriate time step dt is set. Initial saturation S_{in} is prescribed in each block (the same in all the blocks), the corresponding capillary pressure is computed (depending on whether we start on the wetting or draining branch), and all fluxes are initially set to zero.

2. The top boundary condition is set: the flux into the topmost block is set and fixed to q_B. The bottom boundary condition is set: the flux out of the bottom block is set and fixed to zero.

3. Using the current value of the fluxes $q_{i,j}$, saturation S_i in each block is updated according to Equation (3.1).

4. Pressure P_i in each block is updated according to Equations (3.2), (3.3), or (3.4), keeping track whether the block is in the imbibition or draining mode.

5. Fluxes $q_{i,j}$ between neighbouring blocks are updated according to (3.6), keeping the boundary fluxes fixed by step 2.

6. Time is updated to $t + dt$ and the process goes back to step 3.

3.2. Results

In this section, we reproduce the experimental results of DiCarlo [27]. The experiments were performed with water infiltrating a narrow tube filled with 20/30 sand. The diameter of the test tube was chosen by DiCarlo so that the saturation in the column was uniform transverse to the flow direction at all times. There was no observable preferential flow in the columns, as the diameter was less than the finger diameter. The tight packing of the sand ensured there were no observable effects of preferential flow along the tube walls. A tube with the inner diameter of 1.27 cm was used. Saturation and capillary pressure overshoot behavior is reproduced, both qualitatively and quantitatively. The dependence of the saturation overshoot on influx and initial saturation is reproduced, too.

To keep close to the experimental setting (see the Materials and Methods section in the article of DiCarlo [27]), the following parameters are used for the simulation:

- porosity of the material $\theta = 0.35$ [-],

- intrinsic permeability of the material $\kappa = 1 \times 10^{-10}$ m^2,

- dynamic viscosity of water $\mu = 9 \times 10^{-4}$ Pas,

- density of water $\rho = 1000$ kg/m^3,

- acceleration due to gravity $g = 9.81$ m/s^2,

- cross sectional area of the tube $A = 10^{-4}$ m^2 (this will not be needed in the model because it is one dimensional),

- length of the tube $L = 40$ cm (the tube will be divided into 40 blocks of height 1 cm).

The choice of dx is inspired by Glass and Yarrington [52] and reflects the requirement for the blocks to be large enough to retain the characteristics of the original porous medium. At the beginning, all blocks are assumed to be in imbibition mode. The saturation dependence of the relative permeability is modeled by relation $k(S) = S^3$. The retention curve in Figure 3.1 is used with $K_{PS} = 10^5$ Pa.

3.2.1. Saturation overshoot in initially dry medium and its dependence on the influx

First, we want to demonstrate the ability of the semi-continuum model to capture saturation overshoot in infiltration into initially dry homogeneous porous medium, and the dependence of the overshoot on the influx. The dependence of the oversaturation profile on the influx is rather complicated: for a very small influx, there is no visible saturation overshoot. With increasing influx, a distinct overshoot pattern appears. The magnitude of the overshoot and the length of the oversaturated zone increases with increasing influx. If the influx is too large, the fingertip becomes almost completely saturated and the length of the oversaturated zone grows all the way to the upper boundary of the sample. Thus, the overshoot disappears for fluxes which are too large. This rather complicated dependence is well replicated by the semi-continuum model, see the comparison of the experimental data by DiCarlo [27] in the left panel of Figure 3.2 and our numerical simulation in the right panel of the figure. For a technical reasons, we cannot prescribe initial saturation to be zero (this would yield zero hydraulic conductivity) so we chose $S_{in} = 0.003$ everywhere. Since we report the results in SI units and assume the cross-sectional area of the tube to be $A = 1$ cm^2, the conversion factor for the influx between the experiment and the simulation is roughly $60 \times 100 \times 1.27^2 \cong 10000$. Thus, the experimental influx that was small enough not to cause saturation overshoot ($q_B = 8 \times 10^{-4}$ cm/min) corresponds roughly

to $q_B = 2 \times 10^{-8}$ m/s in our simulation. Further, the experimental flux which causes complete flooding of the material ($q_B = 11.8$ cm/min) with no overshoot roughly matches the same situation in our simulation ($q_B = 10^{-3}$ m/s). It can be observed that the model is able to reproduce both the dependencies, magnitude of the overshoot and the length of the oversaturated zone. The quantitative match of the experimental data is not perfect, however, we were not attempting at that. The retention curve we are using is rather arbitrary and matches the 20/30 sand only roughly, we were not trying to fit it to obtain the best fit to experimental data.
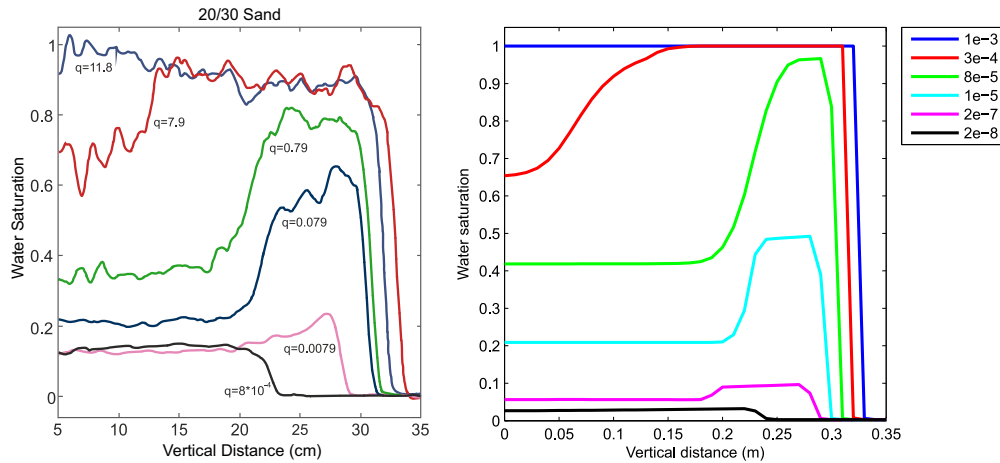
Figure 3.2: Comparison of the saturation profiles for various influx rates. Left panel: Experimental data, infiltration into a narrow tube of initially dry 20/30 sand, reprinted from the article of DiCarlo [27] (Fig. 2), fluxes are reported in cm/min into a test tube of inner diameter of 1.27 cm. Right panel: One dimensional simulation of the same situation by the semi-continuum model, initial saturation $S_{in} = 0.003$, fluxes are reported in m/s into a system of cross-sectional area of 1 cm^2.

Let us also note that the presented model is in no way "tuned" to capture saturation overshoot. When diffusion-like monotonic behavior is expected, the model captures it well, too (see Figures 3.3 for a smooth transition from overshoot to no-overshoot behavior).
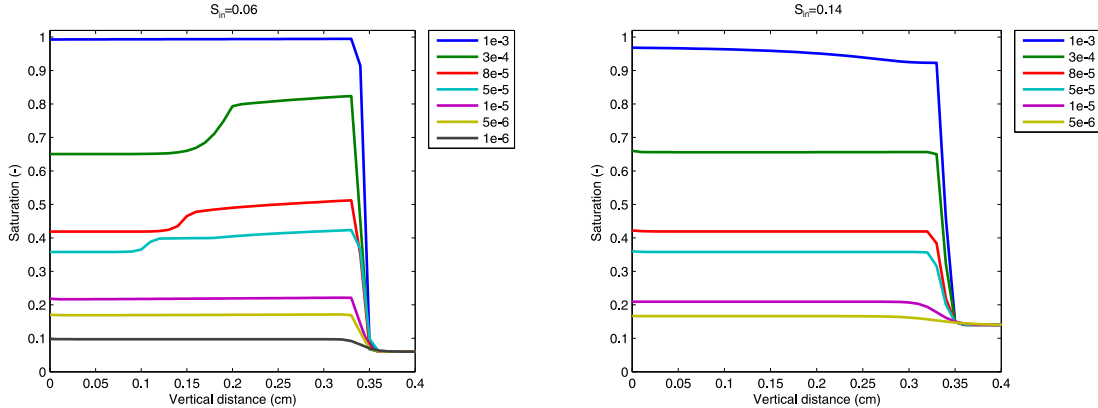
Figure 3.3: Smooth transition from overshoot behavior for large fluxes to no-overshoot behavior for small fluxes. Various influx magnitudes [m/s] color coded. Left panel: Initial saturation $S_{in} = 0.06$. Right panel: Initial saturation $S_{in} = 0.14$. No visible saturation overshoot is present for this initial saturation. However, the model shows a small but distinct pressure overshoot (see the Capillary pressure overshoot section).

3.2.2. The effect of initial saturation

Let us now investigate the effect of initial saturation on the saturation overshoot. It is known [3] that with increasing initial saturation, the overshoot is less and less pronounced and finally disappears completely, and diffusion-like behavior prevails. This seems to be captured well by the semi-continuum model, see Figure 3.4. In the experiments reported by DiCarlo [27], the overshoot disappears completely for $S_{in} = 0.14$, for influx comparable to our simulation. This is in a quantitative agreement with our simulation (see Figure 3.4). Let us further observe that in the simulation, the tail saturation remains independent of the initial saturation S_{in}. This is in agreement with the experimental results of Fritz [39] (see Figure 6.3 in this article).

Further, we want to reproduce the dependence of the magnitude of the overshoot on the initial saturation. Figure 3.5 shows that the model is in qualitative agreement with the experimental data. The experimental data are considerably noisy, so we do not comment on quantitative agreement.

Bauters et al. [3] report a hyperbolic relationship between the initial saturation and the overshoot magnitude. The overshoot magnitude is measured as the difference between the tip saturation and the tail saturation. This observation is very well reproduced by the semi-continuum model, see Figure 3.6.
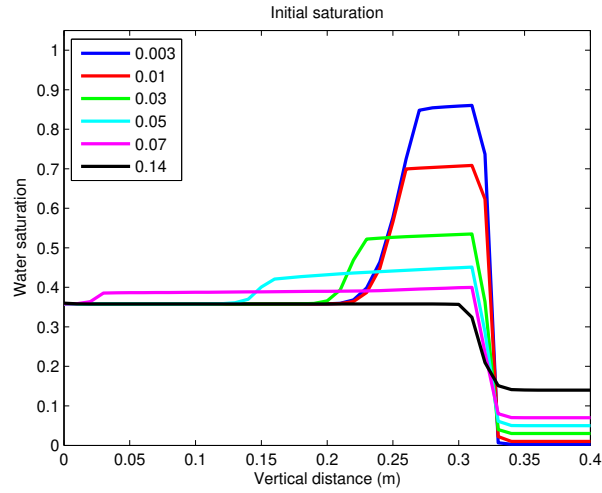
Figure 3.4: Comparison of saturation profiles for various values of initial saturation. Simulation with a constant influx of $q_B = 5 \times 10^{-5}$ m/s.
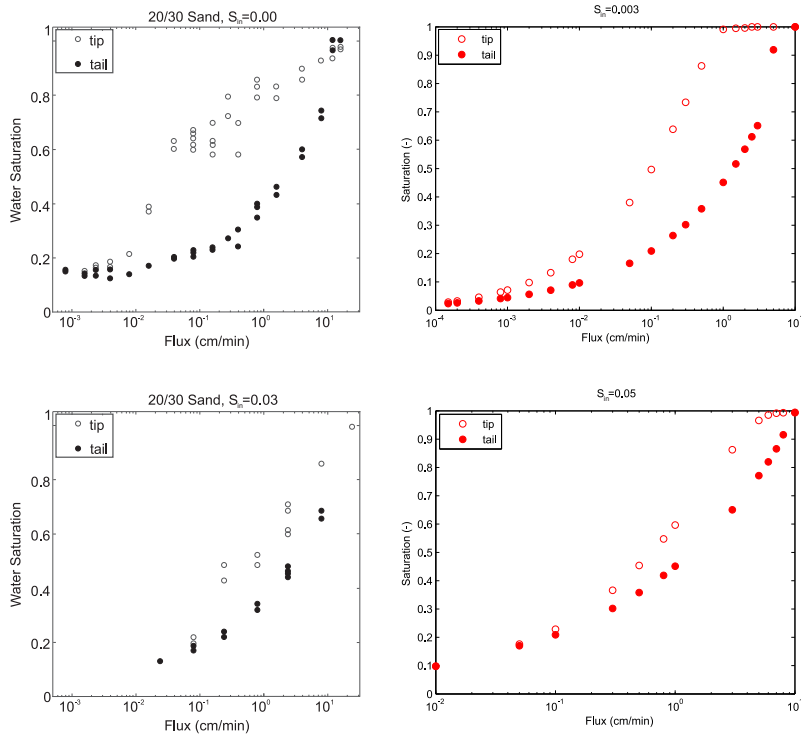

Figure 3.5: Saturation overshoot magnitude. Tip and tail saturations are shown as a function of the influx magnitude for various values of initial saturation. Left panels: Experimental data, infiltration into a narrow tube of initially dry 20/30 sand, reprinted from [27] (Fig. 3 and 4). Right panel: Simulation data.
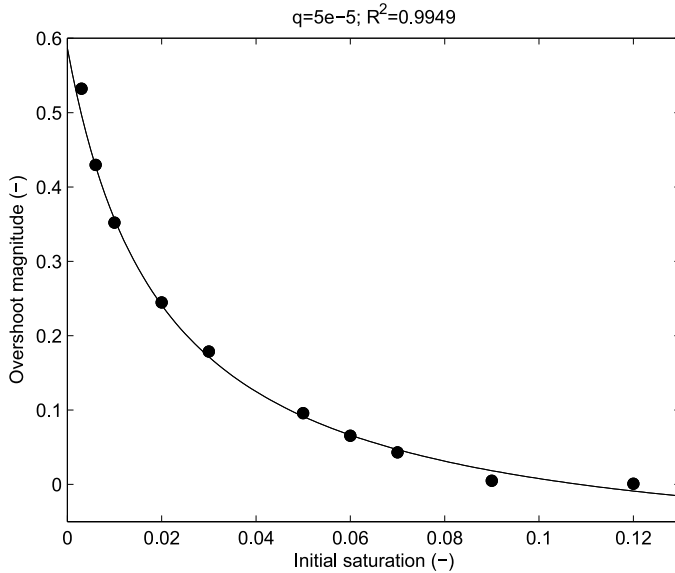
Figure 3.6: Dependence of the overshoot magnitude on initial saturation. A hyperbolic relation fitted to the simulated data.

3.2.3. Capillary pressure overshoot

The capillary pressure overshoot is in agreement with saturation overshoot. If we observe the evolution of capillary pressure at a single point along the tube, and offset the time scale so that $t = 0$ corresponds to the arrival of the finger tip through this point, we obtain behavior depicted in Figure 3.7.

Let us fix a point 12.5 cm from the upper boundary, i.e. a point in the 13th block from the top. Let us offset the time so that $t = 0$ corresponds to the arrival of the fingertip at this point. We now track the evolution of the capillary pressure at this point. The time series of capillary pressure at this point exhibits visible oscillations after the finger tip passes. This is caused by a numerical error: in performing the limit for $dx \to 0$, these oscillations disappear (see Section 3.3). The solid line in Figure 3.7 shows a 20 second moving average of the capillary pressure.

Next, we want to address the dependence of the lowest capillary pressure (i.e. the pressure at the finger tip, at the wettest point) on initial saturation of the medium and on the influx. Figure 3.8 shows capillary pressure at the fingertip for various fluxes and four levels of initial water saturation. DiCarlo [27] observes two basic trends: the capillary pressure at the fingertip increases with decreasing flux and it increases with increasing initial water saturation. Both these trends are reproduced well by the semi-continuum model.
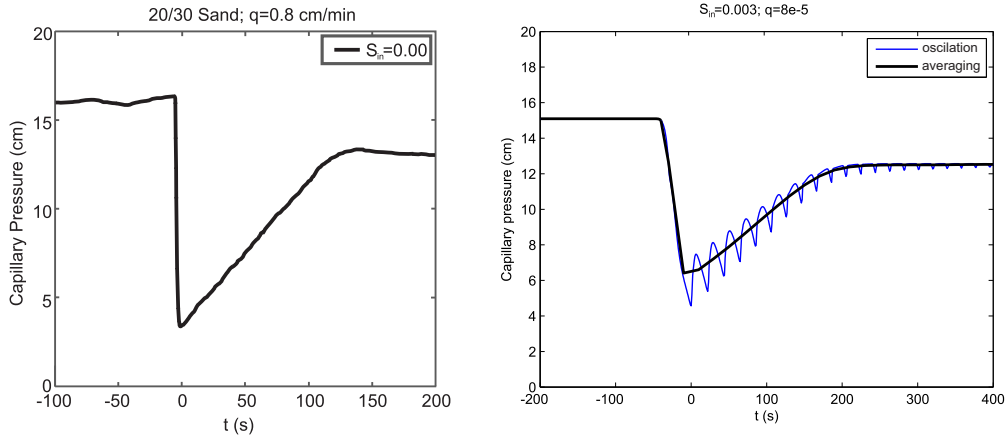
41

Figure 3.7: Evolution of the capillary pressure at a single point in the 13th block from the top. Capillary pressure given as pressure head in cm of water column. The time is offset so that $t = 0$ corresponds to the arrival of the finger tip. Left panel: Experimental data reprinted from the article of DiCarlo [27] (Fig. 5). Influx of $q_B = 0.8$ cm/ min into initially dry 20/30 sand. Right panel: Simulation by the semi-continuum model. The corresponding influx of $q_B = 8 \times 10^{-5}$ m/s into initially dry ($S_{in} = 0.003$) medium. The thin line shows the evolution of the capillary pressure at the point, the thick line shows the moving average over 20 seconds.
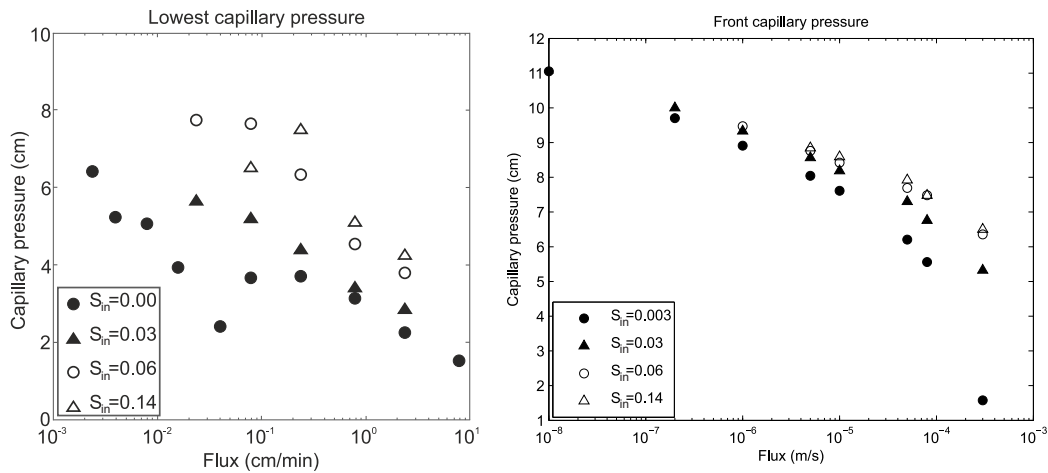

Figure 3.8: Dependence of the lowest capillary pressure (i.e. the pressure at the finger tip) on initial saturation and influx magnitude. Capillary pressure given as pressure head in cm of water column. Left panel: Experimental data reprinted from [27] (Fig. 7). Right panel: Simulation by the semi-continuum model. The fluxes in the simulation are chosen to approximately match the experimental fluxes.

42

Although the pressure overshoot is consistent with the saturation overshoot, a more careful look reveals the following observation: DiCarlo [27] reports that "When a larger initial water saturation of 0.06 was used, the saturation profiles are found to be monotonic at all fluxes, with no saturation overshoot". However, a careful look at Fig. 8 of the original article [27] (not reprinted here) shows that there is, in fact, a small capillary pressure overshoot for initial saturation 0.06 for fluxes higher than 10^{-1} cm/min. Even for initial saturation of 0.14 where no saturation overshoot was observed, the pressure overshoot is still clearly visible for high enough fluxes. This subtle behavior is well reproduced by our semi-continuum model (see Figure 3.9).
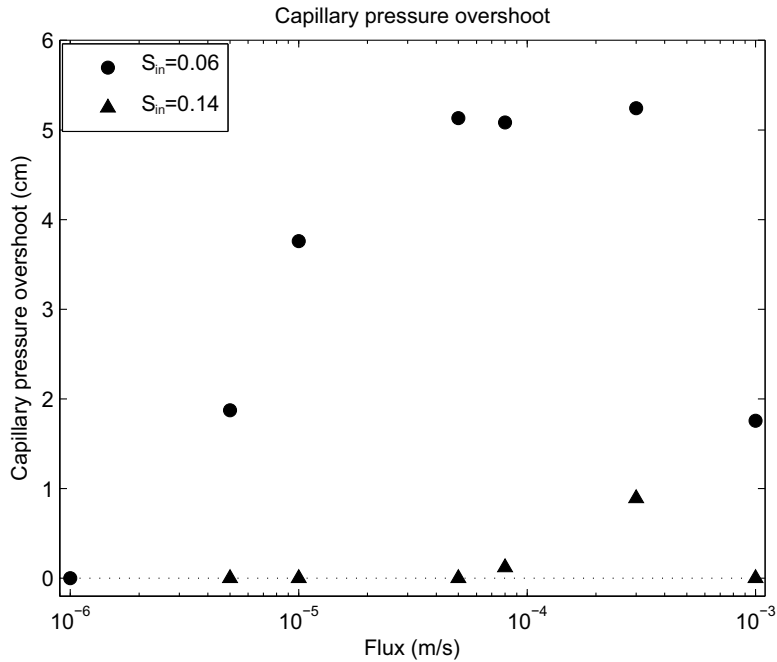

Figure 3.9: Capillary pressure overshoot as a function of the initial saturation and influx magnitude. The pressure overshoot is measured by the difference of the pressure in the finger tip and the pressure in the tail. Capillary pressure given as pressure head in cm of water column.

The model reveals that, indeed, there is saturation overshoot accompanying *any* pressure overshoot but the saturation overshoot magnitude may be negligible (on the order of 10^{-3}) and thus it cannot be observed in experiments. This explains the seemingly self-contradictory observation of DiCarlo.

3.2.4. Finger build up

To understand the formation of the finger, it is convenient to plot the profile of the finger at various time points. Figure 3.10 shows the profile at several successive time points. The finger build up is a gradual process, both in space and in time. It takes several minutes before the saturation profile reaches its final (steady) shape. That is compatible with the experiments reported in the article of Fritz [39], although the author expected, in contrast to his own experimental results, that the finger develops immediately at the inflow boundary and then flattens over time and depth.
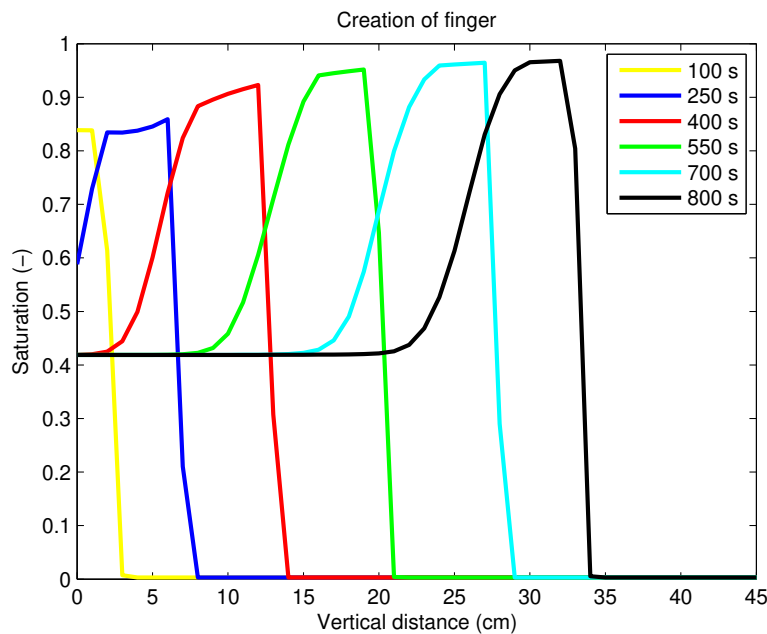

Figure 3.10: The process of finger build up. The profile of the finger at several successive time points.

Two more trends can be observed in the experiments reported in the article of Fritz [39] (Fig. 6.7): (1) the velocity of the finger tip gradually increases before reaching a steady state at a certain depth, (2) the length of the oversaturated zone of the finger increases with time (and thus also with the depth). Both these trends are correctly captured by the semi-continuum model (see Figure 3.11).
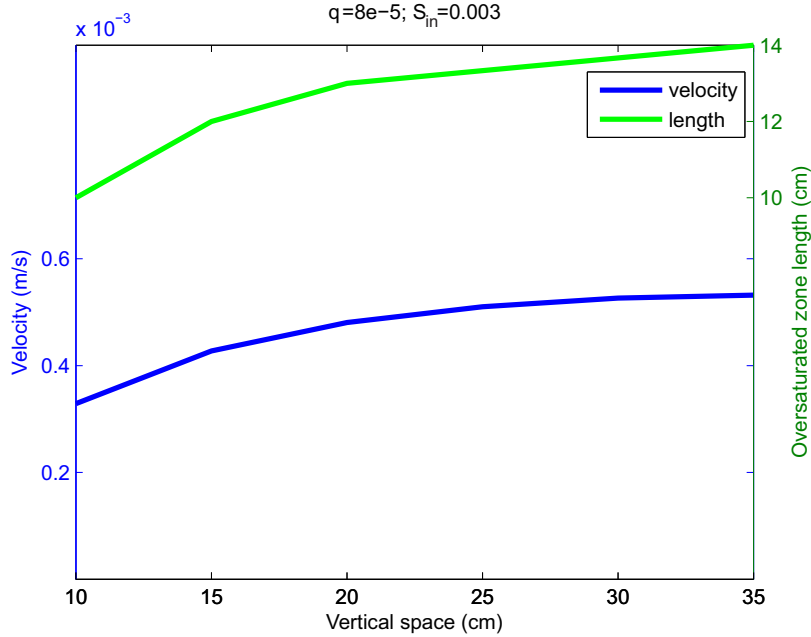
Figure 3.11: Evolution of the finger velocity and the length of the oversaturated zone. Compare with Fig. 6.7 in the article of Fritz [39].

3.2.5. The effect of parameters

Let us now investigate the effect of parameters on the final shape of the finger. It is obvious that each parameter of the simulation forms the finger. However, here we want to demonstrate that each part of the finger is mainly effected by some physical properties of the porous medium. Figure 3.12 (left) shows a representation of the effect for different parts of the finger. A finger is depicted at time 800 s for boundary flux $q_b = 5 \times 10^{-5}$ m/s and initial saturation $S_{in} = 0.01$. Let us subdivide the finger into four segments: finger tail, back part, middle part and front part of the overshoot. In Figure 3.12 (right) saturation and it's corresponding pressure is plotted. It can be seen that the finger tail and the back part of the overshoot is on the draining branch, while the middle part of the overshoot is on the scanning curve and the front part of the overshoot is on the main wetting branch. This corresponds with experimental observations [103]. Each segment of the finger will be commented separately:

- Finger tail: saturation in the finger tail is effected only by intrinsic and relative permeability, dynamic viscosity, density, gravity and boundary flux. It is well known, that saturation in the finger tail is constant. That means that the flux in the finger tail has to be also constant (equal to boundary

flux q_b), and so is. If it was not a true, the saturation would change. A flux balance is then given by Darcy-Buckingham law:

$$\frac{\kappa}{\mu}k(S_{tail})\rho g = q_b,$$

where S_{tail} denotes the saturation in the finger tail. By assuming $k(S) = S^3$, we can write:

$$S_{tail} = \left(\frac{\mu}{\kappa\rho g}q_b\right)^{\frac{1}{3}}.$$

This is exactly the reason why saturation in the finger tail is independent on initial saturation (see Figure 3.4).

- Back part: the back of the overshoot is on drainage mode and thus the biggest impact on forming this part has the main draining branch.

- Middle part: the middle part of the overshoot is mostly effected by the scanning curve. See Figure 3.13 (left), where different exponents K_{PS} of the scanning curve are used. We observed that smaller exponent results in longer middle part of the overshoot with higher inclination. This is caused, because the length of the scanning curve is larger for smaller exponents and thus the block remains on the scanning curve for larger time. For K_{PS} large enough, the distance between branches does not change and thus the effect is negligible. To further demonstrate this behavior, we can simply increase the distance between the main branches of the retention curve. Figure 3.13 (right) shows fingers for three different draining branches. The basic retention curve (given by Figure 3.1) is used for the red finger. Other two fingers are calculated with modified draining branches, such that we add 300 Pa to the main draining branch for the blue finger and we subtract 300 Pa to the main draining branch for the green finger. Basically it means, that the distance between the main branches is smaller for blue finger and larger for green finger. Consequently the middle part of the overshoot changes the length regarding to the distance between the main branches.

- Front part: we observed similar behavior as for the back part of the overshoot. Since the front part is in the imbibition mode, the finger tip is formed especially by the main wetting branch. Moreover, a geometric mean of the permeability between blocks plays a crucial role.
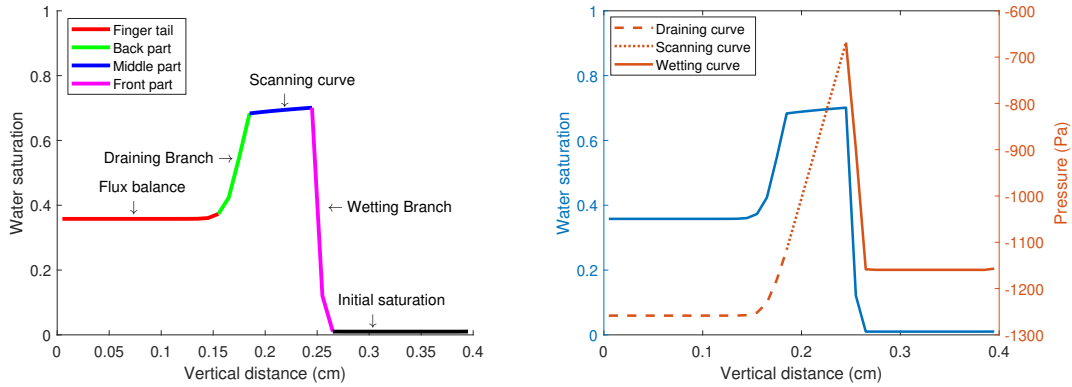
Figure 3.12: Left panel: Representation of the effect of parameters on the final shape of the finger. Right panel: Saturation and corresponding pressure.
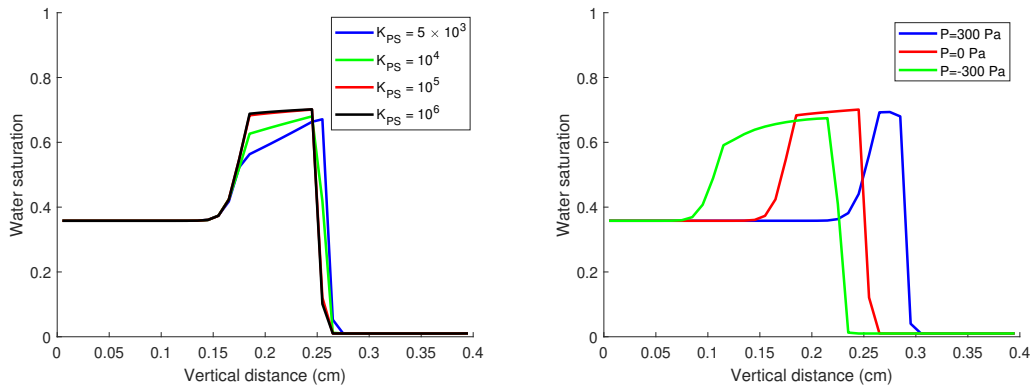

Figure 3.13: Left panel: Effect of the hysteresis exponent K_{PS}. Right panel: Effect of the distance between the main branches. See the text for more details.

3.3. Limit of 1D semi-continuum model

In case of the porous media flow, there are more reasons to doubt the continuum mechanics approach apriori. The discrete nature of the fluid is not a problem – the pores are orders of magnitude larger – it is rather the nature of the acting forces that raises doubts about continuum modelling. In a turbulent fluid (described for instance by well known Navier-Stokes equations [88, 116]), the representation of internal forces (viscosity and pressure) through a smooth tensor field makes sense at each point. On the other hand, a water body inside a porous matrix is "suspended" on its air-water menisci. Tension at each point of the water body is dictated by the geometry of the menisci at its outskirt. Capillary forces act only at the air-water interfaces and it may not be sensible to assume they are "spread out" throughout the porous medium in the form of a "capillary force

field". However, this is exactly the key assumption behind continuum mechanics modelling.

There is a major issue to be clarified before the model can be considered appropriate: the size of the blocks and the behaviour of the model as this size goes to zero. We show that the question is interesting because the correct answer has to live between the two long established "extremes". On one hand, a mathematically trivial but physically incorrect limit of the semi-continuum model yields the RE, which works well for the diffusion-like regime but fails in the fingering regime. On the other hand, passing to the limit in the retention curve without sending the block size to zero yields the original Macro Modified Invasion Percolation model of Glass et al. [50], which works well in the fingering regime but fails in the diffusion-like regime [51, 44, 43, 52]. The correct limiting process has to balance the convergence in the retention curve with the block size. It yields neither a partial differential equation, nor a cellular automaton. In this sense, we believe that the semi-continuum model is the golden mean in porous media flow modelling, and that it is a representative of a rather interesting family of mathematical models. Surprisingly, we are not aware of much work dealing with this type of models.

It is crucial to understand, that in performing the limit $dt \to 0$, $dx \to 0$, one cannot assume that the distribution of the characteristics of the blocks (i.e. their permeability, porosity and retention curve) stays the same. We conjecture that with decreasing dx, the *variance* of this distribution has to increase. As the blocks become smaller and smaller, some of them will likely represent a void of the porous matrix (thus becoming very permeable) and others will likely represent the bulk of the porous matrix (thus becoming negligibly permeable). Note that this idea goes directly against the continuum mechanics paradigm! To stress the contrast further, imagine we treated the problem of heat diffusion by the semi-continuum approach presented above. The heat conducting material would be cut up into blocks and heat would flow between the adjacent blocks according to Fourier's Law. Each block would be described by the same heat conductivity coefficient. Next, the mesh would be refined. Naturally, the heat conductivity coefficients would not be affected by the refinement of the mesh. Taking the limit of the refinements (together with $dt \to 0$) would yield the classical heat equation.

However, in the context of unsaturated porous media flow, the material coefficients cannot stay constant during the limiting process. As the blocks become smaller, the *variance* of the material parameters has to increase. Moreover the variability of the geometry of its pore-space decreases, and consequently its re-

tention curve becomes simpler. If we imagine a block so small that it contains only a single pore, its retention curve becomes completely flat. For a single pore, the transition from zero to unit saturation happens at a constant pressure (the water-entry pressure) and the transition from unit to zero saturation also happens at constant pressure (the air-entry pressure). Thus, in the limit $dx \to 0$, the retention curve of each block collapses to two parallel horizontal lines, one for imbibition and the other one for drainage. Such a retention curve is inadmissible in the context of the RE and so the semi-continuum model does not reduce to the RE in the limit $dx \to 0$.

To simplify the ideas as much as possible, the limiting process of one-dimensional version of the model will be addressed in this chapter. All parameters remain the same as for 1D simulations provided in this chapter.

3.3.1. A numerical limit

We showed in Results section 3.2 that the model is able to reproduce well all the observed features in unsaturated flow in a narrow vertical test tube filled with sand in experiments reported by DiCarlo [23, 26, 28]. The model correctly predicts when a saturation overshoot effect will appear. Moreover, it captures well both the interesting aspects of the overshoot behavior: (1) the non-monotonic dependence of the overshoot magnitude on the influx, and (2) the transition from the overshoot regime to diffusion-like regime for increasing initial saturation.

Fingering regime in a narrow tube does not allow the fingers to exhibit complicated spatial patterns. To observe these, one has to switch to two-dimensional experiments such as [46, 47, 50, 48, 45, 3, 103]. In Chapter 4 we will use the two-dimensional version of the model to show that it is able to correctly reproduce the transition between fingering regime with saturation overshoot (for small initial saturation) and diffusion-like regime of a stable flat water front with a monotonic saturation profile (for large initial saturation), see Figure 4.15. The overshoot magnitude and spatial structure of the fingers are also reproduced correctly [95].

In [29], DiCarlo states the four criteria to evaluate a model for unsaturated porous media flow (see Section 2.5). Since the semi-continuum model can never reduce to the RE, we understand the second criteria in the way that the model should be able to reproduce also diffusion-like regime, not only the fingering regime. The semi-continuum model formulation uses only the physics of the RE (porosity, permeability, the retention curve, mass conservation, and the Darcy-Buckingham Law), thus no new parameters are introduced. In view of Figures 3.2, 4.15 and other results in Chapters 3 and 4, points 2–4 are satisfied, too. One

might be tempted to say that the issue is settled and the semi-continuum model is the appropriate one. However, that would miss the question how to choose the block size. This is clearly a "parameter" of the semi-continuum model, and clearly a rather artificial one.

First, note that the time step is not a free parameter of the model – it is a discretization parameter. Figure 3.14 (left) shows the behavior of the 1D semi-continuum model for a range of dt values. The solution is stable in the limit $dt \to 0$.
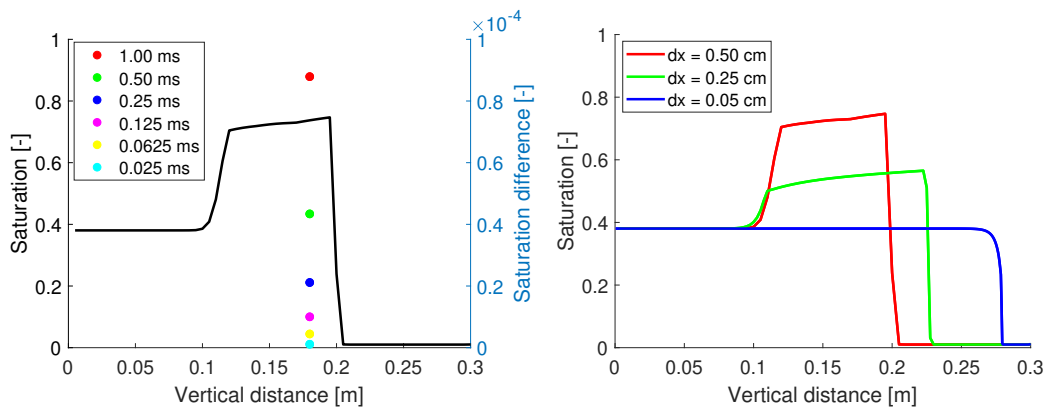

Figure 3.14: Left panel: The dependence of the moisture profile at $t = 10$ minutes on time step dt, the profiles are almost identical for a range of dt between 10^{-3} and 10^{-5}. The right vertical axis denotes the difference of the saturation in the finger tip for various dt, which are plotted with coloured circles. The reference finger is calculated for time step $dt = 0.0125$ ms. Right panel: The dependence of the moisture profile at $t = 10$ minutes on dx. As $dx \to 0$, the overshoot behavior disappears and the semi-continuum model converges to the Richards' equation.

This is not the case for dx. If we let the block size go to zero (dt has to go to zero, too), the overshoot behavior disappears (see right panel of Figure 3.14). This is natural because in the limit $dx \to 0$, $dt \to 0$, the semi-continuum model converges to the RE. The only difference between a numerical scheme for the RE and the semi-continuum model is the use of geometrical mean for flux update. However, in the limit $a \to b$, all means (arithmetic, geometric, and harmonic) converge to the same value a, so this has no effect in the limit. In view of this convergence, one might say that the semi-continuum model is just another wrong numerical scheme for the RE [92, 93] — the scheme is wrong because it produces saturation overshoot while the RE cannot produce overshoot. This line of thinking has a rich history, see the discussion of Eliassi and Glass [35]. We will argue that it is quite the opposite: the RE is a wrong limit of the semi-continuum

model.

The main idea is the following: each block is a sample of the original medium characterized by the porosity, intrinsic permeability, and the retention curve. If we decrease the sample size, the characteristics of the block have to change, especially the retention curve. We claim that smaller samples of the original medium have flatter retention curves. To fix ideas, imagine a single pore in the shape of a cylinder of radius R. Assuming zero contact angle, a drop of water would "sit" inside this capillary cylinder bounded by two hemispherical menisci of radius R. According to the Young-Laplace equation [139], the pressure drop across each of the meniscus is $2\sigma/R$ where σ is the surface tension between water and air. Setting the air pressure to zero, the water drop is under tension (i.e. negative pressure) $P = 2\sigma/R$. Connecting such an empty pore to a water reservoir at a pressure lower than $-P$ will yield zero saturation in the pore — the suction of the pore is not enough to draw any water in. Once the pressure in the reservoir increases above $-P$, the pore will immediately fill with water, switching to unit saturation. Thus, the dependence of saturation on pressure (i.e. the retention curve) is a horizontal line at $-P$. Let us continue this thought experiment and imagine two pores of radii $R_1 < R_2$. At certain pressure $-P_1$, the first pore will fill, and at a higher pressure $-P_2$, the second one will fill. Thus, the retention curve of this system of two pores is a broken horizontal line (see Figure 3.15). A macroscopic sample of a porous medium contains many pores of various shapes. The result of assembling many horizontal lines at different levels is a smooth function such as the one presented in Figure 3.1. The main point of this excursion is to explain that as the sample size converges to zero, its retention curve has to converge to the retention curve of a single pore – i.e. to a horizontal line.

The same idea can also be approached from a different angle: if we want to decrease the block size and yet preserve the character of the flow, the fluxes across the block boundaries must stay roughly the same. The fluxes are given by Equation (3.6) in which decreasing dx to a half increases the flux by a factor of two. To compensate for this, the difference in pressure between the blocks must decrease. And decreasing the pressure difference without changing the saturation in the blocks amounts to the flattening of the retention curve.

Suddenly, a clear picture emerges. Letting $dx \to 0$ without flattening the retention curve should yield a physically unsound model. And so it does — the RE is unable to capture experimentally observed flow patterns. The correct limiting process must include correct scaling of the retention curve. We propose
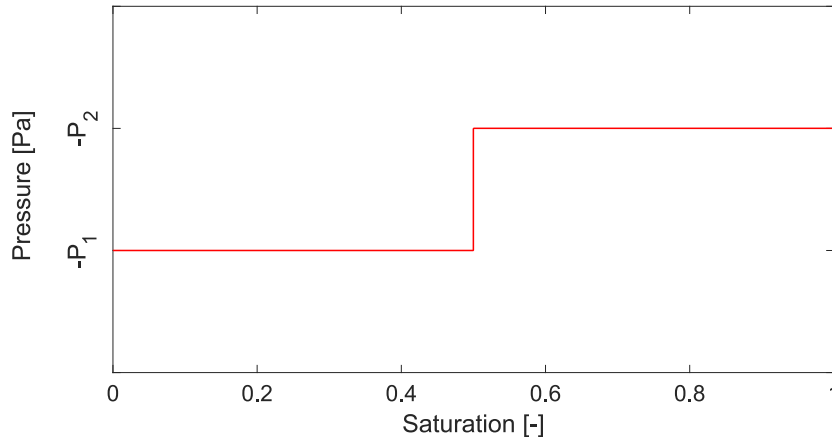
Figure 3.15: The main draining branch of two pores of radii $R_1 < R_2$ and corresponding pressures $-P_1$ and $-P_2$. Both pores have the same volume, thus a break in horizontal line is for $S = 0.5$.

the following simple mechanism in which the retention curve of a block takes the form

$$P = dx \left[-100 \, log \left(\frac{1}{S} - 1 \right) \right] + C, \tag{3.7}$$

where dx denotes the block size, and C is -700 Pa for the main wetting branch and -1300 Pa for the main draining branch. This retention curve is the simplest possible parametrization and roughly matches the characteristics of 20/30 sand in the experiments of DiCarlo [23]. We did not try to fit the constants -- the purpose of this article is to explain the scaling not to produce the best possible fit of experimental data. Figure 3.16 illustrates the scaling of the retention curve as dx goes to zero. Notice that the distance between the two main branches does not change.

Left panel of Figure 3.17 shows the predicted moisture profile in 1D simulation for a decreasing sequence of block size values. The setting is the same as in Figure 3.14 but, unlike in Figure 3.17, this time the flow profile converges to the experimentally correct finger flow pattern, with overshoot in the fingertip and under-saturated finger tail. Notice that the limit saturation profile is almost rectangular. The right panel of Figure 3.17 shows the numerical convergence for $dx \to 0$ in case of a diffusion-like flow regime. Thus, this scaling works in both the regimes, fingering and diffusion-like.

Finally, Figures 3.18 and 3.19 show the predicted pressure profiles for a de-
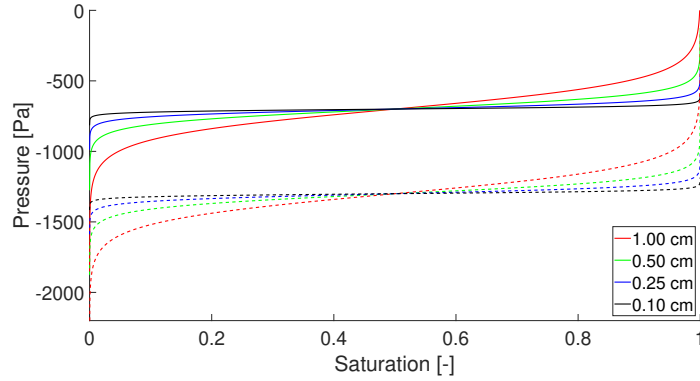
Figure 3.16: The scaling of the retention curve with the block size dx. The solid line denotes the main wetting branch and the dashed line denotes the main draining branch.
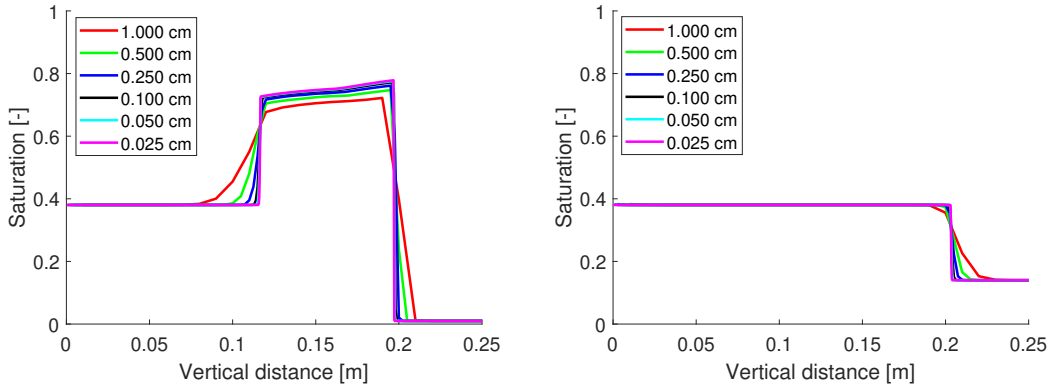

Figure 3.17: Left panel: Convergence of the moisture profile at $t = 10$ minutes for $dx \to 0$ for initial saturation $S_{in} = 0.01$. The moisture profile converges and retains the overshoot pattern. Right panel: Convergence of the moisture profiles at $t = 5$ minutes for $dx \to 0$ for initial saturation $S_{in} = 0.14$. The moisture profile converges to a sharp water-front without saturation overshoot.

creasing sequence of block size values at a point 5 cm from the upper boundary. It is important to mention, that initial setting is crucial for the pressure behavior. While in Figure 3.18, we started on the main wetting branch (the same setup was used in Figure 3.17), in Figure 3.19 all blocks started on the main draining branch.

We can clearly see, that for the first case (all blocks are assumed to be in the imbibition mode), the behaviour of the pressure profile is not consistent with experimental results [27]. In the limit, the pressure first equals -700 Pa (as the block is in the imbibition mode), then the pressure slowly decreases (as the block

is on the scanning curve) and finally the pressure is again constant and equals -1300 Pa (as the block is on the main draining curve). On the other hand, if all blocks are assumed to be in the draining mode, the pressure first increases and then slowly decreases which is consistent with experimental observation. The convergence of moisture profiles is similar as shown in Figure 3.17 and thus it is not presented here. Let us also note, that the oscillations observed in 1D simulation (see Figure 3.7) disappear in limiting process.

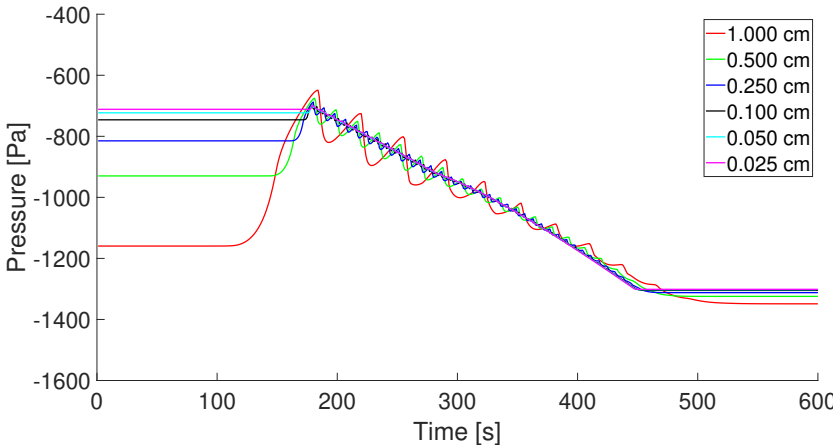Figure 3.18: The predicted pressure profiles for initial saturation $S_i = 0.01$. All blocks started on the main wetting branch.
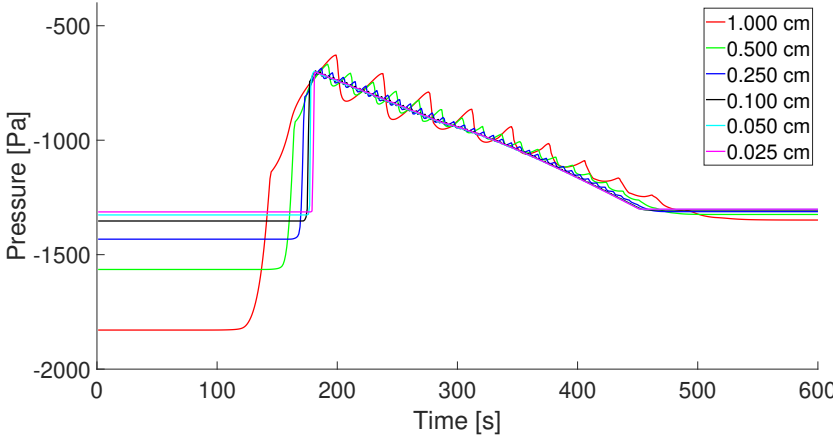

Figure 3.19: The predicted pressure profiles for initial saturation $S_i = 0.01$. All blocks started on the main draining branch.

The semi-continuum allows for a physically reasonable scaling of the retention curve with dx so that the character of the solution remains the same. This numer-

ical evidence suggests there should be a limit form of the semi-continuum model, i.e. a model to which the semi-continuum model converges as $dx \rightarrow 0$, while scaling the retention curve in the appropriate way. The idea of the mathematical limit is presented in the next section.

3.3.2. A mathematical limit

In this section, we pay attention to the limit process suggested above. First, let us complete the model (3.1), (3.6) with initial conditions

$$S_i(x, 0) = S_i(x), \quad \text{for} \quad i = 0, \ldots, n + 1, \tag{3.8}$$

and boundary conditions

$$q_{0,1}(t) = q_0 > 0, \quad \text{and} \quad q_{n,n+1}(t) = 0. \tag{3.9}$$

Let us denote by x_{i+1} the point between block i and $i + 1$. Points x_0 and x_{n+2} form the boundary of the one-dimensional sample. To simplify notation we denote $h := dx$. A single block thus corresponds to the interval $[x_i, x_i + h)$. Further, we define the following notation. A function $\tilde{f}_h(x)$ denotes a piecewise constant function that takes the value f_i on each interval $x \in [x_i, x_i + h)$. In this notation, $\tilde{S}_h(x)$ is the saturation, piecewise constant on each block. A piecewise linear (and thus continuous on $[0, L]$) approximation will be denoted without the tilde, i.e.

$$f_h(x) := \left(1 + \frac{x_i}{h} - \frac{x}{h}\right) f_i + \left(\frac{x}{h} - \frac{x_i}{h}\right) f_{i+1},$$

for $x \in [x_i, x_i + h)$. In the following paragraphs, we will use these piecewise constant and piecewise linear approximations to saturation, pressure, and flux. We will also denote

$$\partial_t := \frac{\partial}{\partial t} \quad \text{and} \quad \partial_x := \frac{\partial}{\partial x}$$

With this notation, Equation (3.1) can be rewritten as a partial differential equation

$$\theta \partial_t \tilde{S}_h(x, t) = -\partial_x q_h(x, t), \quad \text{for } (x, t) \in [0, L] \times [0, T]. \tag{3.10}$$

This approach is inspired by the Rothe's scheme which related a partial differential equation (PDE) to its discrete approximations [108]. Similarly, Equation (3.6) can be rewritten as follows

$$\tilde{q}_h(x + h, t) = \frac{\kappa}{\mu} \sqrt{k(\tilde{S}_h(x, t))} \sqrt{k(\tilde{S}_h(x + h, t))} (\rho g - \partial_x P(h))$$

$$\text{for } (x, t) \in [0, L] \times [0, T]. \tag{3.11}$$

Next, we employ the toolbox of modern PDE theory and pass to the weak formulation. We take a smooth function φ, multiply both sides of (3.10) with it, and integrate over the interval $[0, L]$ to get

$$\theta \int_0^L \partial_t \tilde{S}_h(x,t)\varphi(x)\ dx = \int_0^L q_h(x,t)\partial_x\varphi(x)\ dx + q_0\varphi(0). \tag{3.12}$$

In this equation, the derivative is transferred to the test function φ which enables us to relax the assumptions on the limits performed below.

The retention curve defined by (3.7) can be decomposed into two branches (wetting and draining) in the following symmetrical way

$$g_w(h,S) = f(h,S) + C, \qquad \text{and} \qquad g_d(h,S) = f(h,S) - C, \tag{3.13}$$

with

$$f(h,S) = h\left(-100\log\left(\frac{1}{S}-1\right)\right) - 1000$$

and $C = 300$. The scanning curves $b(S)$ are modelled such that they follow a straight line given by

$$\frac{dP}{dS} = K_{PS}. \tag{3.14}$$

Using the form of the two branches we can see similarity between (3.13) and (3.14) and the classical Prandtl model of elasto-plasticity (the stop operator), see Visintin for more details [129]. The hysteresis operator P defined by (3.13) and (3.14) can be thus express using the differential inequality

$$(K_{PS}\partial_t S - \partial_t P(h))\,(P(h) - v) \geq 0, \qquad \text{for all } v \in [g_d(h,S), g_w(h,S)],$$

$$\text{with}\ \ P(h) \in [g_d(h,S), g_w(h,S)], \qquad \text{and} \qquad S \in [0,1].$$

To see that the equations above really describe the classical Prandtl model of elasto-plasticity, we use the substitution

$$\bar{S}(h) := K_{PS}S - f(h,S),\ \ \bar{P}(h) := P(h) - f(h,S),\ \ w := v - f(h,S). \tag{3.15}$$

The resulting operator form of the semi-continuum model takes the form of the following differential inequality

$$\left(\partial_t \bar{S}(h) - \partial_t \bar{P}(h)\right)\left(\bar{P}(h) - w\right) \geq 0, \quad \text{for all } w \in [-C, C] \ \text{with } \bar{P}(h) \in [-C, C]. \tag{3.16}$$

We now check whether the differential inequality in (3.16) corresponds with the hysteresis operator defined by (3.13) and (3.14):

1. Let $\bar{P}(h) \in [-C, C]$. Then there exists $w_j \in [-C, C]$, $j = 1, 2$, such that $\bar{P}(h) - w_1 > 0$ and $\bar{P}(h) - w_2 < 0$. From (3.16) it follows:

$$\partial_t \bar{S}(h) - \partial_t \bar{P}(h) = 0.$$

Integration in time variable together with (3.15) results in

$$P(h, t) = K_{PS} S(t) - K_{PS} S(t_0) + P(h, t_0),$$

where t_0 is an initial time such that $\bar{P}(h, t_0) \in (-C, C)$. Thus, we are located on the scanning curve for this case.

2. Let $\bar{P}(h) = C$ and thus $P(h) = f(h, S) + C$. Then $\bar{P}(h) - w \geq 0$ and $\partial_t \bar{S}(h) - \partial_t \bar{P}(h) \geq 0$. Hence and from (3.15) it follows

$$K_{PS} \partial_t S \geq \partial_t P(h) \Rightarrow K_{PS} \geq \partial_S f(h, S),$$

because the pressure corresponds to this branch only if $\partial_t S \geq 0$ and moreover $\partial_t f(h, S) = \partial_S f(h, S) \partial_t S$. Without the inequality $\partial_t S \geq 0$ we are unable to connect $K_{PS} S$ and $f(h, S) + C$. From the inequality $K_{PS} \geq \partial_S f(h, S)$ it follows that $K_{PS} S$ and $f(h, S) + C$ are connected.

3. Let $\bar{P}(h) = -C$ and thus $P(h) = f(h, S) - C$. Then $\bar{P}(h) - w \leq 0$ and $\partial_t \bar{S}(h) - \partial_t \bar{P}_h \leq 0$. Hence and from (3.15) it follows

$$K_{PS} \partial_t S \leq \partial_t P(h) \Rightarrow K_{PS} \geq \partial_S f(h, S),$$

because the pressure corresponds to this branch only if $\partial_t S \leq 0$ and moreover $\partial_t f(h, S) = \partial_S f(h, S) \partial_t S$. Without the inequality $\partial_t S \leq 0$ we are unable to connect $K_{PS} S$ and $f(h, S) - C$. From the inequality $K_{PS} \geq \partial_S f(h, S)$ it follows that $K_{PS} S$ and $f(h, S) - C$ are connected.

Finally, assume that as $h \to 0$, the solutions of the operator form of the semi-continuum model (3.16) converge in the following sense

$$\tilde{S}_h \to S, \qquad q_h \to q, \quad \tilde{q}_h \to q, \qquad \text{and} \qquad \bar{P}(h) \to P + 1000. \tag{3.17}$$

The validity of this assumption is suggested by the numerical evidence described above. Performing the limit in (3.12), (3.13) and (3.14) yields

$$\theta \int_0^L \partial_t S(x, t) \varphi(x) \, dx = \int_0^L q(x, t) \partial_x \varphi(x) \, dx + q_0 \varphi(0), \tag{3.18}$$

where

$$q := \frac{\kappa}{\mu} k(S) \left(\rho g - \partial_x P \right) \tag{3.19}$$

and

$$\left(K_{PS} \partial_t S - \partial_t P \right) \left(P - v \right) \geq 0, \ \ \text{for all } v \in [-1300, -700] \text{ and } P \in [-1300, -700]. \tag{3.20}$$

Thus, the limit form of the semi-continuum model is a weak formulation (3.18) for a partial differential equation together with the classical Buckingham-Darcy law (3.19), containing a hysteresis operator of the Prandtl model of elasto-plasticity (3.20). Passing from the weak formulation to the classical one yields

$$\theta \partial_t S + \partial_x \left(\frac{\kappa}{\mu} k(S)(\rho g - \partial_x P) \right) = 0. \tag{3.21}$$

Equation (3.20)–(3.21) represent the classical form of the limit of the semi-continuum model. It is a partial differential equation containing a Prandtl-type hysteresis operator under the derivative, which makes the equation switch between a hyperbolic and parabolic type. This is a rather interesting mathematical object and we are not aware of much research dealing with such equations. Since these equations seem to arise naturally from a limiting process of the semi-continuum model, we think they deserve more attention of the mathematical community.

If P was a differentiable monotonically increasing function (i.e. a retention curve, not a hysteretic operator), Equations (3.20)–(3.21) would reduce to the classical RE defined by equation (3.21). However, in view of the above arguments, that would correspond to a physically unsound limiting process. For a sample size above representative elementary volume (REV), a retention curve is a material characteristic and is independent on the sample size. On the other hand, for the sample size lower than REV (centimeters), the retention curve is dependent on this sample. However, it is obvious, that the size of blocks ("the size of the computational mesh") should be lower than REV; thus for a mathematical model, the retention curve should not be considered as a material characteristic. Taking this into account, one arrives at a model that differs dramatically from the RE.

3.3.3. The golden mean in porous media flow

Many researchers in the community have been circling around the semi-continuum model and its correct scaling. In 1996 (i.e. before it was proven that

58

the RE cannot admit saturation overshoot), Nieber [92] claimed to have produced a finger-like solution to the RE numerically. However, Eliassi and Glass [35] went through the discretization process used by Nieber and demonstrated that his finger-like solution is a numerical artefact. With the benefit of hindsight, we see that Nieber "guessed" the correct mechanism of flux across the fingertip, however, he tried to put it into the context of the RE which is impossible. We might say that he was right by producing an incorrect solution to an incorrect equation.

Another approach came very close to this result. As soon as 1989, Glass and Yarrington [50] proposed a cellular automaton under the title of "mechanistic modelling", or "Macro Modified Invasion Percolation (MMIP)". They first proposed the idea of representing the porous medium as a grid of blocks that retain the character of a porous medium. In their approach, each block is completely characterized by two numbers:

- P_w, the wetting pressure, i.e. the pressure needed for water to fully percolate the block (that means to form a connected network of filled pores throughout the block so that the block becomes conductive),

- P_d, the draining pressure, i.e. the pressure needed for air to reinvade the block.

For zero contact angle, capillary pressure can be related to a radius of curvature by means of the formula $P = 2\sigma/R$, thus, each block can be assigned a wetting radius R_w and a draining radius R_d. Each block is either full (percolated by the invading fluid) or empty (not percolated) so that the model cannot capture saturation as a continuous variable. There are many important details to make the model work (e.g. the wetting and draining radii have a distribution, a mechanism of collective pore filling called "facilitation" has to be implemented, etc.) but once in place, the model produces astonishing match of observed data in a range of different conditions.

From the perspective of the model presented here, the MMIP model is an incomplete limit of the semi-continuum model in the following sense. The characterisation of each block by two critical values of pressure exactly corresponds to a flat retention curve, i.e. to a retention curve of a single pore. Thus, the MMIP model takes the limit in the retention curve but leaves the block size constant (and arbitrary). The RE, on the other hand, arises by taking the limit in the block size but leaving the retention curve of the block without change. We argue that both the limiting processes have to proceed in parallel. In this way we strike

the golden mean between the RE (which works well for diffusion-like flow but fails in the fingering regime), and the MMIP (which works well in the fingering regime but fails for diffusion-like flow). Hence the title of this section.

Let us present an analogy, which we find trivial but useful. The most famous limit in mathematics is undoubtedly the expression

$$\lim_{n \to \infty} \left(1 + \frac{1}{n} \right)^n$$

which defines the Euler constant. A tempting but wrong freshmen approach is to notice that $1/n$ goes to zero, thus the bracket goes to unity, and so the limit must be 1. A similarly wrong approach is to say that the bracket is always greater than one, the exponent goes to infinity, and conclude that the limit must therefore be infinite. The correct answer is the golden mean: the decrease of the bracket to unity is balanced by the increasing power to which the bracket is raised. This resembles rather well the limiting process described here. The decrease in the block size is balanced by the increasing "flatness" of the retention curve.

The price we pay for the semi-continuum approach is the awkward nature of the limit. It is a partial differential equation containing a Prandtl-type hysteresis operator under the derivative, which makes the equation switch between a hyperbolic and parabolic type. The limit derived here is a formal one, i.e. we *assume* the solution of the semi-continuum model converges as $dx \to 0$ to a function and show which equation this function should satisfy. The reader should be warned that the "limit of a model" may be understood in two different ways which we will explain on the example of Navier-Stokes equations. If we let viscosity of the fluid go to zero, the Navier Stokes equations will reduce to Euler equations. This "limit in the model" is easy. However, it is quite another matter to show that if take the *solution* to Navier-Stokes equations and pass to the limit $\nu \to 0$ in the *solution*, the resulting function will be a solution of the Euler system. This "limit in the solutions" is still an open problem and almost no one in the community believes it is true. In this article, Equations (3.20)–(3.21) represent the "limit in the model" approach.

3.4. Discussion

There is an interesting connection between the presented results and the work of Hassanizadeh and Gray [55, 57, 56, 54], who propose a dynamical term in the pressure saturation equation. In their approach, the retention curve takes the

form

$$P_{dyn}(S) = P_{stat}(S) - \tau(S)\frac{\partial S}{\partial t}$$

with $P_{stat}(S)$ the original rate-independent retention curve, and $\tau(S)$ a new saturation dependent material function. There has been a discussion whether the term is physically sound and whether there is any experimental evidence of it [28]. If saturation increases (i.e. if the wetting branch of the retention curve is followed), the dynamical term is negative and so $P_{dyn} < P_{stat}$. On the draining branch, the effect is opposite.

As stated earlier, decreasing dx without flattening the retention curve accordingly produces too large fluxes across the fingertip (due to too large pressure differences) which do not allow water to pile up in the finger and ultimately destroy the overshoot. This is the reason why the RE cannot capture overshoot profiles. Our solution of this problem is to flatten the retention curve along with decreasing dx. Hassanizadeh's solution is to decrease the pressure difference by the dynamical term. The dynamical term is "silent" in most of the medium where the rates of change of saturation are moderate. It kicks in precisely at the edge of the advancing fingertip where the saturation rises quickly. From the numerical point of view, it does not matter how we prevent the pressure differences across the fingertip to increase too much. From the point of view of physics, we believe that our approach is more reasonable. We reach the same effect without introducing any new parameters by a process which is theoretically sound and is backed by experimental evidence. Hassanizadeh needs to introduce a parameter which is saturation dependent, i.e. he needs to introduce a new material function. Although his approach seems to have theoretical backing, experimental evidence for the existence of the dynamical effect is lacking and it is unclear how to measure the function $\tau(S)$.

Averaging of hydraulic conductance has been used before [92, 93] and heavily criticized since then [35]. Nieber used the averaging process in a numerical solution to the RE. That was proven wrong by Eliassi et al. [35] who showed that his "numerical solution" was far from the true solution to the RE. Thus, by the averaging process, Nieber obtained an incorrect numerical solution to the RE. Today we know that the RE is inappropriate for finger flow modelling [40]. In the present semi-continuum model, the averaging process is not used to obtain a numerical solution to any differential equation. The averaging process is based on the studies of the so-called equivalent hydraulic conductivities of spatially varying media [61]. There is theoretical justification to use the harmonic mean of conductivities (as a lower bound) in case of a medium stratified perpendicular to

the flow direction [61]. This is similar to the situation at the fingertip where an almost saturated block is in contact with an almost dry block beneath. In a series of numerical experiments in a random pore networks, Jang et al. [61] report results which are mostly consistent with the averaging process using the geometric mean. Thus, the geometric mean of relative permeability of the neighbouring blocks is used in our model.

Experiments show that the behavior of the finger tip edge is crucial for the flow pattern. The overshoot can be understood as fluid piling up behind the fingertip because the dry medium ahead of the fingertip has insufficient hydraulic conductance thus the flux across the fingertip cannot keep up with the flux in the tail of the finger. The detailed mechanism of the fingertip advance matters here. The fluid menisci "jump" from grain to grain, rather than flow in a continuous way. That is why the overshoot behavior so much depends on the shape of the grains, as reported by DiCarlo [27]. Materials with identical macroscopic characteristics exhibit different overshoot behavior. It may be possible to model this process if we knew the exact positions and shapes of the grains at the fingertip. However, such detailed knowledge is neither available nor wise to incorporate in a porous medium flow model. Our model accounts for this "burst-and-hold" behavior by the following fast positive feedback: the block beneath the finger tip is dry, thus its conductivity is very low. The flux into the dry block is thus negligible and fluid piles up behind the fingertip. Once the pressure at the front increases enough and the previously dry block starts filling with water, the flux from the finger tip increases very quickly, making the block even more wet, which in turn increases the flux even more. This positive feedback fills the dry block with fluid almost instantly. This makes the finger "jump" ahead by one block. Notice that modelling the flux between the blocks by means of the geometric average is crucial in this process. It should also be stressed that it is crucial to take into account the hysteresis of the retention curve which prevents the oversaturated fingertip to drain into the undersaturated tail.

The microscopic origin of the "burst-and-hold" mechanism has been debated for a long time. Capillary pressure arises from the shapes of the water-air interfaces on the pores are dictated by the geometry of the pore space and the incompressibility of the flow. It is probable that velocity dependent effects also play a role [114, 4]. Hoffman [60] describes the dependence of the contact angle on the velocity of the flow. Steenhuis et al. [114] use this result to predict the capillary pressure in the fingertip for various levels of influx and initial saturation. They assume that water at the fingertip advances by bursting through a single

pore with a velocity high enough to cause a decrease in the contact angle. This causes the pressure to build up in the tip of the finger. There is experimental evidence in support of this mechanism [83]. Whatever the microscopic origin of the capillary pressure is, a semi-continuum model has to capture its effect in terms of quantities that are measurable on the level of the blocks. In our case, the macroscopic manifestation of these pore-scale processes is the low relative permeability between the wet block at the fingertip and the dry block directly beneath.

It is well known that forward time discretization (see equation 4.1) may cause instability of the numerical simulations which usually manifest themselves as spurious oscillations in the finger tip. One may suspect that these spurious oscillations cause the overshoot behavior of the model. The explicit and implicit discretizations were compared and it was shown that the overshoot behavior is independent on the discretization scheme used. For more information, see Supplementary Information in [66].

Let us stress again that the presented model is entirely based on well-known physical principles and material properties. The coefficient K_{PS} may be an exception – it is not usually assumed that all the scanning curves between the main wetting and draining branch of the retention curve are lines with a large derivative. However, any measurement is difficult here and sometimes an estimate of the scanning curves is the only option.

By an easy extension, the model can also be used to under fully or partially saturated conditions. If a block becomes fully saturated, the (negative) capillary pressure becomes zero and (positive) hydrostatic pressure appears. The hydrostatic pressure is computed using the height of the water column (i.e. the height of fully saturated blocks) above the considered block. Thus, in Equation (3.6), hydrostatic pressure difference appears on the right hand side instead of the capillary pressure difference.

Chapter 4

2D semi-continuum model

In this chapter, we present the two-dimensional version of the semi-continuum model [66] which is a straightforward extension of the 1D case [65]. We show that the model is able to reproduce both the finger-like regime (for small initial saturation of the matrix) and the diffusion-like regime (for large initial saturation), and the transition between the two. In the finger-like regime, the model reproduces the persistence of the fingers and captures their spatial heterogeneity well. Further, the model helps to explain the inner structure of the finger – the mobile core and immobile fringe – that is observed in experiments. The well-known two-dimensional experiments of Glass et al. [46, 47, 50, 48, 45] and Rezanezhad et al. [103] are reproduced by the model.

A structure of this chapter is similar as for the 1D semi-continuum model. First, we will derive the two-dimensional extension of 1D model in Section 4.1. Next, in Section 4.2 we will demonstrate that the limit of 2D model works equally well as for the 1D model followed by Section 4.3 in which the parameters of the model will be fitted for different types of porous media. In Section 4.4 we will show capability of the model to reproduce experimental observations. The chapter will be again closed with discussion in Section 4.5. Sections 4.1, 4.4 (except Section 4.4.5) and 4.5 are taken from Kmec et al. [66], and are slightly extended here.

4.1. Model derivation

We extend the model to two spatial dimensions because in 2D there are many more features of the finger flow that can be tested. A 2D model aims to capture experiments in a vertical Hele-Shaw cell filled with sand used for experiments e.g. by DiCarlo [23]. The distance between the two parallel plates is small and thus

the dependence of the quantities of interest on this coordinate can be neglected; hence the notion of 2D porous media flow.

The model is again based only on well-established physics, measurable parameters, and material characteristics. The porous medium is modelled as a regular rectangular grid of $N \times M$ small square blocks of uniform size $dx \times dx$. Each block of the material is assumed to retain the characteristics of a porous medium and so each block is fully characterized by two material functions – the pressure-saturation dependence in the wetting phase (known as the retention curve) and the dependence of hydraulic conductivity on saturation. The amount of the wetting fluid (water in our case) in each block is captured by the moisture content (saturation) and the pressure. Both these quantities are assumed to be uniform inside each block but continuously changing with time. For simplicity, the non-wetting phase (air in our case) is assumed to have zero pressure everywhere.

Each block is denoted by its row and column indices $[i, j]$. The model simulates the motion of the wetting fluid inside the 2D porous medium by tracking the following three quantities:

- the saturation $S_t(i, j)$ [-] of the wetting phase in each block at time t. Saturation is assumed to be uniform throughout each block but varying continuously in time;

- the pressure $P_t(i, j)$ [Pa] of the wetting phase in each block at time t. Pressure is assumed to be uniform throughout each block but varying continuously in time;

- the fluxes $q_t[(i_1, j_1) \to (i_2, j_2)]$ [ms^{-1}] of the wetting phase between blocks (i_1, j_1) and (i_2, j_2) at time t. The fluxes are assumed to be continuous in time.

The evolution of these three quantities is modeled by the following three rules.

4.1.1. Saturation update

The update of saturation in each block is based on simple mass balance.

$$\theta \partial_t S(t, x) + \mathrm{div}(q(t, x)) = 0,$$

where θ [-] denotes the porosity of the material. This mass balance is implemented by the following discrete scheme

$$\frac{\theta}{dt}\left[S_{t+dt}(i,j) - S_t(i,j)\right] = \tag{4.1}$$

$$= \frac{1}{dx}\left[q_t[(i-1,j) \rightarrow (i,j)] - q_t[(i,j) \rightarrow (i+1,j)]\right] +$$

$$+ \frac{1}{dx}\left[q_t[(i,j-1) \rightarrow (i,j)] - q_t[(i,j) \rightarrow (i,j+1)]\right].$$

4.1.2. Pressure update

Next, the pressure in each block is updated according to the retention curve. Here we assume that all the blocks share the same retention curve. The standard retention curve consists of the main wetting and draining branches, which are both assumed to be non-decreasing [128]. It is well known that the retention curve exhibits substantial hysteresis, i.e. the pressure-saturation relation also depends on the history of the system. The main wetting and draining branches are modelled by the standard van Genuchten relation [128];

$$P = -\frac{1}{\alpha}\left(\left(S^{\frac{-1}{m}}\right) - 1\right)^{\frac{1}{n}}, \tag{4.2}$$

where $\alpha \in \mathbb{R}^+$ and $n \in \mathbb{R}^+$ are free parameters and $m = 1 - \frac{1}{n}$. Parameters α, n corresponding to the main wetting branch are usually denoted by index w and parameters α, n corresponding to the main draining branch are usually denoted by index d.

We adopt again same approach of hysteresis modelling as for 1D model. Thus, we assume that all the scanning curves are almost vertical line segments. If a block is transitioning between the main wetting and draining branch, it follows a straight line given by

$$\frac{dP}{dS} = K_{PS}, \tag{4.3}$$

where K_{PS} is a large constant. This enables the pressure to change rapidly while keeping the saturation almost constant. If a block undergoes wetting along a scanning line and reaches the main wetting branch, it sticks to it and further wetting proceeds along the main wetting branch. A similar principle applies in the draining mode: once a block reaches the main draining branch, it sticks to it.

Following a change in saturation, the pressure in each block is updated in this way. The pressure-saturation curve is assumed to be satisfied at all times, i.e. there is no relaxation time involved.

4.1.3. Flux update

Once the pressure in each block is updated, new values of the fluxes among the blocks are calculated. The flux is modeled by the standard Darcy-Buckingham law [5], which takes the following form:

$$q = \frac{\kappa}{\mu} k(S) \left(\rho g - \nabla P \right), \tag{4.4}$$

where κ [m^2] denotes the intrinsic permeability of the medium, μ [Pa s] denotes the dynamic viscosity of the fluid, ρ [kgm^{-3}] denotes the density of the wetting fluid, g [ms^{-2}] denotes the acceleration resulting from gravity, and P [Pa] denotes the pressure in the wetting fluid given by the retention curve. The function $k(S)$ [$-$] stands for the relative permeability, i.e. the ratio of the effective permeability at a particular saturation to the intrinsic permeability. The relative permeability is usually modelled by a power law. Here we adopt the form derived in [86, 87, 128]:

$$k(S) = S^\lambda \left[1 - \left(1 - S^{\frac{1}{m}} \right)^m \right]^2, \tag{4.5}$$

where λ is a free parameter and $m = 1 - \frac{1}{n}$ are the parameters of the retention curve given by Equation (4.2). Because we are especially interested in the fingertip behaviour (which is in the imbibition mode), we always use the value m corresponding to the main wetting branch. Let us denote the effective permeability of the porous medium $\gamma(S) = \kappa k(S)$.

The flux update is the only step where we slightly depart from the standard implementation of the Darcy-Buckingham law. We proposed the following discrete implementation

$$q[(i_1, j_1) \rightarrow (i_2, j_2)] = \begin{cases} \frac{1}{\mu} \sqrt{\gamma(S(i_1, j_1) \gamma(S(i_2, j_2)} \left(\rho g - \frac{P(i_2, j_2) - P(i_1, j_1)}{dx} \right) \\ \qquad \text{for } j_1 = j_2, \ i_2 = i_1 + 1 \\ \frac{1}{\mu} \sqrt{\gamma(S(i_1, j_1) \gamma(S(i_2, j_2)} \left(0 - \frac{P(i_2, j_2) - P(i_1, j_1)}{dx} \right) \\ \qquad \text{for } i_1 = i_2, \ j_2 = j_1 + 1 \\ \\ 0 \qquad\qquad\qquad\qquad\qquad \text{otherwise} \end{cases} \tag{4.6}$$

Thus, the lateral fluxes ($i_1 = i_2$) do not include the force of gravity and the vertical fluxes do ($j_1 = j_2$) include the force of gravity. Each block is assumed to have four neighbours; diagonal fluxes are not included. The geometric mean of the permeability of the neighbouring blocks is used. This is crucial because the

effective permeability becomes small if at least one of the blocks is dry enough to have low permeability. This does not hold for the more typical arithmetic mean, so the use of the geometric mean proves essential for correctly capturing the behaviour of the finger tips. Further justification for using this type of averaging comes from [61], where the authors show that the geometric mean is appropriate by means of numerical experiments in random pore networks.

By setting the fluxes among the blocks, we can update the time to $t + dt$ and proceed back to the saturation update step (4.1). This closes the modelling loop.

4.1.4. Initial and boundary conditions

The two dimensional Hele-Shaw cell of a porous medium is modelled by an $N \times M$ grid of blocks. For the model to be specified fully, initial and boundary conditions must be set. The initial condition can be defined either by prescribing the initial saturation $S_{in}(i, j)$ in each block or by prescribing the initial pressure value $P_{in}(i, j)$ in each block. At the beginning, all blocks are set to start on the main wetting branch. A constant flux q_B is prescribed across the top edge of each of the blocks in the top row. In experiments, a layer of very fine sand [46, 50, 45, 103] is usually used instead. This layer smooths out any heterogeneity in the influx, and so it simulates a constant flux across the top boundary. The lateral boundaries are assumed to be impenetrable and so zero lateral flux is prescribed there. Finally, a free discharge is set at the bottom boundary by the relation

$$
\begin{aligned}
q[(N, j) \to \text{out}] &= \frac{1}{\mu}\gamma(S)\left(\rho g + \frac{P(N, j)}{dx}\right), & S(N, j) &\geq S_{rs}, \\
q[(N, j) \to \text{out}] &= 0, & S(N, j) &< S_{rs},
\end{aligned}
\tag{4.7}
$$

where N stands for the bottom row index and S_{rs} stands for a residual saturation. That means, that the flux from the bottom boundary is set to zero if the saturation of the respective block does not exceed a residual saturation S_{rs}. This implementation of initial and boundary conditions is standard and similar to models based on the Richards' equation [133].

4.2. Limit of 2D semi-continuum model

The scaling of the retention curve described in Section 3.3 works equally well for the 2D version of the semi-continuum model. The idea of the 2D limit is same as for the 1D model; hence a mathematical limit will not be performed here.

Since we use different retention curve for the 2D simulations, let us propose the following scaling of the van Genuchten retention curve. Van Genuchten equation (4.2) is dependent on the size of the block dx in the following way:

$$P = -dx_{par}\frac{dx}{\alpha}\left(S^{\frac{-1}{m}} - 1\right)^{\frac{1}{n}} + (P_{basic} - P_{dx}),\qquad(4.8)$$

where dx_{par} is a fixed discretization parameter. Values P_{basic} and P_{dx} are given by relations

$$P_{basic} = -dx_{par}\frac{1}{\alpha}\left(0.5^{\frac{-1}{m}} - 1\right)^{\frac{1}{n}},$$

$$P_{dx} = -dx_{par}\frac{dx}{\alpha}\left(0.5^{\frac{-1}{m}} - 1\right)^{\frac{1}{n}}.$$

Thus, the retention curve converges to the value $P(S)$ for $S = 0.5$. The reason why the values P_{basic} and P_{dx} are used in Equation (4.8) is that we want to keep the constant distance between the two main branches. The idea is the same as for the logistic retention curve (see Figure 3.16). The reference size of the block dx_{ref} (the size of the block for which we use the reference retention curve given by relation (4.2)) can be obtaint as an inverse value of the discretization parameter dx_{par}, i.e:

$$dx_{ref} = \frac{1}{dx_{par}}.\qquad(4.9)$$

Figure 4.1 illustrates the scaling of the retention curve as dx goes to zero for 20/30 sand. The reference retention curve is given for $dx_{ref} = 1.00$ cm, thus $dx_{par} = 1.00$ cm.

Let us now present the predicted moisture profile for 2D simulations for a decreasing sequence of block size values. Figure 4.2 shows the predicted moisture profile for 2D simulation for a decreasing sequence of block size values. Notice analogous behaviour to the 1D case: the saturation in the fingertip increases slightly with decreasing block size but the oversaturated zone remains roughly the same. However, due to numerical error that are not present in 1D, the fingers become more narrow and consequently slightly faster. Let us note, that we selected an example of the convergence, such that we received "nice" convergence solution. The limiting process in 2D requires more attention because the variance and spatial correlation of material parameters has to be addressed. Thus, more thorough research is needed.
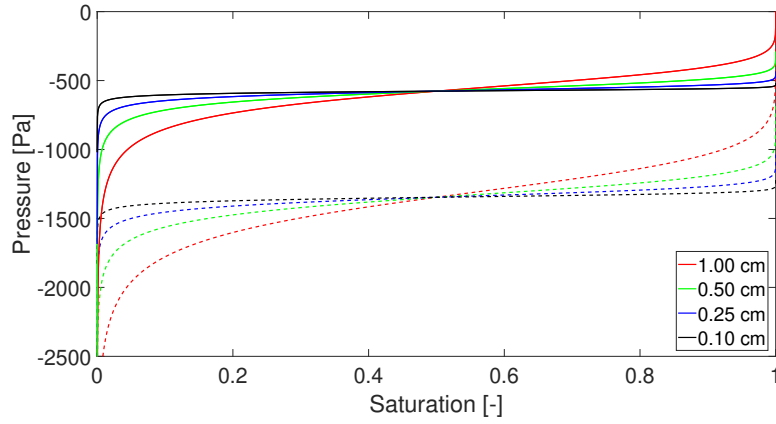
Figure 4.1: The scaling of the retention curve with the block size dx for 20/30 sand for a discretization parameter $dx_{par} = 1.00$ cm. The solid line denotes the main wetting branch and the dashed line denotes the main draining branch.
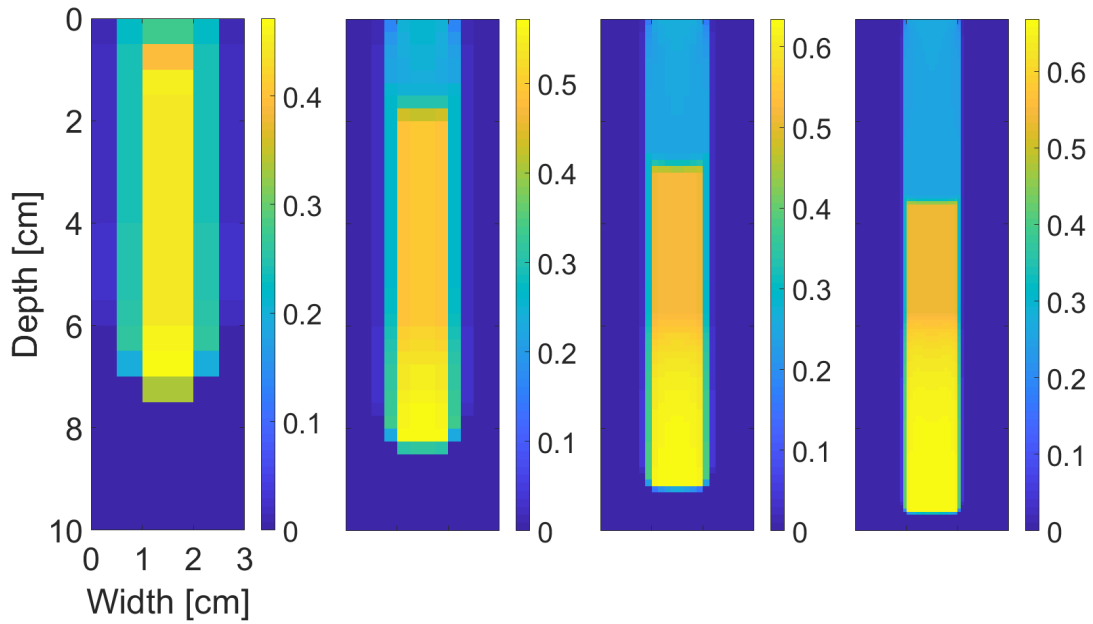

Figure 4.2: Convergence of the moisture profile in 2D at time $t = 14.5$ minutes for $dx = 0.500$ cm, 0.250 cm, 0.125 cm and 0.0625 cm from the left to the right for initial saturation $S_{in} = 0.002$. The moisture profile converges and retains the overshoot pattern. Saturation values are colour-coded according to the colour bar on the right.

4.3. Fitting of parameters

In Sections 3.3 and 4.2, we explained that in performing the limit, the retention curve has to be more flatten. However, we still do not know, what is the block size for the reference retention curve; hence dx_{par} is clearly a parameter of the semi-continuum model and has to be fitted for the simulation. In this Section, we will set two parameters of the model:

- Discretization parameter dx_{par} (see Equation (4.8)) – indicates the size of the block for the reference retention curve. The reference size of the block dx_{ref} is then given by Equation (4.9).

- Relative permeability exponent λ (given by Equation (4.5)) – indicates the relative permeability of the porous medium.

It is important to find a combination of discretization parameter dx_{par} and relative permeability exponent λ, such that we obtain good agreement with experimental results (e.g with [3, 103]). Adjustment of both parameters is a crucial part of the model and should be done separately for each type of a porous material. Both parameters are in principal physical parameters.

Let us note, that we cannot combine both parameters arbitrary. If the parameter dx_{par} is chosen too small, pressure gradients will be very small (see Equation (4.8)) and thus only gravitational force will take a role instead of the retention curve. Consequently, the fingers will be too narrow as water will flow only downwards.

4.3.1. Adjustment of parameters for 20/30 sand

In this section, we will do a thorough analysis for 20/30 sand (used e.g in experiments by DiCarlo [23] and Bauters et al. [3]). A fitting is done in such way, that we want to obtain consistent results with experiments provided by Bauters et al. [3]. The authors showed that with increasing initial saturation, the finger is first more narrow and then wider (this complex behavior is simulated in Section 4.4.5). Therefore, for each combination of dx_{par} and λ we simulate the finger flow for three different initial saturation: a dry, a medium dry and a wet porous medium.

Let us now analyze a possible combinations of parameters $[dx_{par}, \lambda]$ for 20/30 sand. Initial saturation S_{in} equals $0.001, 0.01$ and 0.05 for a dry, medium dry and wet porous medium respectively. The parameters used for the fitting are given in

Table 4.1. A constant flux q_B is prescribed across one centimeter in the middle at the top edge.

Parameter	Symbol	Value
Horizontal width of the chamber	A	17 cm
Vertical length of the chamber	B	50 cm
Block size	dx	0.50 cm
Porosity	θ	0.35
Density of water	ρ	1000 kgm^{-3}
Dynamic viscosity of water	μ	9×10^{-4} Pa s
Intrinsic permeability	κ	2.294×10^{-10} m^2
Acceleration due to gravity	g	9.81 ms^{-2}
Wetting curve parameter	α_w	0.177 Pa^{-1}
Wetting curve parameter	n_w	6.23
Draining curve parameter	α_d	0.0744 Pa^{-1}
Draining curve parameter	n_d	8.47
Slope of scanning curves	K_{PS}	10^5 Pa
Boundary flux	q_B	8×10^{-5} ms^{-1}

Table 4.1: Parameters used for fitting dx_{par} and λ. Parameters for 20/30 sand were adopted from Schroth et al. [110] and DiCarlo [23].

In Figure 4.3, six different variants of parameters $[dx_{par}, \lambda]$ are shown at time 30 minutes. It is crucial to choose parameters $[dx_{par}, \lambda]$ carefully as we want to have sufficiently wide fingers for initially dry porous medium and a diffusion-like behavior for initially wet porous medium. It is observed, that for λ too small, the fingers are thin and conductive for initially dry porous material. On the other hand, for λ too large, a diffusion-like behavior disappears for high initial saturation. This effect is well observed for $[dx_{par} = 1.00, \lambda = 0.5]$ and $[dx_{par} = 1.00, \lambda = 1.2]$. The parameter dx_{par} has a similar behavior. If the parameter dx_{par} is chosen too small, the fingers will be very narrow due to smaller pressure gradients. On the other hand, with increasing dx_{par}, pressure gradients become much larger and thus the fingers are more wider for all initial saturations (see simulation for $[dx_{par} = 1.40, \lambda = 1.2]$). The most optimal combinations are $[dx_{par} = 1.20, \lambda = 0.8]$ and $[dx_{par} = 1.20, \lambda = 1.0]$. It seems, that $dx_{par} = 1.40$ for $\lambda = 1.0$, 1.2 is also possible, however physically irrelevant flow appears for very low initial saturation due to inappropriate choice of the relative permeability function (this will be explained in Section 4.3.2).

Moreover, it can be seen for some variants that the width of the finger is not constant for a dry porous medium, although it is experimentally observed [3].

It is important to mention, that this artificial behavior will disappear, if more realistic porous matrix is used for the simulation. Let us explain it more properly. The porous medium is assumed to be homogeneous, i.e. there are no preferential pathways "hard-wired" in the porous matrix structure. This, however, does not mean that it is sensible to assume the characteristics of all the blocks are the same. Such a model would resemble an artificial medium (e.g. uniformly packed glass beads) rather than realistic porous matrix. If a narrow and spatially correlated distribution of the intrinsic permeability of blocks is introduced, the finger width will be constant for a dry porous medium and thus artificial fingers will not arise anymore (see the Results section).
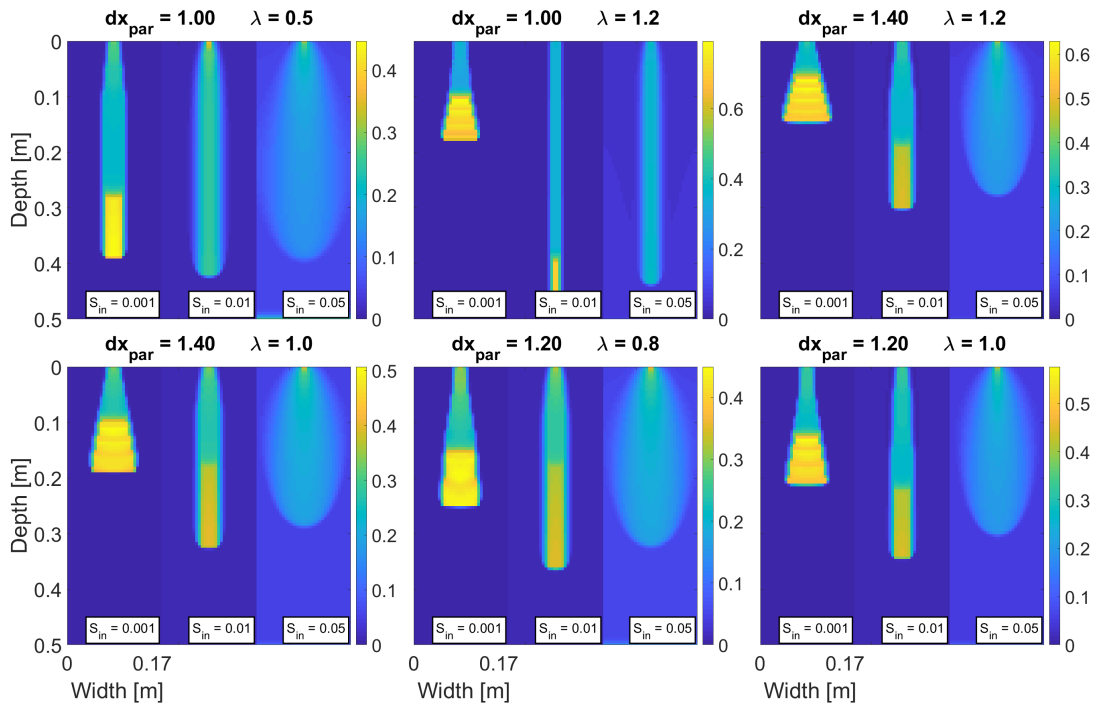
Figure 4.3: Snapshot of the saturation field at 30 minutes for six different combinations of parameters $[dx_{par}, \lambda]$ for initially dry ($S_{in} = 0.001$), a medium dry ($S_{in} = 0.01$) and a wet ($S_{in} = 0.05$) porous material. Saturation values are colour-coded according to the colour bar on the right.

Let us note, that a similar thorough analysis can be provided for 30/40 sand. However, only 20/30 sand was used in the experiments of Bauters et al [3]. Thus, we propose to use the same value λ for 30/40 sand as for 20/30 sand. The parameter dx_{par} is then chosen such that the simulations are consistent with experimental results of Glass et al. [46, 47, 50, 48, 49, 45] and Rezanezhad et al. [103] (see the Results section).

4.3.2. Inappropriate choice of the relative permeability

We observed that the finger would not be able to spread sideways for dry initial saturation, if the relative permeability exponent was chosen too large. See Figure 4.4, where the finger at various simulation times is plotted for a combination $[dx_{par} = 1.40, \lambda = 1.2]$ for $S_{in} = 0.0003$. Let us stress, that this behavior is not a drawback of the semi-continuum model. The lateral fluxes are negligible and thus the flow proceeds only downwards. This is due to inappropriate choice of the relative permeability function as a total permeability of the dry block is approximately 4×10^{-23}. We conjecture, that this issue is caused due to insufficient precision of numerical calculations (double precision was used). The resulting flux into the lateral block is such small, that is already treated as zero for a calculation. At time 30 minutes, the finger finally spread sideways, because the lateral fluxes where high enough. Let us also note, that a similar behavior is observed for the relative permeability function S^m.
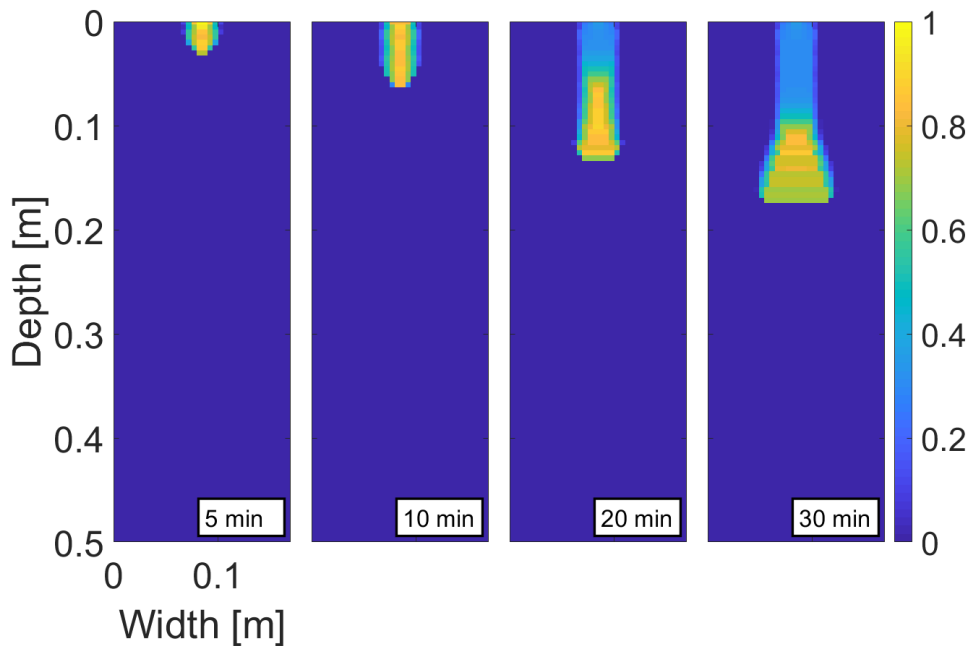

Figure 4.4: Fingering pattern at various simulation times for the combination $[dx_{par} = 1.40, \lambda = 1.2]$ for $S_{in} = 0.0003$. Saturation values are colour-coded according to the colour bar on the right.

To verify this explanation, a precision of numeric calculations has to be increased, however it would be difficult to implement this into the existing code written in MatLab. Moreover, the built-in function *vpa*, which is used for higher

precision in MatLab is very time demanding and is not possible to use it in our case. There are two another solutions to avoid this possible numerical issue. Modify relative permeability function for very low saturation or use a combination of fitting parameters with smaller exponent λ. We conjecture, that the second solution is more appropriate.

4.4. Results

In this section, we demonstrate the capability of the model to reproduce experiments by Glass et al. [46, 47, 50, 48, 49, 45], Rezanezhad et al. [103] and Bauters et al. [3]. The experiments were concerned with the persistence of the fingers, their structure, and the dependence of the fingers on initial saturation and boundary influx.

The porous medium is assumed to be homogeneous. However, as was already explained in Section 4.3.1, there is no reason to assume, that the intrinsic permeability of all the blocks is the same. Thus, we introduce a narrow and spatially correlated distribution of the intrinsic permeability of the blocks. First, let us explain how the distribution of the intrinsic permeability is provided (without any correlation between blocks):

- Assume, that a vertical Hele-Shaw cell consists of $N \times M$ square blocks of size dx.

- First, for each block (i, j) we generate a random number $r(i, j)$ from the normal distribution with mean parameter 0 and standard deviation parameter σ.

- A permeability of each block $\kappa(i, j)$ is then equaled:

$$\kappa(i, j) = R(i, j)\kappa,$$

where κ denotes the default intrinsic permeability and $R(i, j)$ is a multiplication factor such that:

$$R(i, j) = 1 + r(i, j), \quad \text{for} \quad r(i, j) \geq 0,$$
$$R(i, j) = \frac{1}{1 - r(i, j)}, \quad \text{for} \quad r(i, j) < 0, \tag{4.10}$$

so thus, values $R(i, j)$ are always positive. By this approach, we can simply distribute the intrinsic permeability of each block. Moreover, the probability of

being n times smaller is the same as the probability of being n times larger. In Figure 4.5, the histograms for $r(i,j)$ and $R(i,j)$ are plotted, such that we generated field $r(i,j)$ of size 10^8.
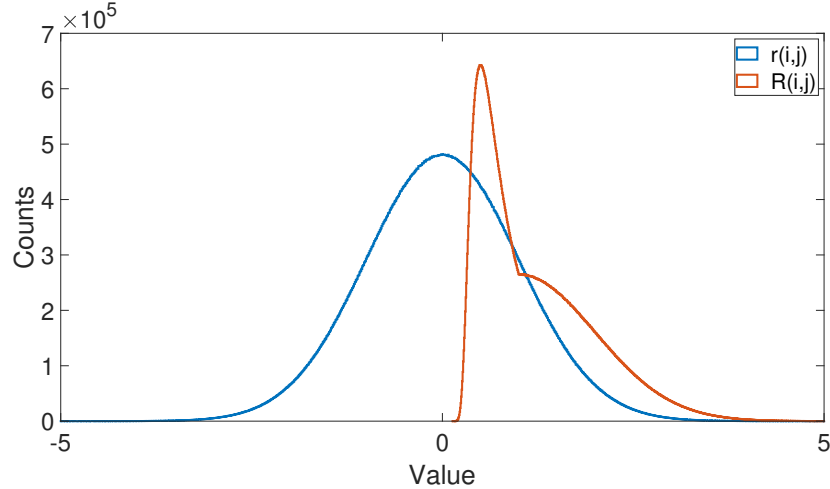

Figure 4.5: Histograms for $r(i,j)$ and $R(i,j)$. Field $r(i,j)$ of size 10^8 was randomly generated from the normal distribution $N(0,1)$. Values $R(i,j)$ are given by Equation (4.10).

However, a correlation between blocks is still not included. We used two different methods, which are usually used in image processing [15]; let us call these methods as filter method and interpolation method. The first method is provided such that we apply a two-dimensional averaging filter of size dx_{L1} on the intrinsic permeability field. The MatLab function *imfilter* is used in this case. The second method is slightly different. First, we do not generate intrinsic permeability for $N \times M$ blocks of size dx. Instead, the intrinsic permeability is generated for larger blocks of size dx_{L2}. Then, we use bicubic interpolation to interpolate the intrinsic permeability of larger blocks on $N \times M$ grid. The MatLab function *imresize* is used in this case. The advantage of this method is that we obtain more smooth field of the distribution of the intrinsic permeability. Let us note, that the intrinsic permeability is the only parameter that is assumed to have a distribution; otherwise the blocks are identical.

4.4.1. Finger persistence

First, we wish to demonstrate the instability of the wetting front – the formation of macroscopic fingers – and their persistence in time. The parameters used for the simulations are given in Table 4.2. The choice of the block size dx was

inspired by the Macro Modified Invasion Percolation model developed by Glass et al. [43, 52]. A constant flux q_B is prescribed across the top edge of each of the blocks in the top row. In experiments, a layer of very fine sand [46, 50, 45, 103] is usually used instead. This layer smooths out any heterogeneity in the influx, and so it simulates a constant flux across the top boundary. The reference retention curve of a 30/40 sand [110, 23] used for this simulation is shown in Figure 4.6 (see Equation (4.2)).

Parameter	Symbol	Value
Horizontal width of the chamber	A	100 cm
Vertical length of the chamber	B	50 cm
Discretization parameter	dx_{par}	2.0 cm
Block size	dx	0.5 cm
Porosity	θ	0.35
Density of water	ρ	1000 kgm^{-3}
Dynamic viscosity of water	μ	9×10^{-4} Pa s
Intrinsic permeability	κ	1.376×10^{-10} m^2
Relative permeability exponent	λ	0.8
Acceleration due to gravity	g	9.81 ms^{-2}
Wetting curve parameter	α_w	0.173 Pa^{-1}
Wetting curve parameter	n_w	10.00
Draining curve parameter	α_d	0.067 Pa^{-1}
Draining curve parameter	n_d	13.10
Slope of scanning curves	K_{PS}	10^5 Pa
Residual saturation	S_{rs}	0.05
Boundary flux	q_B	8×10^{-5} ms^{-1}

Table 4.2: Parameters used for reproducing the wetting front instability experiments. The parameters for 30/40 sand were adopted from Schroth et al. [110] and DiCarlo [23].

The distribution of the intrinsic permeability was provided by interpolation method with standard deviation $\sigma = 0.3$ and $dx_{L2} = 2.5$ cm (see Equation (4.10)). The distribution satisfies $\kappa_{max}/\kappa_{min} \approx 4$ and the mean of the intrinsic permeability approximately equals κ. The distribution of the values of intrinsic permeability is shown in Figure 4.7. A similar spatially correlated permeability field was also used in [21, 53].

In experiments, the wetting front instability is observed for low initial saturation of the matrix [112, 46], and thus we set $S_{in} = 0.01$. Figure 4.8 shows six snapshots of the saturation field at various simulation times. The wetting front
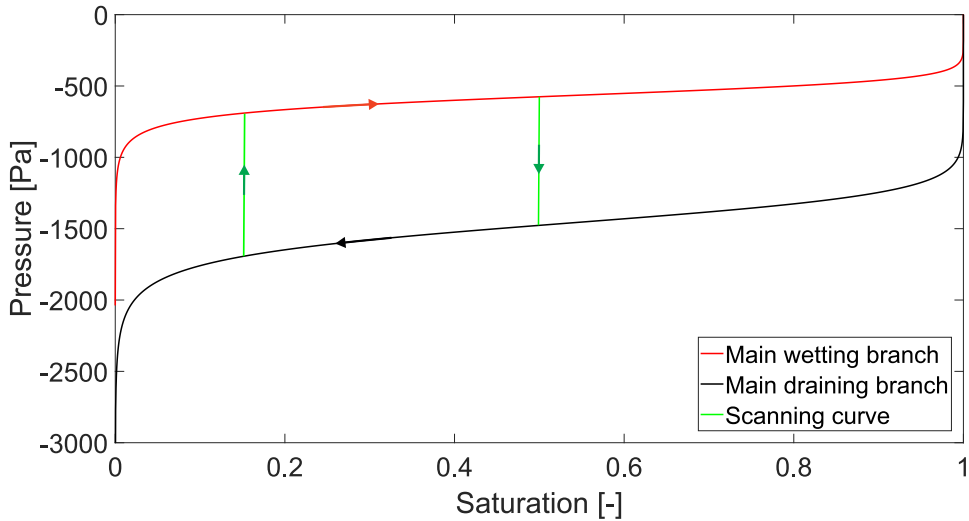
Figure 4.6: The reference retention curve a 30/40 sand [110, 23] used for two dimensional simulations. The reference size of block $dx_{ref} = 0.50$ cm (thus $dx_{par} = 2.0$ cm, see Section 4.3).
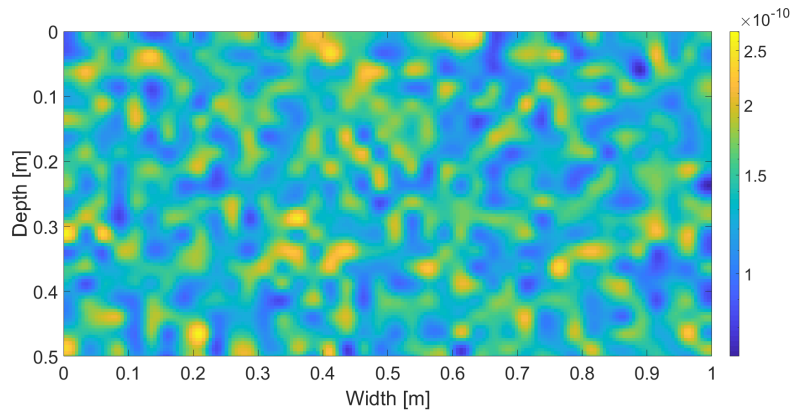

Figure 4.7: The distribution of the intrinsic permeability generated by interpolation method with standard deviation $\sigma = 0.3$ and $dx_{L2} = 2.5$ cm (see Equation (4.10)). Intrinsic permeability values are colour-coded according to the colour bar on the right.

becomes unstable and produces fingers that are very typical of an initially almost dry porous medium – a spatial structure of the fingers is reproduced correctly [95]. Note that the flux across the top boundary is constant and no perturbation is used to initialize any instability. This is in contrast with e.g. [21, 53] who produced

78

fingers by introducing a perturbation directly into the wetting front at the beginning of the simulation. The fingers are fully developed after approximately 10 minutes and then they proceed downward until they reach the bottom boundary. The saturation in the fingers exhibits the typical overshoot pattern – the bottom part of the finger is close to full saturation while the finger tail is much drier. The length of the oversaturated zone is approximately 17 cm, which matches well with the experiments [47]. One may observe the long persistence of the fingers (the numerical experiment ran for 12 hours), which was experimentally observed e.g. in [46, 47, 48, 103]. Moreover, Glass et al. [46, 47, 48] and DiCarlo et al. [31] reported that after hours or days of steady infiltration, the chamber was fully wet; however, most of the flow was confined to the original finger cores and the saturation was much lower around the fingers. This is exactly what can be seen in the last snapshot shown in Figure 4.8 after 12 hours of simulation.
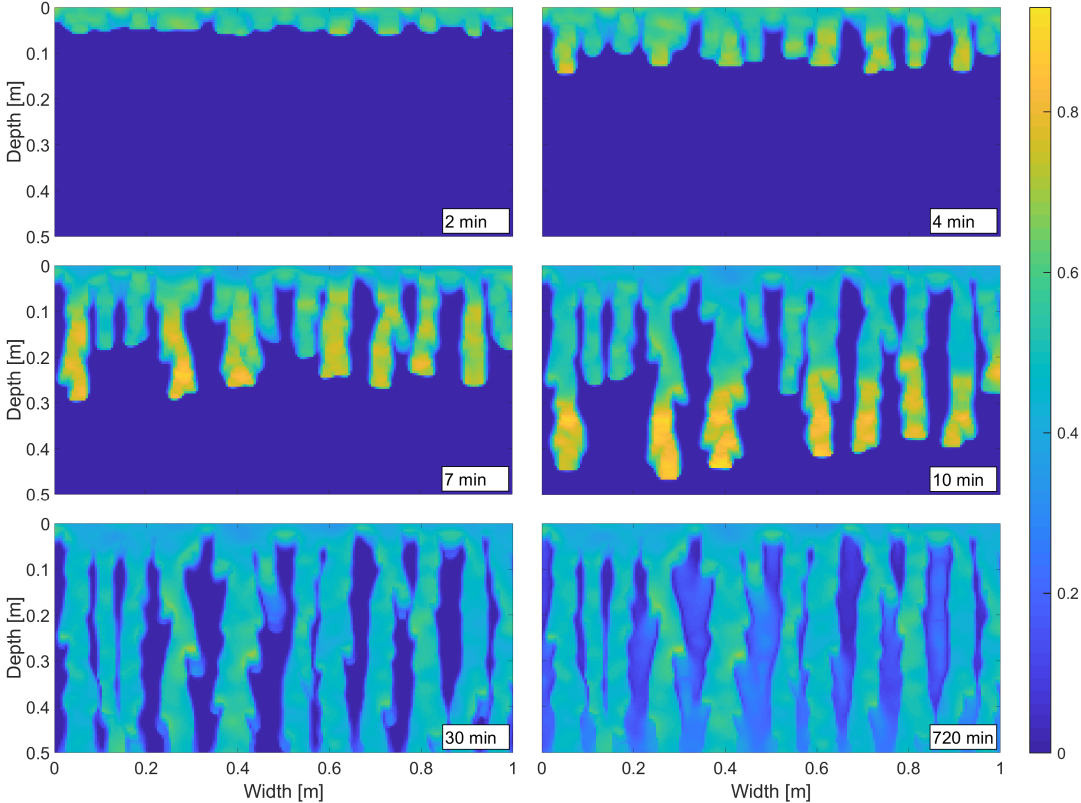

Figure 4.8: Fingering pattern at various simulation times. Constant flux over the top boundary into an almost dry isotropic porous medium. See Table 4.2 for the simulation parameters. For details, refer to the text. Saturation values are colour-coded according to the colour bar on the right.

The persistence of fingers was explained e.g. by Rezanezhad et al. [103] and Glass et al. [46]. Using a dye tracer, the authors showed that the flow is dominant in the centre of the fingers (the finger core) and water stagnates at the periphery (the finger fringe). Therefore, each finger is separated into a mobile core and an immobile fringe. Figure 4.9 shows the velocity field in the left-most finger at the time 10 minutes. For better visualization, each arrow was produced by averaging the flux vector over four neighbouring blocks. It is observed that the magnitude of the flow decreases rapidly toward the boundary of the finger and becomes negligible at the fringe.
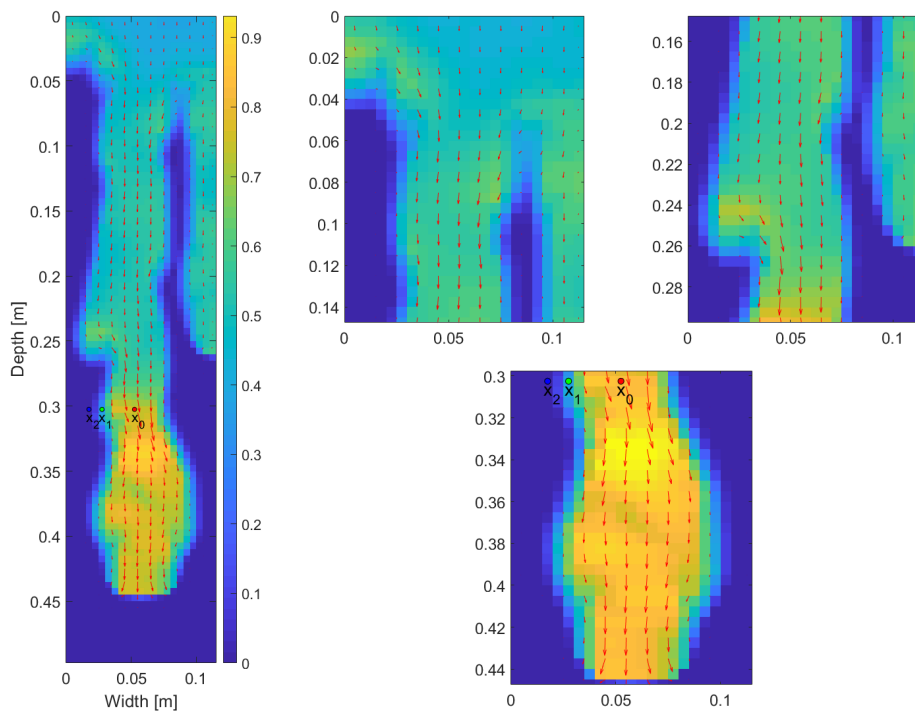

Figure 4.9: A manifestation of the mobile core and immobile fringe of a finger. Detail of the left-most finger in Figure 4.8 at time 10 minutes. Each arrow was produced by averaging the flux over four neighbouring blocks. Saturation values are colour-coded according to the colour bar on the right.

Understanding the stability of such a flow structure is crucial and it can be explained by tracking the pressure-saturation states of the blocks on the retention curve during the passage of the finger [47, 103]. Figure 4.10 tracks the pressure-saturation states of three points inside the finger. Point x_0 lies at the centre of the core (see Figure 4.9), point x_1 lies between the core and the fringe, and point x_2 lies at the outer edge of the fringe. At the beginning, the porous medium was almost dry and so the pressure was negative and quite high at all three points.

All three points started at the wetting branch (the top curve in Figure 4.10) of the retention curve, close to its left-most point. When the finger tip was passing through x_0, the saturation increased quickly and the block followed the main wetting branch of the retention curve. Behind the finger tip, saturation started to decrease and the block jumped down to the main draining branch (the almost vertical red line segment) and then moved to the left along the draining branch. During the same time, the saturation first increased at x_1 (the top part of the green curve) and then it decreased somewhat so that this point stayed between the main branches of the retention curve and reached almost the same pressure as the point x_0. Thus, the pressure difference between the points x_0 and x_1 is negligible and no flow is induced between them. This means that the structure becomes stable although the difference in saturation is large. At the point x_2 the evolution of pressure and saturation is similar to the point x_1. The finger does not expand laterally, because the pressure at x_2 is less negative than the pressure at x_1. This is due to the chosen shape of the retention curve – the pressure at the finger tail (given by the middle part of the draining curve) is always more negative than the initial pressure (given by the left-most point of the wetting curve). This is in contradiction with Rezanezhad et al. [103] where the authors claim that the pressure at x_2 is much more negative than at x_1, and hence the finger expands slowly. Moreover, this lateral finger expansion was also experimentally observed [46, 47, 48].
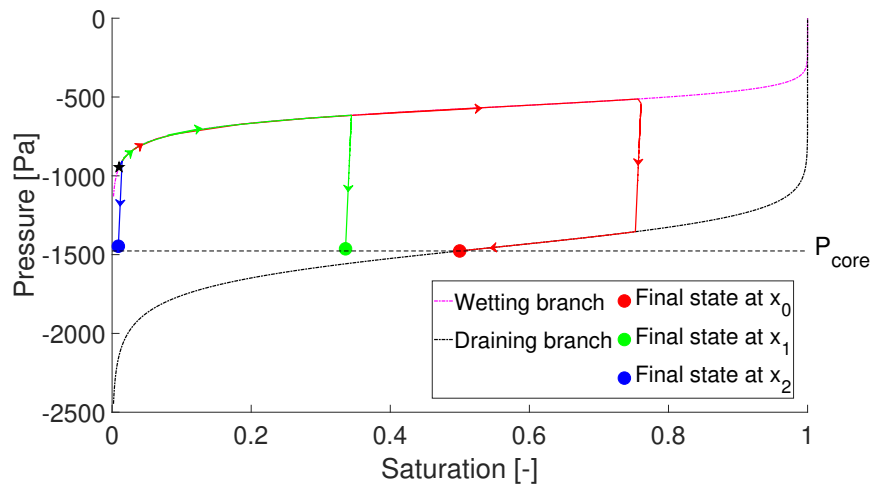

Figure 4.10: Evolution of the pressure-saturation states of three blocks x_0 (core), x_1 (between the core and the fringe), and x_2 (outer block of the fringe) during the first 12 minutes of the simulation. All three points started at the location denoted by a black pentagram. See the text for details.

We suggest that the model presented here may help to explain the question of the later expansion of the fingers. In the previous paragraph, we explained that our choice of the retention curve led to fingers that do not expand laterally. However, a different choice of the retention curve shape allows for lateral expansion. Let us assume a retention curve with larger gradients in the left part (i.e. steeper dependence of pressure on saturation in a dry medium). Since it is difficult to obtain such a retention curve by the van Genuchten model [128], we modified the wetting branch by means of a cubic spline. Figure 4.11 shows the modified wetting branch (dotted red line) compared to the original van Genuchten model (full red line). The main draining branch (full black line) was not modified. This modification allows blocks in the wetting branch at initial saturation to attain more negative pressure compared to the finger tail.
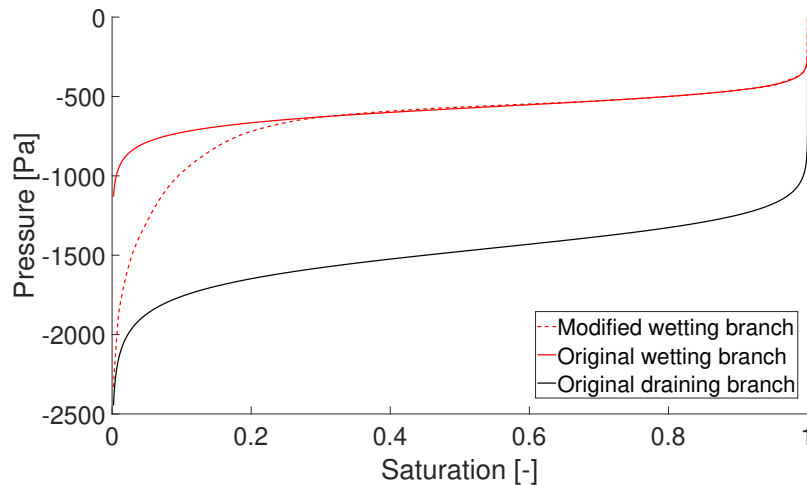

Figure 4.11: The modified retention curve of 30/40 sand. Original van Genuchten wetting curve (full red line) and its modification by a cubic spline (dotted red line). The draining branch (full black line) was not modified.

Let us repeat the simulation shown in Figure 4.8 with this modified retention curve. As a result of the high gradients of the retention curve for low saturations, it was necessary to increase the parameter λ in the relative permeability Equation (3.4). Here, we set $\lambda = 1.5$. All the remaining parameters of the simulation remained the same. The evolution of the saturation field is shown in Figure 4.12. At first, the character of the flow is almost identical to the model using the van Genuchten retention curve (cf. Figure 4.8). This shows that the fingering regime is very robust – a rather dramatic change in the retention curve has little effect on the finger formation process. However, in this case, gradual lateral expansion

of the fingers may be observed (the difference is already visible after 30 minutes of simulation). The speed of the expansion of the fingers is comparable to the experiments reported in [46], but it is faster than in the experiments reported in [47]. After 12 hours of simulation, the matrix is fully wet, and yet most of the flow proceeds through the cores of the original fingers. The speed of the lateral expansion of the fingers can be altered by modification of the retention curve and/or the relative permeability.
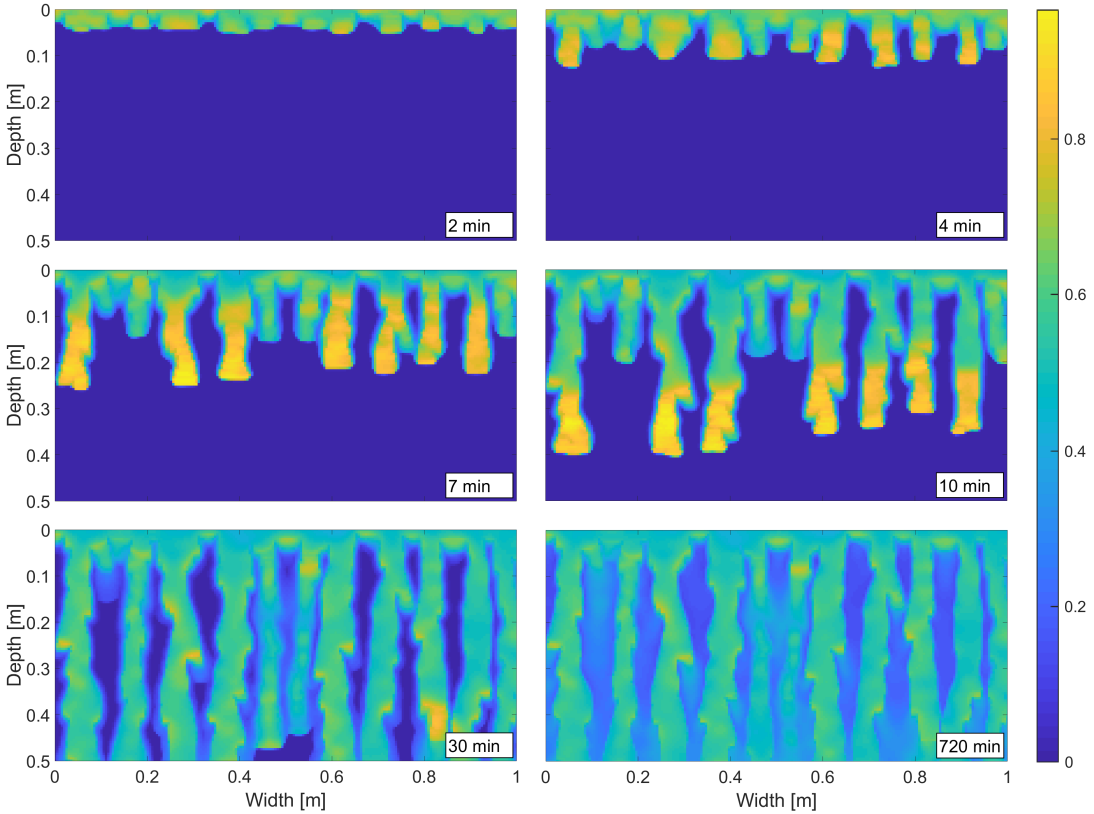

Figure 4.12: Fingering pattern at various simulation times for the modified retention curve. Constant flux over the top boundary into an almost dry isotropic porous medium. For details, refer to the text. Saturation values are colour-coded according to the colour bar on the right.

Figure 4.13 shows the velocity field in the left-most finger in Figure 4.12 10 minutes after the start of the simulation. The modification of the retention curve did not affect the flow magnitude in the core and at the fringe of the fingers. Still, most of the flow happened through the mobile core of the finger, while the fringe remained almost stationary.

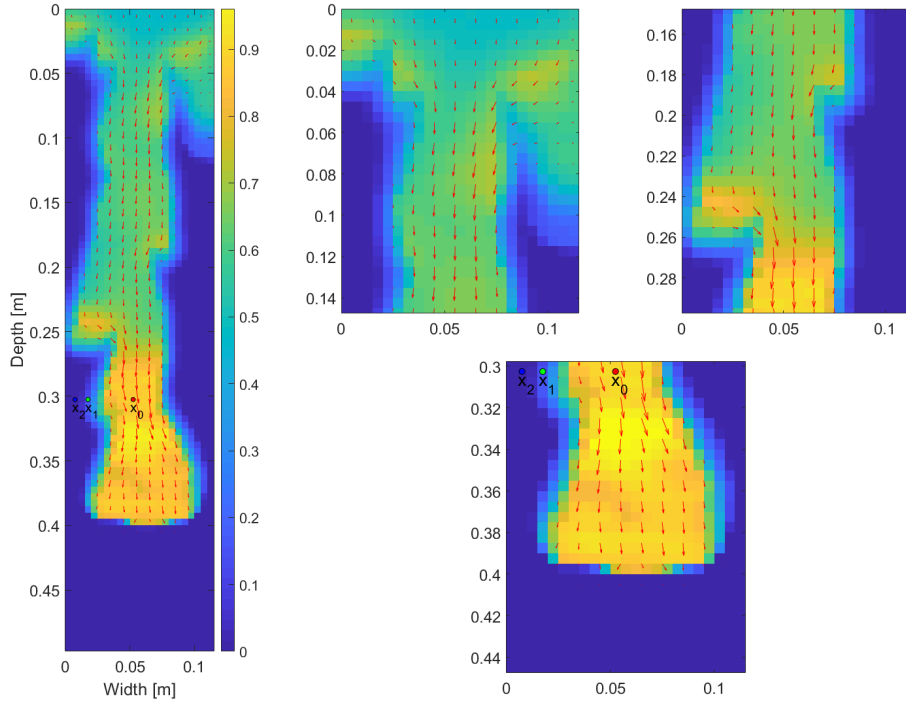To understand the difference between the original (van Genuchten) and modi-

Figure 4.13: A manifestation of the mobile core and immobile fringe of a finger for the modified retention curve. Detail of the left-most finger in Figure 4.12 at time 10 minutes. Each arrow was produced by averaging the flux over four neighbouring blocks. Saturation values colour-coded according to the colour bar on the right.

fied retention curve, we again demonstrate the evolution of the pressure-saturation hydraulic states for three locations, x_0, x_1, and x_2 in Figure 4.14. Analogously to Figure 4.10, the pressure difference between the points x_0 and x_1 was negligible after the first 20 minutes of the simulation and so the flux between the points was also negligible. The saturation at the point x_2 increased slightly from its initial value and so the pressure moved along the main wetting branch. But because of the modified retention curve, the pressure at x_2 was still lower than the pressure at the fringe, and so there was outward lateral flux from the fringe of the finger. This is in agreement with the observation of Rezanezhad et al. [103]. This explains the slow lateral expansion of the fingers in Figure 4.12.
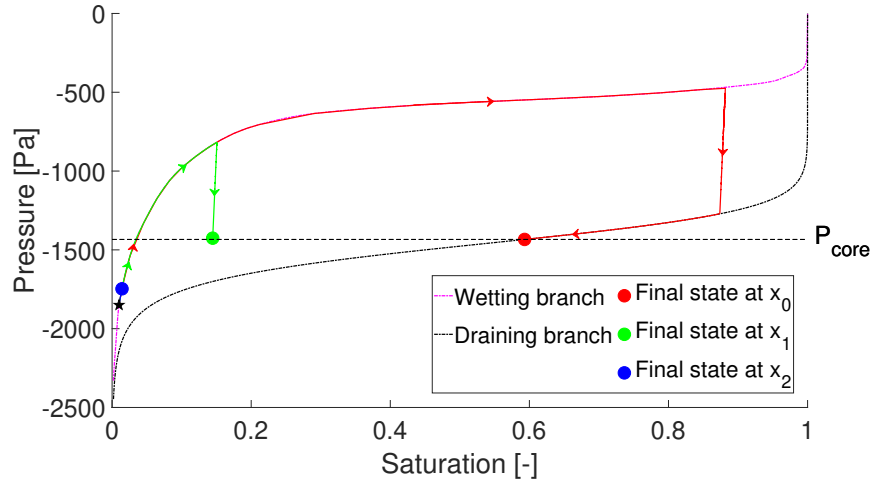
Figure 4.14: Evolution of the pressure-saturation states of three blocks x_0 (core), x_1 (between the core and the fringe), and x_2 (outer block of the fringe) during the first 20 minutes of the simulation. All three points started at the location denoted by a black pentagram. See the text for details.

4.4.2. The effect of initial saturation

Let us now examine the effect of the initial saturation S_{in} on the evolution of the flow patterns. The parameters used for the simulations are given in Table 4.2 and the distribution of intrinsic permeability is shown in Figure 4.7.

In experiments, the dependence on initial saturation is observed to exhibit very interesting qualitative and quantitative features [3, 28]. Most interestingly, as the initial saturation increases from dry to fully saturated, the flow pattern changes qualitatively from the fingering regime (a complex network of preferential pathways, each with the saturation overshoot effect) to a diffusion-like wave water front travelling uniformly (without any overshoot). Moreover, the transition from the fingering regime to the diffusion regime is not monotonic. With increasing initial saturation, the fingers first become faster and narrower, but then they become slower and wider again before disappearing completely into the diffusion-like regime. The model presented here correctly captures both the qualitative and quantitative aspects of this wonderful transition. We again wish to stress that the model does not introduce any artificial or non-measurable parameters to do so.

Figure 4.15 shows a snapshot of the saturation field at 10 minutes for six different values of the initial saturation. See the Supplementary Material for full videos. The model seems to be in complete agreement with the observed

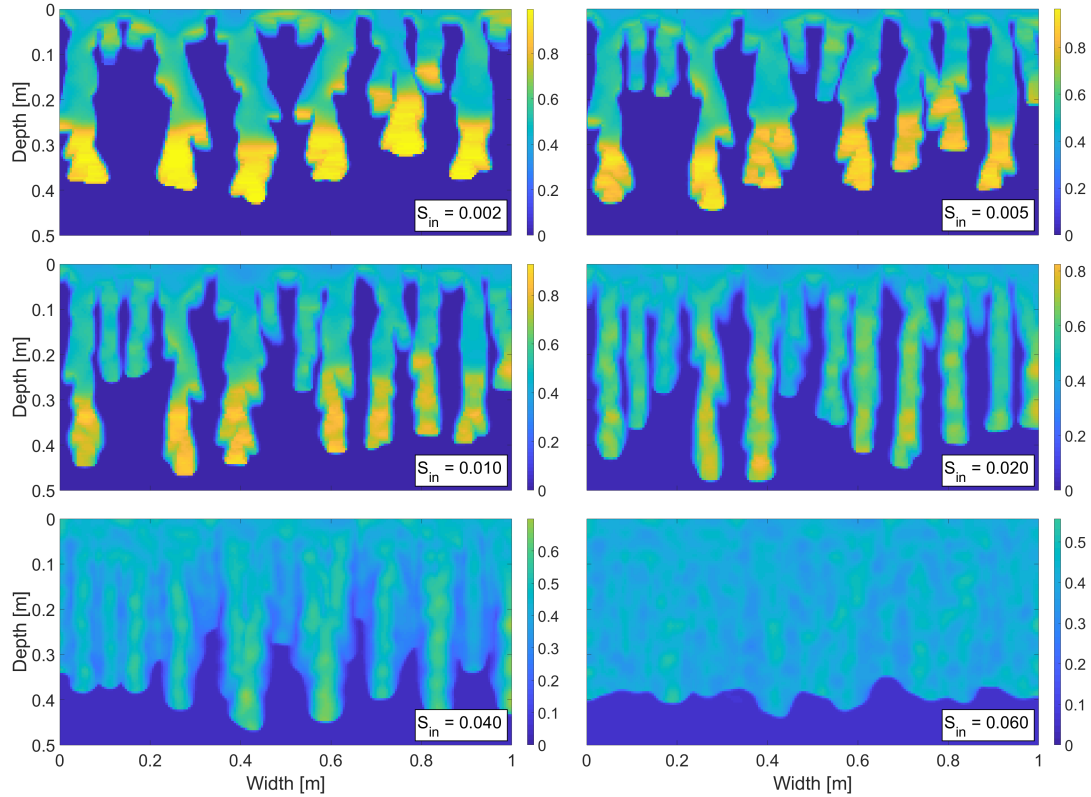transition from the fingering regime to the diffusion-like regime.

Figure 4.15: Snapshot of the saturation field at 10 minutes for six different values of the initial saturation. See the Supplementary Material for full videos. Saturation values are colour-coded according to the colour bar on the right.

4.4.3. Flow across layers of porous media with different characteristics

The experiments of Rezanezhad et al. [103] provide us with an opportunity to test the model in the situation when a layered porous medium is subject to a constant influx of water across the top boundary. Rezanezhad et al. [103] use a Hele-Shaw cell ($160 \times 60 \times 0.3$ cm) filled with four layers of porous material with different characteristics. The top layer (5 cm deep) was composed of fine sand with a grain size diameter between 0.063 mm and 0.25 mm, the second and the bottom layers (both 50 cm deep) consisted of sand with a grain size $0.63 - 1.25$ mm (called homogeneous sand), and these two layers were separated by a layer of horizontally arranged sand (also 50 cm deep) with a grain size between 0.25 mm and 1.25 mm (called heterogeneous sand).

Thus, the separating layer (heterogeneous sand) has smaller grains on average, and therefore its retention curve should be steeper compared to the homogeneous layers. The saturated hydraulic conductivity of the heterogeneous layer was approximately three times lower than that of the homogeneous layers. For details, see Rezanezhad et al. [103].

In the experiment, the top 5 cm layer served as a "randomizer" to smooth out any heterogeneity in the influx. In the model, it is not a problem to keep the influx exactly homogeneous, and thus we do not simulate the top layer. For the simulation of the three 50 cm layers beneath, we used the parameters shown in Table 4.3. All the other parameters of the simulation were identical to the previous two runs of the model. Both the retention curves and the spatial distribution of intrinsic permeability are shown in Figure 4.16. The horizontal arrangement of the heterogeneous layer was ignored in the simulation.
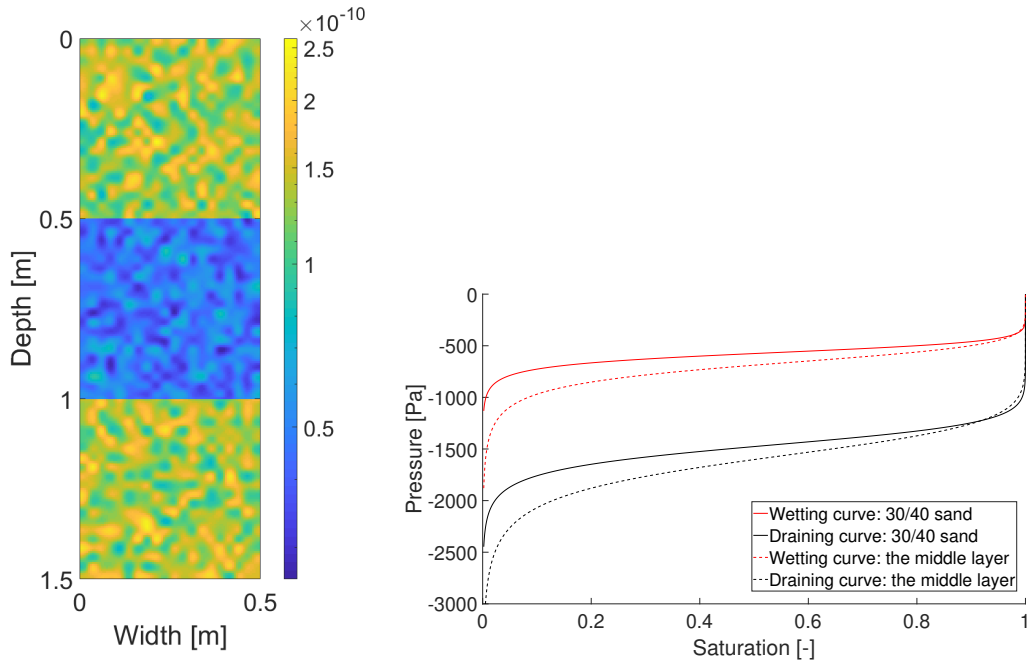

Figure 4.16: Reproducing the flow across layers of porous media with different characteristics. Left panel: The distribution of the intrinsic permeability generated by interpolation method with standard deviation $\sigma = 0.3$ and $dx_{L2} = 2.5$ cm (see Equation (4.10)) The values of intrinsic permeability are colour-coded according to the colour bar on the right. Right panel: The retention curves of the respective layers.

Parameter	Symbol	Value
Intrinsic permeability (homogeneous):	κ	1.376×10^{-10} m^2
Retention curve parameters (homogeneous):	α_w	0.173 Pa^{-1}
	n_w	10.00
	α_d	0.067 Pa^{-1}
	n_d	13.10
Intrinsic permeability (heterogeneous):	κ	4.587×10^{-11} m^2
Retention curve parameters (heterogeneous):	α_w	0.1471 Pa^{-1}
	n_w	7.00
	α_d	0.0623 Pa^{-1}
	n_d	9.17
Width of the chamber	A	50 cm
Depth of the chamber	B	150 cm

Table 4.3: Parameters used for reproducing the flow across layers of porous media with different characteristics. Parameters not included in this table were the same as in Table 4.2.

Rezanezhad et al. [103] showed that stronger capillary forces in the heterogeneous layer (because of the smaller grains) were sufficient to disturb the finger flow. However, the fingering pattern re-appeared immediately in the bottom layer (see Figure 5 in Rezanezhad et al. [103] or the supplementary video therein). We reproduce this behaviour in Figure 4.17, which shows six successive snapshots of the saturation field produced by the model. Observe that the second layer wiped out the typical fingering pattern and a more diffusive regime appeared. When the fingers re-appeared in the bottom layer, there were fewer of them compared to the top layer. This is also consistent with the experimental findings [103]. If we introduced stronger horizontal spatial correlation of the intrinsic permeability in the middle layer (corresponding to the horizontal arrangement), the flow pattern would be disturbed even more. Here, we only wanted to show that this effect can be reproduced by a small change in the retention curve.
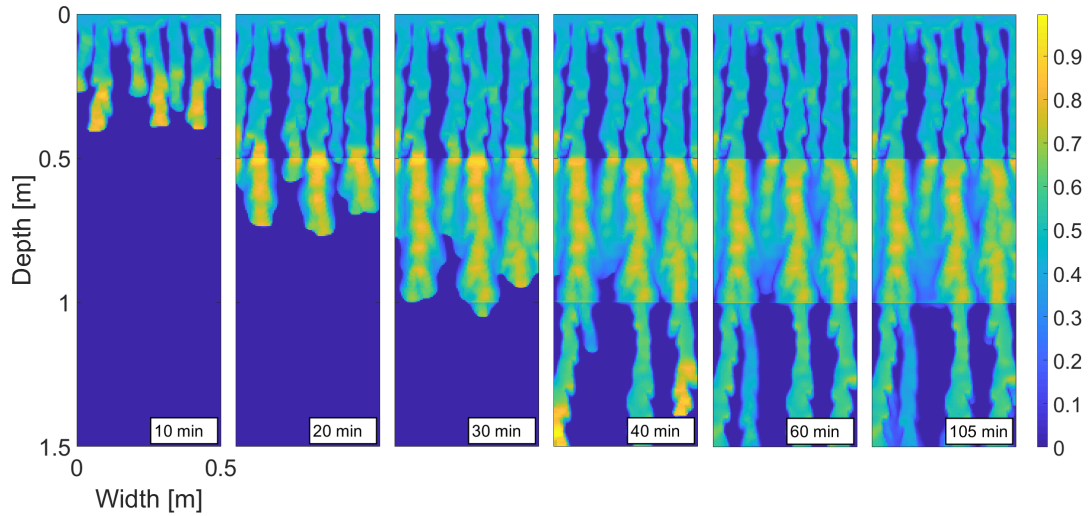
Figure 4.17: Simulated flow across layers of porous media with different characteristics. Snapshots of the saturation field for several successive time points. Saturation values are colour-coded according to the colour bar on the right.

4.4.4. The fingers merging

Experiments show that fingers can merge or bifurcate [47, 49, 103], which is well reproduced by the semi-continuum model. A close look at the simulations performed in Sections 4.4.1-4.4.3 (see also videos in the Supplementary Material) reveals two different scenarios of finger conjunction: the fingers either merge (usually by coalescence of their tips) or they converge and flow side by side without merging. In the first case, the saturation at the finger tip is high enough to break through the immobile fringes. Fingers also merge if the hydraulic conductance below the finger tip is low enough to force lateral expansion of the finger. On the other hand, sometimes two fingers converge without merging. This happened e.g. to the second and the third fingers from the left in Figure 4.8. In this case, neither of the fingers was able to penetrate the fringe of the other. Let us also note, that the fingers finally merged at around 16 minutes (see video *SatIni_0,010.avi* in the Supplementary Material). To understand this phenomenon more thoroughly, see Figure 4.18.
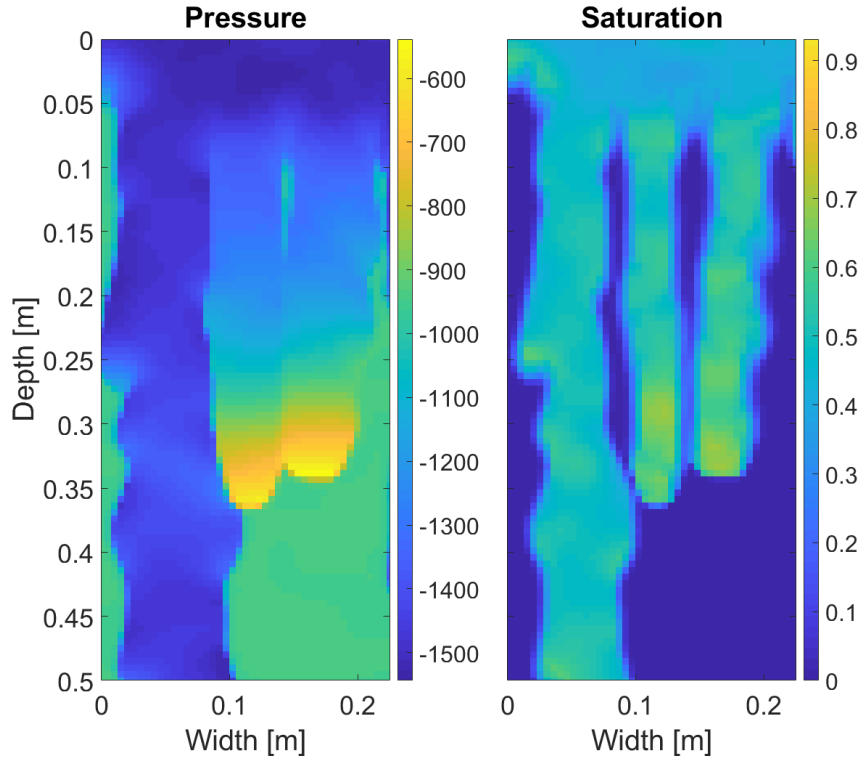
Figure 4.18: A snapshot of the pressure [Pa] and saturation [−] fields 13 minutes after the start of the simulation. The second and third fingers did not merge because the gradient between the fingers was equal to zero (as a result of the equality of pressure at the fringes) and thus the flux between them was negligible. The situation was different for the first and second fingers, as the slower finger collided with the tail of the faster finger. In this case, the gradient was high, but still not sufficient to break through the immobile parts of both fingers. Neither of the effects – merging of the fingers and side-by-side flow – is affected by the modification of the retention curve described above. Pressure and saturation values are colour-coded according to the colour bar on the right for each snapshot.

4.4.5. Point source infiltration

We showed in Section 4.4.2, that the model captured the dependence on initial saturation well. However, a constant flux q_B was prescribed across the top boundary instead of the point source influx, which was experimentally used by Bauters et al. [3]. In this section, we want to thoroughly reproduce experiments provided in [3]. The authors use a Hele-Shaw cell ($50 \times 30 \times 0.94$ cm) filled with homogeneous 20/30 sand. Both water content and matric potential were measured. Water content was measured with Synchrotron X-rays at the Cornell High Energy Synchrotron Source and matric potential with fast responding tensiome-

ters. Unfortunately, it is not clear what a top boundary condition was used in experiments. The authors claim that water was injected at a rate of 2 $\mathrm{cm}^3 \mathrm{min}^{-1}$ through a hypodermic needle located near the sand surface. However, it is not possible to derive Darcy's flux q_B (which is in units ms^{-1}) due to lack of information of the experiment (we do not know the affected area by a needle at the top sand surface). Thus, a point source infiltration is modeled such that a constant flux is prescribed across one centimeter at the top edge (in the middle). Zero discharge at the bottom boundary is prescribed. The reference retention curve of a 20/30 sand [110, 23] used for simulations is shown in Figure 4.19 (see Equation (4.2)). The parameters used for the simulations are given in Table 4.4.

Parameter	Symbol	Value
Horizontal width of the chamber	A	31 cm
Vertical length of the chamber	B	50 cm
Discretization parameter	dx_{par}	1.2 cm
Block size	dx	0.25 cm
Porosity	θ	0.35
Density of water	ρ	1000 kgm^{-3}
Dynamic viscosity of water	μ	9×10^{-4} Pa s
Intrinsic permeability	κ	2.294×10^{-10} m^2
Relative permeability exponent	λ	0.8
Acceleration due to gravity	g	9.81 ms^{-2}
Wetting curve parameter	α_w	0.177 Pa^{-1}
Wetting curve parameter	n_w	6.23
Draining curve parameter	α_d	0.0744 Pa^{-1}
Draining curve parameter	n_d	8.47
Slope of scanning curves	K_{PS}	10^5 Pa
Boundary flux	q_B	8×10^{-5} ms^{-1}

Table 4.4: Parameters used for reproducing the experiments of Bauters et al. [3]. Parameters for 20/30 sand were adopted from Schroth et al. [110] and DiCarlo [23].

The distribution of the intrinsic permeability was provided by interpolation method with standard deviation $\sigma = 0.3$ and $dx_{L2} = 2.5$ cm (see Equation (4.10)). The distribution satisfies $\kappa_{max}/\kappa_{min} \approx 3.75$ and the mean of the intrinsic permeability approximately equals κ. The distribution of the values of intrinsic permeability is shown in Figure 4.20.

In experiments, it is observed that with increasing initial saturation, the wetting front changes gradually from unstable to a stable Richards' flow. However,
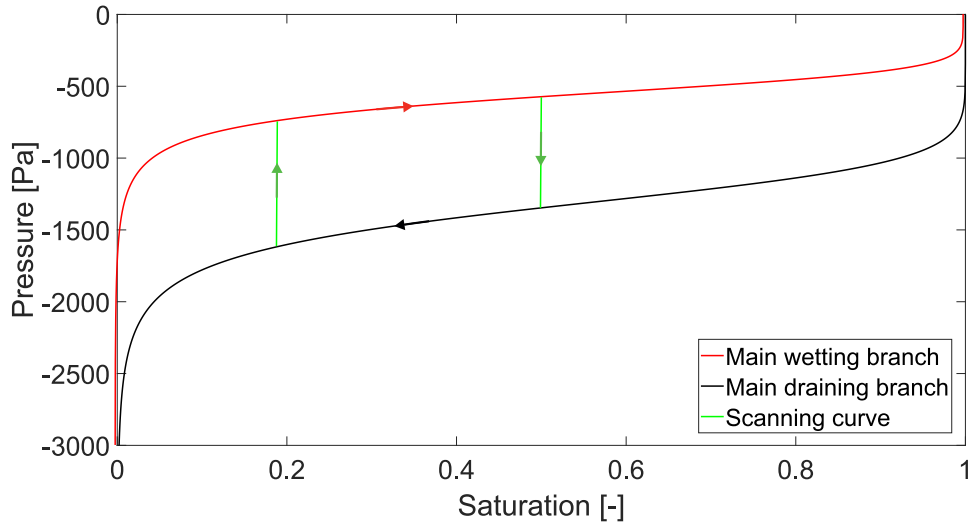
Figure 4.19: The reference retention curve of a 20/30 sand [110, 23] used for the two dimensional simulations. The reference retention curve is given by parameter $dx_{par} = 1.20$ cm, thus the reference size of the block dx_{ref} is approximately 0.83 cm (see Section 4.3.1 for more information).
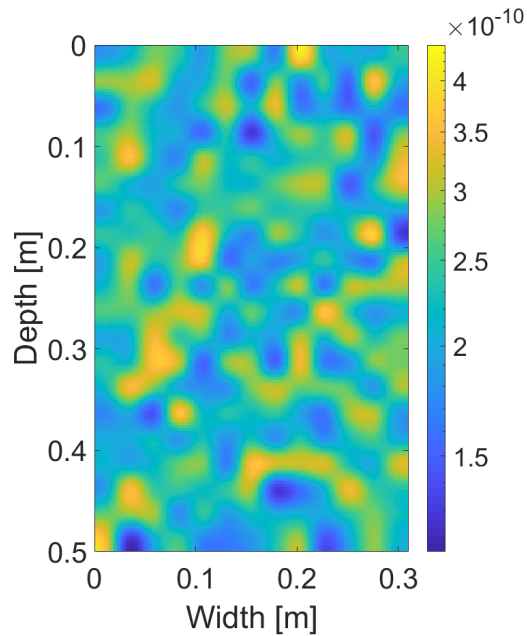

Figure 4.20: The distribution of the intrinsic permeability generated by interpolation method with standard deviation $\sigma = 0.3$ and $dx_{L2} = 2.5$ cm (see Equation (4.10)). The distribution satisfies $\kappa_{max}/\kappa_{min} \approx 3.75$. Intrinsic permeability values are colour-coded according to the colour bar on the right.

this transition is very complex and not monotonic [3]. With increasing initial saturation, first the width of the finger is decreasing and then is increasing. Moreover, the fingers become faster with increasing initial saturation, but then the fingers slow down again and finally the diffusion-like behavior dominates (see Figure 3 in [3]). This very interesting behavior is captured well by the semi-continuum model. Let us note, that the authors only recorded the wetting front patterns 15 cm from the top. Therefore, we are not able to compare wetting fronts at the upper part of the chamber.

Figure 4.21 shows a snapshot of the saturation field at 25 minutes for seven different initial saturations.
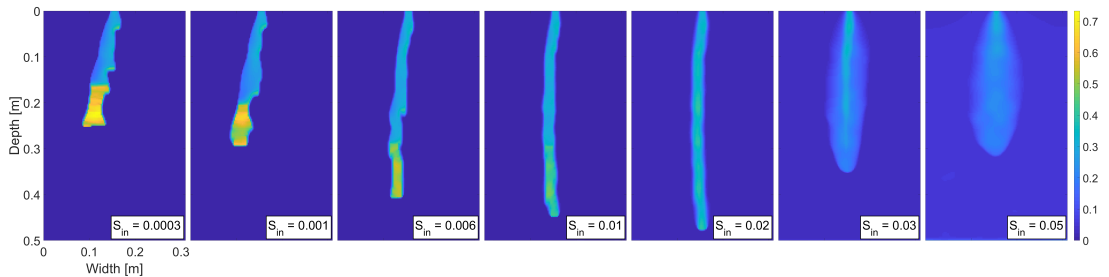

Figure 4.21: Snapshot of the saturation field at 25 minutes for seven different values of the initial saturation. Saturation values are colour-coded according to the colour bar on the right.

The transition between unstable and stable flow is in good agreement with experimental observation: the non-monotonic behavior of the finger width and velocity is captured correctly as well as the shape of the wetting front. Moreover, a stable wetting front appears for initial saturation higher than 0.03, which is also consistent with experiments. However, there is still a small discrepancy compared with the experiments of Bauters et al. [3]. The authors observed that for initial saturation high enough ($S_{in} = 0.047$), water filled the whole chamber. We can clearly see the diffusion-like behavior for $S_{in} = 0.05$ in our simulation, however the chamber is not fully wet. One possible explanation might be followed: the flux used in experiments is very high and thus the porous medium is not able to conduct all the water infiltrated from the point at the upper boundary. The affected area by a needle then slightly increases as the initial saturation is higher. This does not happen for dryer porous medium, because the gradients are much larger and thus the water does not spill at the top boundary. Since the authors did not record the upper part of the chamber (the first 15 centimeters), it is not able to experimentally verify whether the affected area slightly increased or not. Thus we are not able to reproduce properly the behavior of the wetting front for

a residual initial saturation. Moreover, more pronounced diffusion can be obtaint by introducing the space distribution in the retention curve. We conjecture, that the model should be as simple as possible and thus it was not included in the simulation. Another possibility how to increase the diffusion-like behavior can be done by a change in the retention curve or/and relative permeability or/and other parameters of the model. Here, still a good qualitative agreement with experiments is provided without any "fitting" of the parameters. Let us also note that the latter expansion of the finger is not allowed due to the chosen shape of the retention curve because the pressure at the finger tail is always lower than the initial pressure (see Figure 4.10 in Section 4.4.1).

Let us now investigate the effect of the distribution of the intrinsic permeability. Both, filter method and interpolation method, were used to generate seven different distributions (see Figure 4.22) for repeating the same simulations as above.
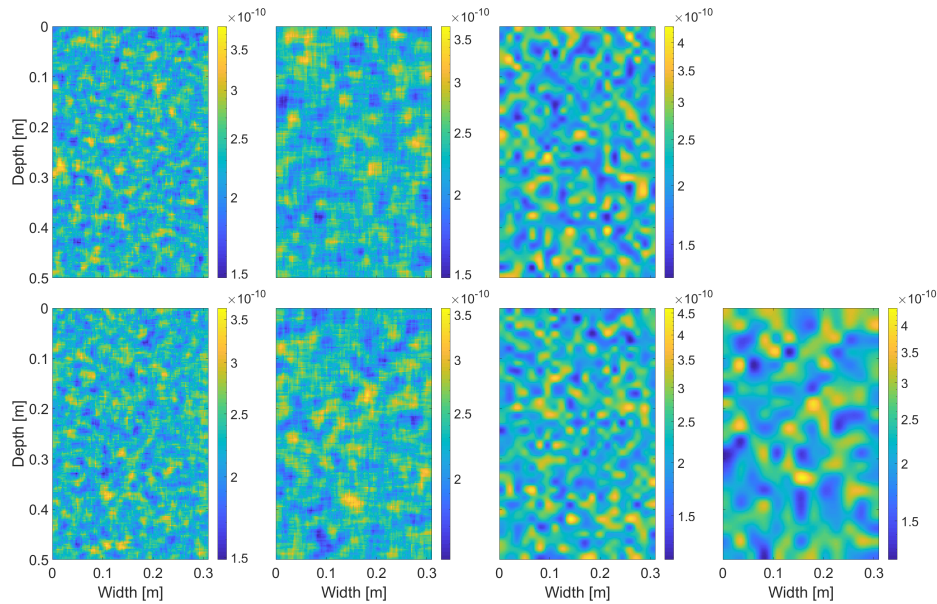

Figure 4.22: The distribution of the intrinsic permeability generated by either filter or interpolation method. The first column: Filter method with standard deviation $\sigma = 0.9$ and $dx_{L1} = 1.5$ cm. The second column: Filter method with standard deviation $\sigma = 1.4$ and $dx_{L1} = 2.5$ cm. The third column: Interpolation method with standard deviation $\sigma = 0.3$ and $dx_{L2} = 1.5$ cm. The fourth column: Interpolation method with standard deviation $\sigma = 0.3$ and $dx_{L2} = 2.5$ cm. From the left up to the right bottom the distributions satisfy respectively: $\kappa_{max}/\kappa_{min} \approx 2.60, 2.50, 3.40, 2.45, 2.35, 3.90, 3.50$. Intrinsic permeability values are colour-coded according to the colour bar on the right.

Figures 4.23-4.29 show a snapshot of the saturation field at 25 minutes for seven different distributions of the intrinsic permeability given by Figure 4.22. The character of the flow remains the same for all types of the distributions. With increasing initial saturation, the fingers are first more narrow and faster and then they are more wider and slower. Thus, the distribution of the intrinsic permeability does not affect this complex transition from the finger flow to the diffusion-like behavior.
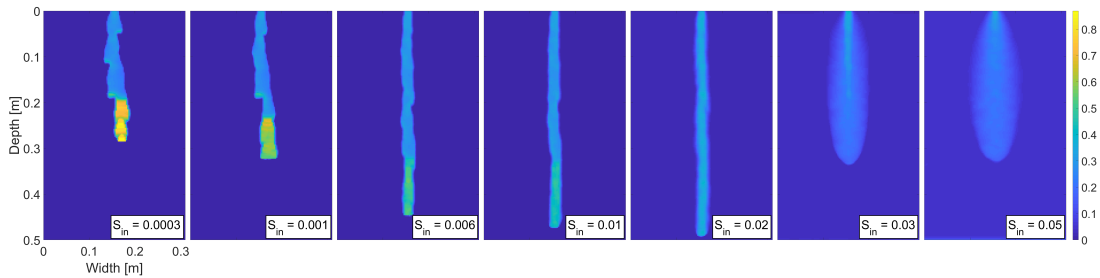

Figure 4.23: Snapshot of the saturation field at 25 minutes for seven different values of the initial saturation for the distribution which satisfies $\kappa_{max}/\kappa_{min} \approx 2.60$ (the first top distribution in Figure 4.22). Saturation values are colour-coded according to the colour bar on the right.

Figure 4.24: Snapshot of the saturation field at 25 minutes for seven different values of the initial saturation for the distribution which satisfies $\kappa_{max}/\kappa_{min} \approx 2.50$ (the second top distribution in Figure 4.22). Saturation values are colour-coded according to the colour bar on the right.

95

Figure 4.25: Snapshot of the saturation field at 25 minutes for seven different values of the initial saturation for the distribution which satisfies $\kappa_{max}/\kappa_{min} \approx 3.40$ (the third top distribution in Figure 4.22). Saturation values are colour-coded according to the colour bar on the right.
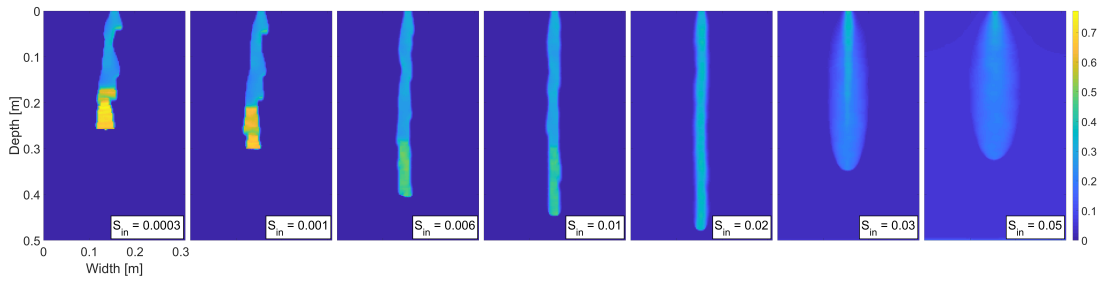

Figure 4.26: Snapshot of the saturation field at 25 minutes for seven different values of the initial saturation for the distribution which satisfies $\kappa_{max}/\kappa_{min} \approx 2.45$ (the first bottom distribution in Figure 4.22). Saturation values are colour-coded according to the colour bar on the right.
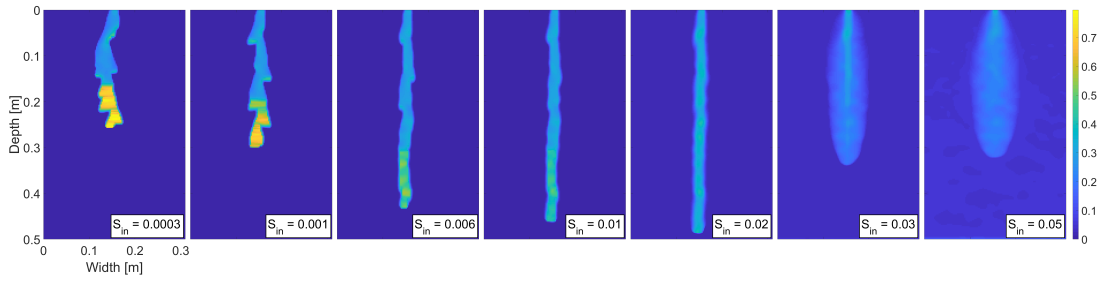

Figure 4.27: Snapshot of the saturation field at 25 minutes for seven different values of the initial saturation for the distribution which satisfies $\kappa_{max}/\kappa_{min} \approx 2.35$ (the second bottom distribution in Figure 4.22). Saturation values are colour-coded according to the colour bar on the right.

Figure 4.28: Snapshot of the saturation field at 25 minutes for seven different values of the initial saturation for the distribution which satisfies $\kappa_{max}/\kappa_{min} \approx 3.90$ (the third bottom distribution in Figure 4.22). Saturation values are colour-coded according to the colour bar on the right.
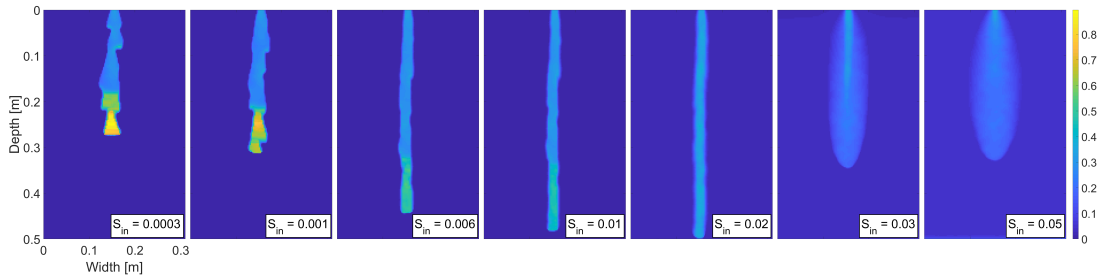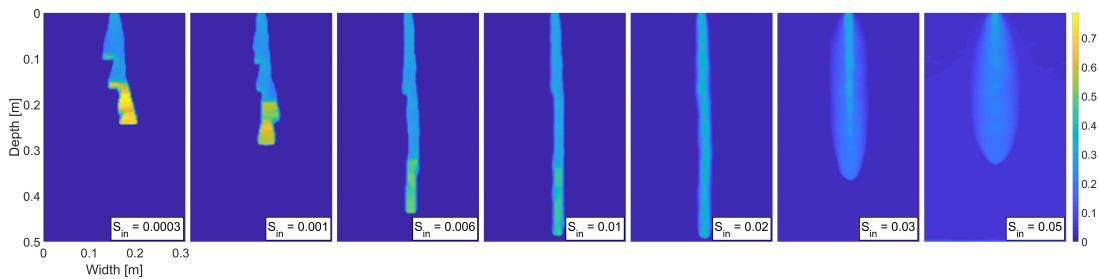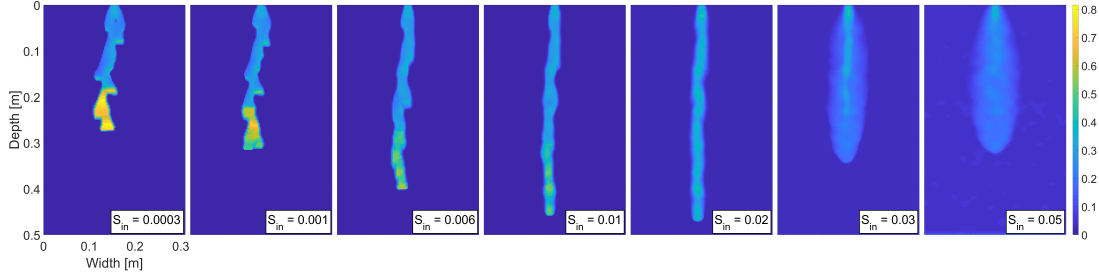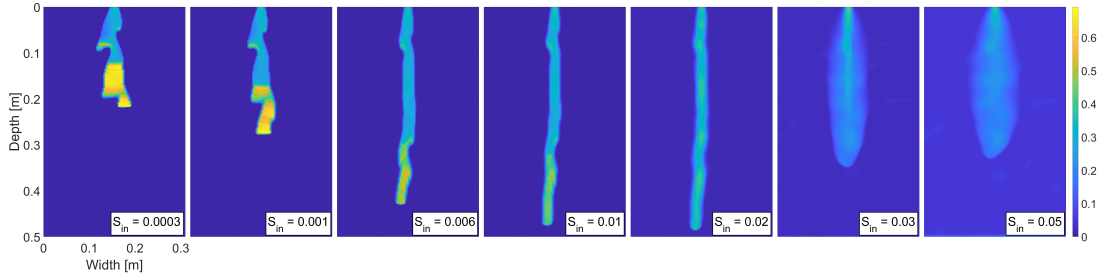

Figure 4.29: Snapshot of the saturation field at 25 minutes for seven different values of the initial saturation for the distribution which satisfies $\kappa_{max}/\kappa_{min} \approx 3.50$ (the fourth bottom distribution in Figure 4.22). Saturation values are colour-coded according to the colour bar on the right.

Figure 4.30 (left) shows the width of fingers for the simulation given by Figure 4.21 (wetting profiles for $S_{in} = 0.0005$, 0.002, 0.04 are not included). The width of each finger is calculated in the following way: first, we calculate the width of each row, which equals $n_{row} \times dx$, where n_{row} is a number of blocks for which saturation is higher than 0.06. The finger width is then calculated as an average width of all the rows. We can clearly see that the finger width first slightly decreases and then increases. The most narrow finger is for $S_{in} = 0.01$ (2.71 cm) which is consistent with experiments (see Figure 5 in [3]). Moreover, the width for unstable flow is also captured well. However, the finger width for $S_{in} = 0.0003$ (3.76 cm) is a little bit smaller than for $S_{in} = 0.0005$ (3.85 cm). This is due to the distribution of the intrinsic permeability. In Figure 4.31 (left), the average finger width for all simulations given by eight different distributions of the intrinsic permeability (see Figures 4.20 and 4.22) is depicted. It is observed, that in average, the finger width for the lowest initial saturation used in simulation is

97

higher than for $S_{in} = 0.0005$. Let us also note, that the average width for a stable wetting fronts is always lower than the maximum width due to the finger expansion. For instance, the average width for $S_{in} = 0.05$ in Figure 4.30 (left) equals 9.27 cm, however the maximum width in the middle of the wetting front equals 12.25 cm.
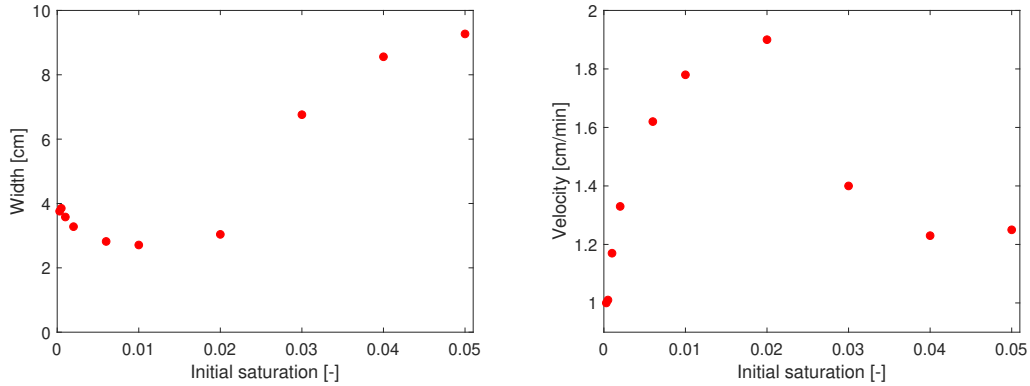

Figure 4.30: The width and the velocity of the wetting front is plotted against the initial saturation for the simulation given by Figure 4.21.

The wetting front velocity for the simulation given by Figure 4.21 is summarized in Figure 4.30 (right). The advance of the wetting front was slower for the diffusion-like behavior compared to the lower initial saturation (but higher than $S_{in} = 0.002$). This is very counterintuitive, since the classical Richards' based theory predicts increase in velocity with increasing initial saturation. The highest finger velocity is observed for $S_{in} = 0.02$, and is approximately five times lower than the highest finger velocity experimentally observed in [3] (for $S_{in} = 0.01$). This is a consequence of mass balance law; we used four times lower influx in our simulations compared with experiments. We observed that the character of the flow remains again the same for different distributions of the intrinsic permeability (see Figure 4.31).

Bauters et al. [3] report a hyperbolic relationship between the initial saturation and the saturation overshoot magnitude. The overshoot magnitude is measured as the difference between saturation at the tip and the tail. We showed that this observation is very well replicated by the 1D semi-continuum model (see Figure 3.6 in Section 3.2). A hyperbolic decay relationship is also observed for two-dimensional simulations as can be seen in Figure 4.32 ($R^2 = 0.952$). The fit is clearly not such accurate as for the 1D model ($R^2 = 0.995$), however this is obviously caused by the distribution of the intrinsic permeability. Moreover,

there is a minor saturation overshoot for $S_{in} = 0.02$, which is not seen in Figure 4.21. This is very well consistent with experiments from Bauters et al. [3], where the authors observed saturation overshoot for $S_{in} = 0.02$ but no overshoot for $S_{in} = 0.03$.
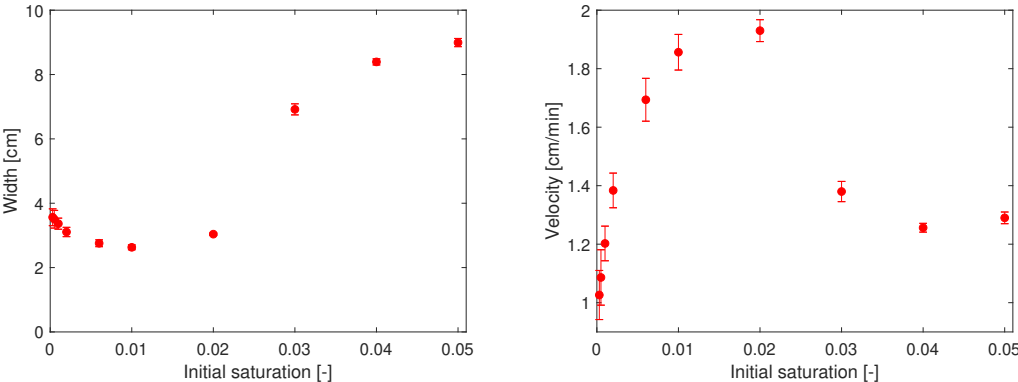
Figure 4.31: The average width and the average velocity of the wetting fronts is plotted against the initial saturation for the all simulations given by eight different distributions of the intrinsic permeability (see Figures 4.20 and 4.22). The standard deviations are also plotted on the graph.
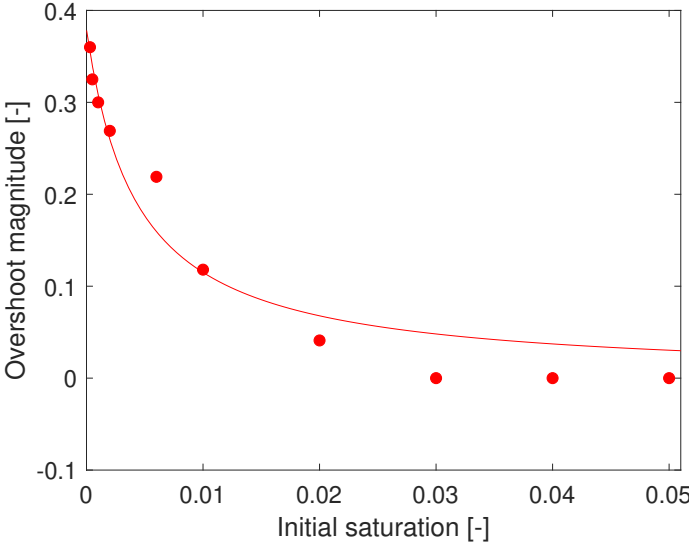

Figure 4.32: Dependence of the overshoot magnitude on initial saturation. A hyperbolic relation fitted to the simulated data has a R^2 value of 0.952.

4.5. Discussion

The difficulty of modelling unsaturated porous media flow can be best understood by studying the effect of the initial saturation of the matrix on the flow pattern. As the initial saturation increases, the flow pattern changes qualitatively from the fingering regime to the diffusion-like regime. During this transition, the saturation overshoot gradually disappears and the finger width depends non-monotonically on the initial saturation (see the Results section). Macro Modified Invasion Percolation models [51, 52] are moderately successful in reproducing the finger-like regime; however, the diffusion-like behaviour is beyond their capacity because there is no way to recover continuous saturation levels and physically meaningful time. At the other end, the Richards' equation is known to reproduce the diffusion-like behaviour but the fingering regime is beyond its power as a result of impossibility of its producing the saturation overshoot [40]. Other models capture some features of the flow in the diffusion like regime or in the fingering regime, but there is usually a price – new parameters that are impossible to measure [54, 142, 21], and/or artificial boundary conditions [109, 115] and/or disagreement with the experiments in other flow regimes except for the one that the model was tuned to [75]. The model presented here correctly captures both the qualitative and quantitative aspects of unsaturated porous media flow both in the fingering regime and in the diffusion regime. The model is based on standard and century-old physics and its only departure is the use of the geometric mean for the flux update.

Let us note again that the typical shape of the retention curve [110, 23] may not always be appropriate, especially for long simulations. This retention curve seems to underestimate the gradient of the wetting branch for small saturations which makes slow lateral expansion of fingers impossible. However, such lateral expansion is often observed in experiments [46, 47, 48]. We conjecture that under certain circumstances, the left-most part of the wetting branch of the retention curve has to be modified to allow for the reproduction of experimental observations. It is exactly this insight that should be expected from a mathematical model.

Chapter 5

Conclusion

The following text was published in [65, 66], and is slightly extended and modificated here.

In this thesis, we propose combining the virtues of continuum and discrete modelling of fluid flow through an unsaturated porous medium. Continuum models work well for diffusion-like regimes but fail to capture preferential flow (finger flow) and its characteristics, especially the saturation overshoot phenomenon. Invasion percolation models and their modifications, on the other hand, capture some features of finger flow but usually describe saturation as a binary variable thus missing a large part of the physical reality. The proposed semi-continuum model describes pressure and saturation as fields that are continuous in time but piecewise constant in space. The model fully rests on well-known theoretical and experimental concepts developed in soil physics [5] and soil hydrology [67]. From mathematical point of view, the model is not a partial differential equation and is based on the Macro Modified Invasion Percolation concept of dividing the porous medium into blocks which are not infinitesimal and are assumed to retain the characteristics of a porous medium. In discrete time steps (which are considered infinitesimal), the semi-continuum model repeats three successive rules: (1) saturation update in each block based on known fluxes between the neighboring blocks, (2) pressure update in each block based on saturation known from the previous step and the retention characteristics of the material, (3) flux update between neighboring blocks based on the Darcy-Buckingham law and a geometric mean of the hydraulic conductivity of the two blocks.

The model captures well all the features of one dimensional unsaturated porous media flow (i.e. three dimensional flow in a thin tube), especially finger flow, including the saturation overshoot, capillary pressure overshoot and their dependence on initial saturation of the medium and influx intensity. The

shape of the saturation overshoot profile and it's evolution in time and space also agrees with observations.

Moreover, the 2D semi-continuum model is able to reproduce (1) gravity-induced preferential flow with a spatially rich system of rivulets (fingers) characterized by saturation overshoot, (2) diffusion-like flow with a monotonic saturation profile, (3) the transition between the two. The model helps to explain the formation of the preferential pathways, their persistence and structure (the core and fringe of the fingers), the slow lateral expansion of the fingers, the effect of the initial saturation of the matrix, and the saturation overshoot phenomenon. Moreover, well known experiments from Bauters et al. [3] are also reproduced well.

The limit of the proposed model for the block size going to zero is a subtle issue. In performing the limit, the retention curve has to become simpler, so that it collapses to a horizontal line. Let us stress again, that this idea is not compatible with continuum mechanics. We conjecture that the semi-continuum approach may also be applicable outside the scope of porous media flow modelling.

Notation

t, x	time and space variables.
$S(t, x)$	relative moisture content (saturation).
$P_c(S)$	capillary pressure.
q	flux.
S_{in}	initial saturation.
P_{in}	initial pressure.
$h(S)$	capillary height.
θ	porosity of the material.
κ	intrinsic permeability of the material.
$k(S)$	relative permeability of the material.
$\gamma(S)$	effective permeability of the material.
μ	dynamic viscosity of fluid.
ρ	density of fluid.
σ	surface tension between fluid and gas.
$K(S)$	hydraulic conductivity.
g	acceleration due to gravity.
$\alpha_w, \ n_w$	wetting curve parameters.
$\alpha_d, \ n_d$	draining curve parameters.
λ	relative permeability coefficient.
S_{rs}	residual saturation.
$S_i(t)$	saturation in block i at time t for 1D simulations.
$P_i(t)$	capillary pressure in block i at time t for 1D simulations.
$S_t(i, j)$	saturation in block $[i, j]$ at time t for 2D simulations.
$P_t(i, j)$	capillary pressure in block $[i, j]$ at time t for 2D simulations.
$q_{i,j}(t)$	fluxes between the blocks i and j at time t for 1D simulations.
$q_t[(i_1, j_1) \rightarrow (i_2, j_2)]$	fluxes between the blocks (i_1, j_1) and (i_2, j_2) at time t for 2D simulations.
q_B	influx at the top boundary.
dx	size of the block.
dx_{par}	discretization parameter.
dx_{ref}	reference size of the block.
K_{PS}	a slope of scanning curves.
$P_{stat}(S)$	equilibrium pressure-saturation curve.
$P_{dyn}(S)$	dynamic pressure-saturation curve.
$\tau(S)$	saturation dependent coefficient.

ϕ	contact angle.
Ψ_{we}	water-entry pressure.
P_w	the pressure needed for the invading phase to fully percolate the block.
P_d	the pressure needed for the defending (retreating) phase to reinvade the block.
R_w	critical wetting radius.
R_d	critical draining radius.
div	divergence operator.
∇	gradient operator.

Abbreviations

CFJ	Cueto-Felgueroso and Juanes Model
IP	Invasion Percolation
MIP	Modified Invasion Percolation
MMIP	Macro Modified Invasion Percolation
RE	Richards' Equation
REV	Representative Elementary Volume
UHPM	Unsaturated Homogeneous Porous Media

Data availability

No experimental data were generated or analysed during the current study. The codes of 1D semi-continuum model and 2D semi-continuum model written in MatLab are available in the Supplementary material.

Bibliography

[1] AKER, E., MALOY, K. J., AND HANSEN, A. Simulating temporal evolution of pressure in two-phase flow in porous media. *Phys. Rev. E 58* (1998), 2217–2226.

[2] ARMANDI, M., BONELLI, B., BOTTERO, I., AREÁN, C. O., AND GARRONE, E. Synthesis and characterization of ordered porous carbons with potential applications as hydrogen storage media. *Micropor. Mesopor. Mat. 103(1-3)* (2007), 150–157.

[3] BAUTERS, T. W. J., DICARLO, D. A., STEENHUIS, T., AND PARLANGE, J.-Y. Soil water content dependent wetting front characteristics in sands. *J. Hydrol. 231-232* (2000), 244–254.

[4] BAVER, C. E., PARLANGE, J. Y., STOOF, C. R., DICARLO, D. A., WALLACH, R., DURNFORD, D. S., AND STEENHUIS, T. S. Capillary pressure overshoot for unstable wetting fronts is explained by hoffman's velocity-dependent contact-angle relationship. *Water Resour. Res. 50* (2014), 5290–5297.

[5] BEAR, J. *Dynamics of Fluids in Porous Media*. American Elsevier Publishing Company, 1972.

[6] BIROVLJEV, A., WAGNER, G., MEAKIN, P., FEDER, J., AND JOSSANG, T. Migration and fragmentation of invasion percolation clusters in two-dimensional porous media. *Phys. Rev. E 51* (1995), 5911–5915.

[7] BLUNT, M. J., AND SCHER, H. Pore-level modelling of wetting. *Phys. Rev. E 52* (1995), 6387–6403.

[8] BÖTTCHER, N., WATANABE, N., GÖRKE, U., AND KOLDITZ, O. *Geoenergy Modeling I - Geothermal Processes in Fractured Porous Media*. Springer, 2016.

[9] BRAY, A. J. Theory of phase-ordering kinetics. *Adv. Phys. 43* (1994), 357–459.

[10] BRINDT, N., AND WALLACH, R. The moving-boundary approach for modeling gravity-driven stable and unstable flow in soil. *Water Resour. Res. 53(1)* (2017), 344–360.

[11] BRINDT, N., AND WALLACH, R. The moving-boundary approach for modeling 2D gravity-driven stable and unstable flow in partially wettable soils. *Water Resour. Res. 56(5)* (2020), e2019WR025772.

[12] BRUSTKERN, R. L., AND MOREL-SEYTOUX, H. J. Description of water and air movement during infiltration. *J. Hydrol. 24(1-2)* (1975), 21–35.

[13] BUCKLEY, S., AND LEVERETT, M. Mechanism of fluid displacement in sands. *Trans. AIME 146* (1942), 107–116.

[14] BUNDT, M., ALBRECHT, A., FROIDEVAUX, P., BLASER, P., AND FLÜHLER, H. Impact of preferential flow on radionuclide distribution in soil. *Environ. Sci. Technol. 44(18)* (2000), 3895–3899.

[15] BURGER, W., AND BURGE, M. J. *Principles of Digital Image Processing: Core Algorithms.* Springer-Verlag, London, 2009.

[16] CAHN, J. W. On spinoidal decomposition. *Acta Metall. 9* (1961), 795–801.

[17] CAHN, J. W., AND HILLIARD, J. E. Free energy of non-uniform systems. i. interfacial free energy. *J. Chem. Phys. 28* (1958), 258–267.

[18] CANCES, C., CHOQUET, C., FAN, Y., AND POP, I. S. Existence of weak solutions to a degenerate pseudo-parabolic equation modelling two-phase flow in porous media. *CASA Report, Eindhoven University of Technology* (2010), 10–75.

[19] CHAPWANYA, M., AND STOCKIE, J. Numerical simulations of gravity-driven fingering in unsaturated porous media using a nonequilibrium model. *Water Resour. Res. 46(9)* (2010).

[20] CHUOKE, R. L., VAN MEURS, P., AND VAN DER POEL, C. The instability of slow, immiscible, viscous liquid-liquid displacements in permeable media. *Trans. AIME. 216* (1959), 88–194.

[21] CUETO-FELGUEROSO, L., AND JUANES, R. A phase field model of unsaturated flow. *Water Resour. Res. 45(10)* (2009), W10409.

[22] CUETO-FELGUEROSO, L., AND JUANES, R. Reply to comment by david a. dicarlo on "a phase field model of unsaturated flow". *Water Resour. Res. 46* (2010), W12802.

[23] DICARLO, D. A. Experimental measurements of saturation overshoot on infiltration. *Water Resour. Res. 40(4)* (2004), W04215.

[24] DICARLO, D. A. Modelling observed saturation overshoot with continuum additions to standard unsaturated theory. *Adv. Water Resour. 28* (2005), 1021–1027.

[25] DICARLO, D. A. Quantitative network model predictions of saturation behind infiltration fronts and comparison with experiments. *Water Resour. Res. 42* (2006), W07408.

[26] DICARLO, D. A. Capillary pressure overshoot as a function of imbibition flux and initial water content. *Water Resour. Res. 43(8)* (2007), W08402.

[27] DICARLO, D. A. Can continuum extensions to multiphase flow models describe preferential flow? *Vadose Zone J. 9(2)* (2010), 268–277.

[28] DICARLO, D. A. Comment on "a phase field model of unsaturated flow" by l. cueto-felgueroso and r. juanes. *Water Resour. Res. 46* (2010), W12801.

[29] DICARLO, D. A. Stability of gravity-driven multiphase flow in porous media: 40 years of advancements. *Water Resour. Res. 49* (2013), 4531–4544.

[30] DICARLO, D. A., AMINZADEH, B., AND DEHGHANPOUR, H. Semicontinuum model of saturation overshoot and gravity-driven fingering in porous media. *Water Resour. Res. 47(3)* (2011), W03201.

[31] DICARLO, D. A., BAUTERS, T. W. J., DARNAULT, C. J. G., STEENHUIS, T., AND PARLANGE, J.-Y. Lateral expansion of preferential flow paths in sands. *Water Resour. Res. 35(2)* (1999), 427–434.

[32] DICARLO, D. A., JUANES, R., LAFORCE, T., AND WITELSKI, T. P. Nonmonotonic traveling wave solutions of infiltration in porous media. *Water Resour. Res. 44* (2008), W02406.

[33] DiCarlo, D. A., Mirzaei, M., and Aminzadeh, B. Fractional flow approach to saturation overshoot. *Transp. Porous. Med. 91* (2012), 955–971.

[34] Egorov, A. G., Dautov, R. Z., Nieber, J. L., and Sheshukov, A. Y. Stability analysis of gravity-driven infiltrating flow. *Water Resour. Res. 39(9)* (2003), 1266.

[35] Eliassi, M., and Glass, R. J. On the continuum-scale modeling of gravity-driven fingers in unsaturated porous media: The inadequacy of the richards equation with standard monotonic constitutive relations and hysteretic equations of state. *Water Resour. Res. 37* (2001), 2019–2035.

[36] Eliassi, M., and Glass, R. J. On the porous-continuum modeling of gravity-driven fingers in unsaturated materials: Extension of standard theory with a hold-back-pile-up effect. *Water Resour. Res. 38(11)* (2002), 16–1–16–11.

[37] Eliassi, M., and Glass, R. J. On the porous continuum-scale modeling of gravity-driven fingers in unsaturated materials: Numerical solution of a hypodiffusive governing equation that incorporates a hold-back-pile-up effect. *Water Resour. Res. 39(6)* (2003), 1167.

[38] Flekkøy, E. G., Schmittbuhl, J., Løvholt, F., Oxaal, U., Maløy, K. J., and Aagaard, P. Flow paths in wetting unsaturated flow: Experiments and simulations. *Phys. Rev. E 65* (2002), 036312.

[39] Fritz, S. *Experimental investigations of water infiltration into unsaturated soil – analysis of dynamic capillarity effects.* Diploma Thesis, University of Stuttgart, Germanys, 2012.

[40] Fürst, T., Vodák, R., Šír, M., and Bíl, M. On the incompatibility of richards' equation and finger-like infiltration in unsaturated homogeneous porous media. *Water Resour. Res. 45(3)* (2009), W03408.

[41] Glass, R. J., Cann, S., King, J., Baily, N., Parlange, J.-Y., and Steenhuis, T. S. Wetting front instability in unsaturated porous media: a three-dimensional study in initially dry sand. *Transp. Por. Med. 5* (1990), 247–268.

[42] GLASS, R. J., CONRAD, S. H., AND PEPLINKSI, W. Gravity-destabilized nonwetting phase invasion in macroheterogeneousporous media: Experimental observations of invasion dynamics and scale analysis. *Water Resour. Res. 36(11)* (2000), 3121–3137.

[43] GLASS, R. J., CONRAD, S. H., AND YARRINGTON, L. Gravity destabilized nonwetting phase invasion in macroheterogeneous porous media: Near pore scale macro modified invasion percolation model. *Water Resour. Res. 37(5)* (2001), 1197–1207.

[44] GLASS, R. J., NICHOLL, M. J., AND YARRINGTON, L. A modified invasion percolation model for low-capillary number immiscible displacements in horizontal rough-walled fractures: Influence of local in-plane curvature. *Water Resour. Res. 34(12)* (1998), 3215–3234.

[45] GLASS, R. J., OOSTING, G. H., AND STEENHUIS, T. S. Preferential solute transport in layered homogeneous sands as a consequence of wetting front instability. *J. Hydrol. 110(1-2)* (1989), 87–105.

[46] GLASS, R. J., PARLANGE, J.-Y., AND STEENHUIS, T. S. Wetting front instability as a rapid and farreaching hydrologic process in the vadose zone p.f. germann (ed.), rapid and farreaching hydrologic processes in the vadose zone. *J. Contam. Hydrol. 3(2-4)* (1988), 207–226.

[47] GLASS, R. J., PARLANGE, J.-Y., AND STEENHUIS, T. S. Mechanism for finger persistence in homogenous unsaturated, porous media: Theory and verification. *Soil Science 148(1)* (1989), 60–70.

[48] GLASS, R. J., PARLANGE, J.-Y., AND STEENHUIS, T. S. Wetting front instability. 1. theoretical discussion and dimensional analysis. *Water Resour. Res. 25(6)* (1989), 1187–1194.

[49] GLASS, R. J., PARLANGE, J.-Y., AND STEENHUIS, T. S. Wetting front instability. 2. experimental determination of relationships between system parameters and two-dimensional unstable flow field behavior in initially dry porous media. *Water Resour. Res. 25(6)* (1989), 1195–1207.

[50] GLASS, R. J., AND YARRINGTON, L. Analysis of wetting front instability using modified invasion percolation theory. *Eos Trans. AGU 70* (1989), 1117.

[51] GLASS, R. J., AND YARRINGTON, L. Simulation of gravity fingering in porous media using a modified invasion percolation model. *Geoderma 70(2-4)* (1996), 231–252.

[52] GLASS, R. J., AND YARRINGTON, L. Mechanistic modeling of fingering, nonmonotonicity, fragmentation, and pulsation within gravity/buoyant destabilized two-phase/unsaturated flow. *Water Resour. Res. 39(3)* (2003), 1058.

[53] GOMEZ, H., CUETO-FELGUEROSO, L., AND JUANES, R. Three-dimensional simulation of unstable gravity-driven infiltration of water into a porous medium. *J. Comput. Phys 238* (2013), 217–239.

[54] HASSANIZADEH, S. M., CELIA, M. A., AND DAHLE, H. K. Dynamic effects in the capillary pressure-saturation relationship and its impact on unsaturated flow. *Vadose Zone J. 1* (2002), 38–57.

[55] HASSANIZADEH, S. M., AND GRAY, W. G. Mechanics and thermodynamics of multiphase flow in porous media including interphase boundaries. *Adv. Water Resour. 13* (1990), 169–186.

[56] HASSANIZADEH, S. M., AND GRAY, W. G. Thermodynamic basis of capillary pressure in porous media. *Water Resour. Res. 29* (1993), 3389–3405.

[57] HASSANIZADEH, S. M., AND GRAY, W. G. Toward an improved description of the physics of two-phase flow. *Adv. Water Resour. 16* (1993), 53–67.

[58] HILFER, R., AND STEINLE, R. Saturation overshoot and hysteresis for two phase flow in porous media. *Eur. Phys. J. Spec. Top. 223(11)* (2014), 2323–2338.

[59] HILL, D. E., AND PARLANGE, J. Y. Wetting front instability in layered soils. *Soil Sci. Soc. Am. Proc. 36* (1972), 697–702.

[60] HOFFMAN, R. L. A study of the advancing interface. i. interface shape in liquid—gas systems. *J. Coll. Inter. Sci. 50* (1975), 228–241.

[61] JANG, J., NARSILIO, G. A., AND SANTAMARINA, J. C. Hydraulic conductivity in spatially varying media - a pore-scale investigation. *Geophysical J. International 184* (2011), 1167–1179.

[62] KATSUSHIMA, T., YAMAGUCHI, S., KUMAKURA, T., AND SATO, A. Experimental analysis of preferential flow in dry snowpack. *Cold Reg. Sci. Tech. 85* (2013), 206–216.

[63] KIRKPATRICK, S. Percolation and conduction. *Rev. Mod. Phys. 45* (1973), 574.

[64] KISSLING, F., HELMIG, R., AND ROHDE, C. Simulation of infiltration processes in the unsaturated zone using a multiscale approach. *Vadose Zone J. 11(3)* (2012).

[65] KMEC, J., FÜRST, T., VODÁK, R., AND ŠÍR, M. A semi-continuum model of saturation overshoot in one dimensional unsaturated porous media flow. *Scient. Rep. 9* (2019), 8390.

[66] KMEC, J., FÜRST, T., VODÁK, R., AND ŠÍR, M. A two dimensional semi-continuum model to explain wetting front instability in porous media. *Scient. Rep. 11* (2021), 3223.

[67] KUTÍLEK, M., AND NIELSEN, D. *Soil Hydrology*. Catena Verlag, Germany, 1994.

[68] KUTÍLEK, M., AND NIELSEN, D. R. Interdisciplinarity of hydropedology. *Geoderma 138* (2007), 252–260.

[69] LAKE, L. *Enhanced Oil Recovery*. Prentice Hall: Englewood Cliffs, 1989.

[70] LENHARD, R. J., AND PARKER, J. C. A model for hysteretic constitutive relations governing multiphase flow: 2. permeability-saturation relations. *Water Resour. Res. 23(12)* (1987), 2197–2206.

[71] LENORMAND, R. Liquids in porous media. *J. Phys.: Condens. Matter 2* (1990), SA79–SA88.

[72] LENORMAND, R., TOUBOUL, E., AND ZARCONE, C. Numerical models and experiments on immiscible displacement in porous media. *J. Fluid Mech. 189* (1988), 165–187.

[73] LENORMAND, R., AND ZACONE, C. Invasion percolation in an etched network: Measurement of a fractal dimension. *Phys. Rev. Lett. 54* (1985), 2226–2229.

[74] LENORMAND, R., ZACONE, C., AND SARR, A. Mechanisms of the displacement of one fluid by another in a network of capillary ducts. *J. Fluid Mech. 135* (1983), 337–353.

[75] LEROUX, N. R., AND POMEROY, J. W. Simulation of capillary pressure overshoot in snow combining trapping of the wetting phase with a nonequilibrium richards' equation model. *Water Resour. Res. 55* (2019), 236–248.

[76] LICHNER, L., ELDRIDGE, D. J., SCHACHT, K., ZHUKOVA, N., HOLKO, L., ŠÍR, M., AND PECHO, J. Grass cover influences hydrophysical parameters and heterogeneity of water flow in a sandy soil. *Pedosphere 21(6)* (2011), 719–729.

[77] LIU, Y., STEENHUIS, T. S., AND PARLANGE, J. Y. Formation and persistence of fingered flow fields in coarse grained soils under different moisture contents. *J. Hydrol. 159* (1994), 187–195.

[78] LØVOLL, G., MÉHEUST, Y., TOUSSAINT, R., SCHMITTBUHL, J., AND MALØY, K. J. Growth activity during fingering in a porous hele-shaw cell. *Phys. Rev. E 70* (2004), 026301.

[79] MEAKIN, P., FEDER, J., FRETTE, V., AND JOSSANG, T. Invasion percolation in a destabilizing gradient. *Phys. Rev. A 46* (1993), 3357–3368.

[80] MEHEUST, Y., LOVOLL, G., MALOY, K. N., AND SCHMITTBUHL, J. Interface scaling in a two-dimensional porous medium under combined viscous, gravity, and capillary effects. *Phys. Rev. E 66* (2002), 051603.

[81] MIKELIĆ, A. A global existence result for the equations describing unsatured flow in porous media with dynamic capillary pressure. *J. Diff. Eq. 248* (2010), 1561–1577.

[82] MITRA, K., AND VAN DUIJN, H. Wetting fronts in unsaturated porous media: the combined case of hysteresis and dynamic capillary pressure. *Nonlin. Anal. Real World Appl. 50* (2019), 316–341.

[83] MOEBIUS, F., AND OR, D. Interfacial jumps and pressure bursts during fluid displacement in interacting irregular capillaries. *J. Coll. Inter. Sci. 377* (2012), 406–415.

[84] MOREL-SEYTOUX, H. J., AND KHANJI, J. Derivation of an equation of infiltration. *Water Resour. Res. 10(4)* (1974), 795–800.

[85] MUALEM, Y. A conceptual model of hysteresis. *Water Resour. Res. 10(3)* (1974), 514–520.

[86] MUALEM, Y. A new model for predicting the hydraulic conductivity of unsaturated porous media. *Water Resour. Res. 12(3)* (1976), 513–522.

[87] MUALEM, Y., AND DAGAN, G. Hydraulic conductivity of soils: unified approach to the statistical models. *Soil Sci. Soc. Am. J. 42* (1978), 392–395.

[88] NAVIER, L. M. H. Mémoire sur les lois du mouvement des fluides. *Mem. Acad. Roy. Sci. 6* (1823), 389–416.

[89] NIASAR, J. V., HASSANIZADEH, S. M., PYRAK-NOLTE, L. J., AND BERENTSEN, C. Simulating drainage and imbibition experiments in a high-porosity micromodel using an unstructured pore network model. *Water Resour. Res. 45* (2009), W02430.

[90] NIEBER, J., DAUTOV, R., EGOROV, A., AND SHESHUKOV, A. Dynamic capillary pressure mechanism for instability in gravity-driven flows; review and extension to very dry conditions. *Transp. Por. Med. 58(1-2)* (2005), 147–172.

[91] NIEBER, J., SHESHUKOV, A., EGOROV, A., AND DAUTOV, R. Non-equilibrium model for gravity-driven fingering in water repellent soils: Formulation and 2D simulations. *Soil Water Rep.: Occ., Cons., Amel. 23* (2003), 245–257.

[92] NIEBER, J. L. Modeling finger development and persistence in initially dry porous media. *Geoderma 70* (1996), 207–229.

[93] NIEBER, J. L., BAUTERS, T. W. J., STEENHUIS, T. S., AND PARLANGE, J. Y. Numerical simulation of experimental gravity-driven unstable flow in water repellent sand. *J. Hydrol.* (2000), 231–232:295–307.

[94] OR, D. Scaling of capillary, gravity and viscous forces affecting flow morphology in unsaturated porous media. *Adv. Water Resour. 31* (2008), 1129–1136.

[95] PALES, A. R., LI, B., CLIFFORD, H. M., KUPIS, S., EDAYILAM, N., MONTGOMERY, D., W.-Z. LIANG, M. DOGAN, N. T., MARTINEZ, N., MOYSEY, S., POWELL, B., AND DARNAULT, C. J. G. Preferential flow systems amended with biogeochemical components: imaging of a two-dimensional study. *Hydrol. E. Sys. Sci. 22(4)* (2018), 2487–2509.

[96] PARKER, J. C., AND LENHARD, R. J. A model for hysteretic constitutive relations governing multiphase flow: 1. saturation-pressure relations. *Water Resour. Res. 23(12)* (1987), 2187–2196.

[97] PARLANGE, J., AND HILL, D. E. Theoretical analysis of wetting front instability in soils. *Soil Sci. 122(4)* (1976), 236–239.

[98] PRAŽÁK, J., TYWONIAK, J., AND ŠÍR, M. Einige bemerkungem zur begriff des kritischen feuchtigkeitsgehaltes. *Ges. – Ing. – Haust. – Bauph. – Umwelt. 109* (1988), 258–261.

[99] PRAŽÁK, J., ŠÍR, M., KUBÍK, F., TYWONIAK, J., AND ZARCONE, C. Oscillation phenomena in gravity-driven drainage in coarse porous media. *Water Resour. Res. 28* (1992), 1849–1855.

[100] PRAŽÁK, J., ŠÍR, M., AND TESAŘ, M. Retention curve of simple capillary networks. *J. Hydrol. Hydromech. 47* (1999), 117–131.

[101] RAATS, P. A. C. Unstable wetting fronts in uniform and nonuniform soils. *Soil Sci. Soc. Am. J. 37(5)* (1973), 681–685.

[102] RÄTZ, A., AND SCHWEIZER, B. Hysteresis models and gravity fingering in porous media. *Z. Angew. Math. Mech. 94(7-8)* (2013), 645–654.

[103] REZANEZHAD, F., VOGEL, H.-J., AND ROTH, K. Experimental study of fingered flow through initially dry sand. *Hydrol. E. Sys. Sci. D. 3(4)* (2006), 2595–2620.

[104] RICHARDS, L. A. Capillary conduction of liquid through porous media. *Physics 1* (1931), 318–333.

[105] RICHARDS, L. A., AND FIREMAN, M. Pressure-plate apparatus for measuring moisture sorption and transmission by soils. *Soil Sci. 56* (1943), 395–404.

[106] ROOIJ, G. H. Modeling fingered flow of water in soils owing to wetting front instability: a review. *J. Hydrol. 231-232* (2000), 277–294.

[107] Ross, C. A., Ali, G., Bansah, S., and Laing, J. R. Evaluating the relative importance of shallow subsurface flow in a prairie landscape. *Vadose Zone J. 16* (2017), 1–20.

[108] Roubíček, T. *Nonlinear partial differential equations with applications.* Birkhäuser Basel, 2013.

[109] Schneider, M., Köppl, T., Helmig, R., Steinle, R., and Hilfer, R. Stable propagation of saturation overshoots for two-phase flow in porous media. *Transp. Por. Med. 121* (2017), 621–641.

[110] Schroth, M., Ahearn, S., Selker, J., and Istok, J. Characterization of miller-similar silica sands for laboratory hydrologic studies. *Soil Science Society of America journal 60* (1996), 1331–1339.

[111] Selker, J., Parlange, J.-Y., and Steenhuis, T. Fingered flow in two dimensions: 2. predicting finger moisture profile. *Water Resour. Res. 28* (1992), 2523–2528.

[112] Smith, W. O. Infiltration in sands and its relation to groundwater recharge. *Water Resour. Res. 3(2)* (1967), 539–555.

[113] Stauffer, D. Scaling theory of percolation clusters. *Phys. Reports 54(1)* (1979), 1–74.

[114] Steenhuis, T. S., Baver, C. E., Hassanpour, B., Stoof, C. R., DiCarlo, D. A., and Selker, J. S. Pore scale consideration in unstable gravity driven finger flow. *Water Resour. Res. 49* (2013), 7815–7819.

[115] Steinle, R., and Hilfer, R. Hysteresis in relative permeabilities suffices for propagation of saturation overshoot: A quantitative comparison with experiment. *Phys. Rev. E 95 95* (2017), 043112.

[116] Stokes, G. G. On the theories of the internal friction of fluids in motion, and of the equilibrium and motion of elastic solids. *Trans. Cambridge Phil. Soc. 8* (1845), 287–319.

[117] Sutherland, K., and Chase, G. *Filters and Filtration Handbook, 5th Ed.* Elsevier, Oxford, 2008.

[118] Szulczewski, M. L., Cueto-Felgueroso, L., and Juanes, R. Scaling of capillary trapping in unstable two-phase flow: Application to CO2 sequestration in deep saline aquifers. *Energy Proc. 1(1)* (2009), 3421–3428.

[119] TEGNANDER, C. Models for ground water flow: A numerical comparison between richards' model and the fractional flow model. *Transp. Por. Med. 43* (2001), 213–224.

[120] TOUMA, J., AND VAUCLIN, M. Experimental and numerical analysis of two-phase infiltration in a partially saturated soil. *Transp. Por. Med. 1* (1986), 27–55.

[121] TURTON, D. J., JR., D. R. B., AND DE JESUS NÁVAR, J. Old and new water in subsurface flow from a forest soil block. *J. Environ. Qual. 24* (1986), 139–146.

[122] ULAM, S. M. On some mathematical problems connected with patterns of growth of figures. *Appl. Math. 14* (1962), 215–224.

[123] VAFAI, K. *Porous media: Applications in Biological Systems and Biotechnology.* Taylor & Francis, 2011.

[124] VALVATNE, P. H., AND BLUNT, M. J. Predictive pore-scale modelling of two-phase flow in mixed wet media. *Water Resour. Res. 40* (2004), W07406.

[125] VALVATNE, P. H., PIRI, M., LOPEZ, X., AND BLUNT, M. J. Predictive porescale modeling of single and multiphase flow. *Transp. Por. Med. 58* (2005), 23–41.

[126] VAN DUIJN, PELETIER, L. A., AND POP, I. S. A new class of entropy solutions of the buckley–leverett equation. *SIAM J. Math. Anal. 39* (2007), 507–536.

[127] VAN DUIJN, C. J., PIETERS, G. J. M., AND RAATS, P. A. C. Steady flows in unsaturated soils are stable. *Transp. Por. Med. 57* (2004), 215–244.

[128] VAN GENUCHTEN, M. T. A closed-form equation for predicting the hydraulic conductivity of unsaturated soils. *Soil Sci. Soc. Am. J. 44* (1980), 892–898.

[129] VISINTIN, A. *Differential models of hysteresis.* New York: Springer, 1993.

[130] VON NEUMANN, J., AND BURKS, A. W. *Theory of self-reproducing automata.* Urbana, University of Illinois Press, 1966.

[131] VONDRKA, A. *Separace hydrogramu dešťového odtoku pomocí elektro-chemických měření.* Doctoral dissertation, Czech Technical University in Prague, Czech Republic, 2012.

[132] VONDRKA, A., TESAŘ, M., AND ŠÍR, M. Vyplavování sodného a drasel-ného iontu z malého horského povodí na Šumavě. *Vodní hospodářství 7* (2013), 21–25.

[133] ŠIMŮNEK, J., AND SUAREZ, D. L. Two-dimensional transport model for variably saturated porous media with major ion chemistry. *Water Resour. Res. 30* (1994), 1115–1133.

[134] ŠÍR, M., LICHNER, L., KMEC, J., FÜRST, T., AND VODÁK, R. Mea-surement of saturation overshoot under grass cover. *Biologia 13* (2020).

[135] WALLACH, R., MARGOLIS, M., AND GRABER, E. R. The role of con-tact angle on unstable flow formation during infiltration and drainage in wettable porous media. *Water Resour. Res. 49(10)* (2013), 6508–6521.

[136] WILKINSON, D. Percolation effects in immiscible displacement. *Phys. Rev. A 34* (1986), 1380.

[137] XIONG, Y. Flow of water in porous media with saturation overshoot: A review. *J. Hydrol. 510* (2014), 353–362.

[138] YAO, T., AND HENDRICKX, J. M. H. Stability of wetting fronts in dry homogeneous soils under low infiltration rates. *Soil Sci. Soc. Am. J. 60* (1996), 20–28.

[139] YOUNG, T. An essay on the cohesion of fluids. *Phil. Trans. Roy. Soc. Lond. 95* (1805), 65–87.

[140] ZHANG, H., AND ZEGELING, P. A. A moving mesh finite difference method for non-monotone solutions of non-equilibrium equations in porous media. *Comm. Comp. Phy. 22(4)* (2017), 935–964.

[141] ZHANG, H., AND ZEGELING, P. A. Numerical investigations of two-phase flow with dynamic capillary pressure in porous media via a moving mesh method. *J. Comp. Phy. 345* (2017), 510–527.

[142] ZHANG, H., AND ZEGELING, P. A. A numerical study of two-phase flow models with dynamic capillary pressure and hysteresis. *Transp. Porous Med. 116* (2017), 825–846.

Supplementary material

Here, complete videos are provided for some simulations presented in this thesis. All videos were published in [66]. The MatLab code used to generate the videos is available upon request from the author. A brief description of the videos follows:

- *Supplementary Video* 1.*avi*: Simulation of the first 20 minutes of the evolution of the saturation field, $S_{in} = 0.010$ (see subsection 4.4.1 "Finger persistence" in the thesis).

- *Supplementary Video* 2.*avi*: Simulation of the first 20 minutes of the evolution of the saturation field for the modified retention curve, $S_{in} = 0.010$ (see subsection 4.4.1 "Finger persistence" in the thesis).

- *Supplementary Video* 3.*avi*: Simulation of the first 10 minutes of the evolution of the saturation field, $S_{in} = 0.002$ (see subsection 4.4.2 "The effect of initial saturation" in the thesis).

- *Supplementary Video* 4.*avi*: Simulation of the first 10 minutes of the evolution of the saturation field, $S_{in} = 0.005$ (see subsection 4.4.2 "The effect of initial saturation" in the thesis).

- *Supplementary Video* 5.*avi*: Simulation of the first 10 minutes of the evolution of the saturation field, $S_{in} = 0.020$ (see subsection 4.4.2 "The effect of initial saturation" in the thesis).

- *Supplementary Video* 6.*avi*: Simulation of the first 10 minutes of the evolution of the saturation field, $S_{in} = 0.030$ (see subsection 4.4.2 "The effect of initial saturation" in the thesis).

- *Supplementary Video* 7.*avi*: Simulation of the first 10 minutes of the evolution of the saturation field, $S_{in} = 0.040$ (see subsection 4.4.2 "The effect of initial saturation" in the thesis).

- *Supplementary Video* 8.*avi*: Simulation of the first 10 minutes of the evolution of the saturation field, $S_{in} = 0.050$ (see subsection 4.4.2 "The effect of initial saturation" in the thesis).

- *Supplementary Video* 9.*avi*: Simulation of the first 10 minutes of the evolution of the saturation field, $S_{in} = 0.060$ (see subsection 4.4.2 "The effect of initial saturation" in the thesis).

- *Supplementary Video* 10.*avi*: Simulation of the first 60 minutes of the evolution of the saturation field for flow across layers of porous media with different characteristics, $S_{in} = 0.010$ (see subsection 4.4.3 "Flow across layers of porous media with different characteristics" in the thesis).